ANALYSIS AND OPTIMIZATION OF MONOPILE TYPE OFFSHORE WIND TURBINES UNDER WIND AND WAVE LOADING

by

Can Aydın

B.Sc., Civil Engineering, Bogazici University, 2007

Submitted to the Institute for Graduate Studies in
Science and Engineering in partial fulfillment of
the requirements for the degree of
Master of Science

Graduate Program in Civil Engineering
Boğaziçi University
2011

ACKNOWLEDGEMENTS

I would like to express my gratitude to all the people who in one way or another contributed to the development of this research. I would like to express my sincere appreciation to my advisor Assist. Prof. Dr. Serdar Soyöz; thank you for your valuable help in instructing, guiding and supporting me throughout the duration of this project.

Also, I would like to thank the members of my Master's thesis examination committee: Assoc. Prof. Dr. Emre Otay, and Assist. Prof. Dr. Çetin Yılmaz for their knowledgeable and in-depth comments and advice.

Special thanks to my sister Dilek Aydın for encouraging me to choose this subject of the thesis and helping me with her knowledge in the sector.

Further, I would like to thank my friends and colleagues: H. Altun, A. Dimoutsis and B. Oluç for their help, the support and for the fun times during MSc. I wish you all success, luck and happiness.

Finally, I would like to thank my family for their continuous support and encouragement.

ABSTRACT

ANALYSIS AND OPTIMIZATION OF MONOPILE TYPE OFFSHORE WIND TURBINES UNDER WIND AND WAVE LOADING

The development of offshore wind technology is rapidly improving because of the energy need in the world. One of the main concerns about the design is to make an economically feasible offshore wind turbine system. The design of the support structure should be strong and stiff enough to endure the time varying wind and wave loads because the offshore wind turbines are very large structures and continuously subjected to the time varying loads.

In this study, 5MW monopile type offshore wind turbine (OWT) was analyzed according to design guidelines. Cost optimization of monopile regarding to steel weight has been done. The standard analysis procedure for the OWT is such that the first structural natural frequency is far away from the first wave frequency to eliminate the resonance; however, it was found that there is an increase in the response of the structure significantly due to the higher wave harmonics (i.e 2^{nd} and 3^{rd} harmonics). Therefore, the results of the thesis may be valuable to designers in terms of the effects of higher wave harmonics on the structural response.

It was found that higher wave harmonics can increase the overturning moment of the monopile (the most important design parameter) about 40% depending on the change in the wave period. The most important outcome of the optimization study was that change in the penetration depth of the monopile into the soil may result in 20% lighter i.e. cheaper structure.

ÖZET

KAZIK TİPİ AÇIK-YAPI RÜZGAR TÜRBİNLERİNİN RÜZGAR VE DALGA YÜKLERİ ALTINDA ANALİZİ VE OPTİMİZASYONU

Dünyadaki enerji ihtiyacından dolayı öncellikle açık-yapı rüzgar teknolojiside olmak üzere teknolojik gelişmeler her geçen gün artıyor. Açık-yapı rüzgar türbin tasarımındaki asıl amaçlardan biri sistemi ekonomik olarak uygun kılabilmektir. Açık-yapı rüzgar türbinleri çok büyük yapılar oldukları gibi sürekli olarak değişken rüzgar ve dalga yüklerine maruz kaldıkları için destek yapılarının bu değişken yüklere karşı yeterince dayanıklı ve direngen olması gerekir.

Bu çalışmada, tasarım klavuzlarına göre analizin yapılması için 5MW lık kazık tipi açık-yapı rüzgar turbini (ART) seçildi. Çelik ağırlığına bağlı olarak maliyet optimizasyon çalışması yapıldı. ART için kullanılan standart analiz prosedürü; resonans etkisini gidermek için, yapının ilk doğal frekansını, dalganın ilk frekansından uzak olacak şekilde seçmektir. Fakat, yüksek dalga frekanlarından (2. ve 3. frekansları) dolayı, yapının tepkisi önemli derecede arttırdığı görüldü. Bu yüzden, belirtilen yüksek dalga frekanslarının yapıya etkisi ile bağlantılı sonuçların tasarımcılar için değerli olabileceği düşünülmektedir.

Yüksek dalga frekansları, maksimum dalga periodunun değişimine bağlı olarak kazık tipi destek yapısının momentini (en önemli tasarım parametresi) yaklaşık %40 oranında arttırabileceği bulundu. Optimizasyon çalışmasının en önemli sonucu ise kazık derinliğinin toprak içindeki değişimiyle %20 oranında daha hafif ve daha ekonomik yapı elde edilebileceği olmuştur.

TABLE OF CONTENTS

LIST OF FIGURES

LIST OF TABLES

LIST OF SYMBOLS / ABBREVIATIONS

a	Induction factor
A	Area of exposure, m
A_p	Gross end area of pile, m^2
A_{rotor}	Area of the rotor disk, m^2
c	Undrained shear strength, kPa
c_a	Airfoil chord length, m
C	Critical elastic buckling coefficient
C_A	Normalized hydrodynamic-added-mass coefficient
C_D	Normalized viscous drag coefficient
C_M	Inertia coefficient
C_s	Aerodynamic shape coefficient
$C_D(\alpha)$	Aerodynamic drag coefficient
$C_L(\alpha)$	Aerodynamic lift coefficient
d	Water depth, m
D	Outside diameter, m
E	Young's Modulus of elasticity, MPa
E_f	Effective Young's modulus, MPa
f	Frequency of excitation force, Hz
f_n	Natural frequency of the structure, Hz
f	Shaft or skin friction, kPa
f_a	Maximum compression stress, MPa
f_{bx}	Computed bending tensile stress in x direction, MPa
f_{by}	Computed bending tensile stress in y direction, MPa
f_v	Maximum beam shear stress, MPa
F	Force action on monopile, kN
F_D	Aerodynamic drag, N
F_L	Aerodynamic lift, N
F_a	Allowable compression stress, MPa
F_b	Allowable bending stress, MPa
F_x	Axial load on blade, N

F_{wind}	Wind force, N
F_v	Allowable shear stress, MPa
F_y	Yield strength, MPa
H	Wave height, m
H_{max}	Maximum wave height, m
I	Inertia of the section, m^4
J	Dimensionless empirical constant
k	Soil spring constant, kN/m^2
K	Coefficient of lateral earth pressure
$k_{u,F}$	Stiffness of lateral deflected structure under lateral load
$k_{u,M}$	Stiffness of lateral deflected structure under moment
$k_{\varphi,F}$	Stiffness of angular deflected structure under lateral load
$k_{\varphi,M}$	Stiffness of angular deflected structure under moment
l	Length of the monopile, m
L_f	Effective fixity length, m
m	Rank of the wind speeds from lowest to highest
M	Moment action on monopile, kNm
M_b	Over turning moment, kNm
N	Total number of annual maximum observation
N_b	Number of rotor blades
p	Actual lateral resistance, kPa
p_o	Effective overburden pressure, kPa
p_u	Ultimate resistance, kPa
P	Probability of non-exceedance
q	In earth calculations: Unit end bearing capacity, kPa
	In structural calculations: Displacement of tower/monopile node, m
$\dot{q}$	Particle velocity, m/s
$\ddot{q}$	Particle acceleration, m/s^2
Q	Mobilized end bearing capacity, KN
Qp	Total end bearing, KN
r	Radius of gyration, m
Δr	Radial length of blade element, m
t_{max}	Maximum soil pile adhesion, kPa

t	In earth calculations: Mobilized soil pile adhesion, kPa
	In structural calculations: Wall thickness, m
T_{max}	Maximum wave period, sec
u	In wave calculations: particle velocity, m/s
	In foundation calculations: lateral deflection, m
w	Excitation frequency, sec
w_n	Natural frequency of structure, sec
W_s	Wind speed, m/s
V	Volume of the cylinder per unit length, m^3
V_b	Base Shear, kN
V_{max}	Maximum annual wind speeds, m/s
V_{rel}	Relative wind speed at a blade section, m/s
V_{rot}	Linear rotation speed at a blade section, m/s
V_{rotor}	Wind velocity at the rotor, m/s
V_R	Extreme wind speed, m/s
V_{tr}	Transverse shear force, MN
V_{wake}	Wind velocity at far wake, m/s
V_o	Wind velocity, m/s
V_1	Wind speed at height h_1, m/s
V_2	Wind speed at height h_2, m/s
y	Actual lateral deflection, mm
X	Depth below soil surface, mm
X_R	Depth below soil surface to bottom of reduced resistance zone, mm
z	Local pile deflection, mm
α	Coefficient for roughness of ground
α_a	Angle of attack, deg
γ	Effective unit weight of soil, MN/m^3
ε_c	Strain which occurs at one-half the maximum stress on laboratory undrained compression tests of undisturbed soil samples
ϕ	Angle of inflow, deg
δ	Friction angle between the soil and pile wall
μ	Mean of random values

ρ_{air}	Air density, kg/m^3
σ^2	Standard deviation
θ	Pitch angle, deg
φ	Angular deflection, rad
Ω	Angular rotation speed, rad/s

ACRONYMS / ABBREVIATIONS

API	American Petroleum Institute
BEM	Blade element momentum
DAF	Dynamic amplification factor
DNS	Direct numerical simulation
DOWEC	Dutch Offshore Wind Energy Converter
EMRA	Energy Market Regulatory Authority
EWEA	European Wind Energy Association
FAST	Fatigue, Aerodynamics, Structures, and Turbulence
FFT	Fast Fourier Transform
FRF	Frequency response function
IEC	International Electrotechnical Commission
GL	Germanischer Llyod
LES	Large-eddy simulation
NREL	National Renewable Energy Laboratory
MSL	Mean sea level
RP	Return period
OWT	Offshore wind turbine
SAP	Structural Analysis Program
SDOF	Single degree of freedom
TurbSim	Turbulence Simulator
WWEA	World Wind Energy Association

1. INTRODUCTION

Wind has been used for years as a source of energy. Nowadays, onshore wind energy is becoming a big industry for the energy needs all around the world. The good locations for onshore wind energy has already been occupied in many countries, therefore, carrying wind turbines to offshore is a natural step for wind energy industry.

The development of offshore wind technology in European waters is rapidly increasing. The main concern is to make an economically feasible offshore turbine system. The amount of steel needed for the support structure has great importance to reduce the cost of the system because the support structures are one of the main cost drivers for offshore wind turbines (OWT).

OWTs are very large structures that carry heavy top mass. They are continuously subjected to the time varying wind and wave loads. Therefore, the design of the support structure should be carried out comprehensively to make the structure strong and stiff enough to endure the time varying loads. Traditionally, the structure is designed according to stiffness and strength criteria. The stiffness criteria specify that the first natural frequency of a structure should be in a region (soft-stiff region) between excitation frequencies (1P and 3P) to avoid resonance.

The foundation types (i.e. ground based foundations, monopiles, and jacked type foundations) of OWTs mostly depend on the depth of the water. The most commonly used support structures in offshore wind industry are the monopile type structures. Those are single cylinder piles with 4 - 6 meters diameter that are driven into the seabed. They are used for shallow waters (i.e. 15-30 meters water depth).

1.1. Scope

In this study, a monopile type OWT was analyzed according to design procedures. Optimization studies were carried out for the monopile foundation, as well. The chosen offshore site is located south of Massachusetts with water depth of 25 meters.

Firstly, the properties of a 5 MW monopile OWT was introduced (i.e. the tower properties, the monopile diameter and thickness, the rotor diameter and weight, cut in and cut out speeds). Constant diameter over thickness ratio was used for the monopile design.

OWTs are exposed to vibration-induced forces (i.e. wind and wave forces) throughout their operational lives that may cause a catastrophic failure; therefore, the stiffness design (i.e. sufficient separation of the natural frequency of the structure from the turbine operational frequency) has initially been checked. The modeling of soil structure interaction is important in the determination of the natural frequency of the structure. The p-y curves (force–displacement curves) were examined with soil springs for large diameter piles. Simplified foundation models were introduced because the software that has been used to simulate the loads is not capable to run the distributed soil spring foundation model. As a last step, the strength of the simplified monopile model was checked.

The effect of the higher wave harmonics on structural response was examined, which is the main objective of this study. A comparison of dynamic structural response was made between two monopile with the same natural period but under the effect of waves with two different periods. The dynamic structural response (i.e. frequency response function) is a function of the ratio of the natural frequency and the forcing frequency (i.e. wave frequency) [6]. Therefore, some cases that can affect the natural frequency (i.e. penetration depth of the monopile, or soil stiffness), and the changes in wave period were analyzed. Finally, the optimization study was carried out for the steel weight of the OWT support structure.

The other types of support structures (e.g. jacket type, ground base support type structures) for OWTs were not examined throughout this thesis. Moreover, fatigue analysis of the support structure, corrosion effect, the water depth effect, and the analyses of the connection parts of the structure were out of the scope of this study.

1.2. Literature Review

Numerous studies have been published concerning the design of OWTs. NREL (National Renewable Energy Laboratory)’s baseline wind turbine model was used in

various concept studies of OWTs analyses [1]. The general properties of the turbine that was studied in this thesis are based on the NREL's baseline model.

1.2.1. Design Parameters

Among the general properties, the main parameter of a monopile is the ratio between the diameter (D) and the wall thickness (t). According to one of the Michiel B. Zaaijer's study [2], D/t ratio equals to 100 is a good representation for foundation pile. Increase in this ratio results in a lighter construction but buckling risk would be encountered during the installation of the pile.

The standard design procedure of OWT starts with defining the turbine type and the weight, the wind and wave data, the water depth, and the soil conditions. In the classical design approach, structure has to fulfill frequency (stiffness) and fatigue limitation [3].

The fatigue limitation is given by the turbine characteristics. The rotational speed of a turbine corresponds to 1P-frequency which is the lower frequency limit for design. If maximum rotational speed of a turbine is very close to its natural frequency, amplification in the response due to resonance occurs. Generally, 10% margin is also added to 1P frequency as a safety. On the other hand, the upper frequency limit for the structure is the higher harmonics of rotor speed (i.e. 3P-frequency). The frequency region between 1P and 3P for the structure is called soft-stiff which is commonly used for current design of OWTs [3, 4].

OWT can be designed with a natural frequency beyond 3P range but that leads to high cost and wind induced fatigue. On the other hand, it can be designed with a natural frequency below 1P range but in this case, OWT would have excessive movement due to wave excitation. Moreover, if the natural structural frequency is lower than the wave excitation, then only inertia dominated response can be expected. Therefore, choosing the natural frequency of the OWT between 1P and 3P range, and closer to 1P range ensures the lightest and most cost effective design solution [3, 5, 6].

In the study of M. Küln [5], an overview was presented on the effects of structural

dynamics due to aero-dynamic and hydro-dynamic loads, and interaction between soil and sub-structures. The stiffness has been identified as the major aspect in the design of support structure that is examined in this paper. The softer design for support structure suffers higher dynamic amplification. This amplification can be reduced with a stiff foundation i.e. pile driven deep enough into the soil.

Moreover, the monopile type structures suffer more from the wave loads then lattice type structures. Several studies show that decrease in pile diameter (3.2m to 2.5m) reduces the hydrodynamic loading by 20-25% [5].

1.2.2. Guidelines

Different design guidelines for OWTs were compared [7]. These guidelines have been developed by organizations such as the American Petroleum Institute (API), and the International Electrotechnical Commission (IEC). The comparison was made between API RP-2A and IEC 61400-3. The main difference is about the return period of the extreme environmental conditions (i.e. API takes 100-year return period and IEC takes 50-year return period).

The Design Methods for Offshore Wind Turbines at Exposed Sites (OWTES) project compares the design loads with measured values [8]. The design has been made according to IEC 61400-3. It was found that the design loads derived from the extreme conditions are much higher than the measured maximum loads. Therefore, the design is on the safe side when it is analyzed according to the guideline.

1.2.3. Design Loads

The monopile type OWT is a slender structure. It vibrates dramatically under wave loads depending on how close the wave and structural frequencies are. Therefore, it is recommended that nonlinear regular waves and combination of linear stochastic seas should be assumed for analyses of the structure [8].

A designer needs to estimate peak loads on a structure over (i.e.) 20 years. Running

20 years of computer simulation is not practical; therefore, representative 20 year spectrum of loads is used. The study by P.S. Veers and S. Butterfield [9] reviews the current practice for loads on wind turbines, and, statistical modeling techniques.

The study [9] mentions that, designers generally use the extreme load models to simulate operational and extreme wind speeds. Parked loads (i.e. loads on non-operating turbine in extreme storm condition) are introduced because highest loads usually occur in the highest wind. Therefore, the parked case specifies the controlling parameters of the worst inflow condition and estimates the turbine response. On the other hand, the operational loads resemble the fatigue load case where long term distribution of fatigue load cycles should be calculated to estimate the total damage over the design lifetime [9].

1.2.4. Foundation Design

The most common method to design monopile foundation in offshore wind industry is the p-y method described in API. The p-y method has been derived from some field test results for the piles having diameters of 0.6 meters. And, that may be acceptable for pile diameter up to 1 m or 2 m [10]. It is quite small compared to large diameter monopiles. The scale effect has been studied and it was found that when pile diameter increases, p-y method overestimates the soil stiffness to determine the necessary embedded pile length [11].

There are some studies on comparison of p-y method with large diameters. Based on those studies [10, 12], p-y method should be modified in order to take the pile soil interaction into account for large diameter monopiles. However, this modification was not considered in this thesis.

The study by Patric Passon [13] shows nonlinear soil effect under dynamic load; however, no validated models for such effect are available. Therefore, only linearized soil models based on p-y method was taken into account. The study by Patric Passon [13] mentions that increase in structural response results in decrease of soil stiffness if deflections exceed the linear portion of p-y curves. The simple approach to substitute a complex distributed spring model is the widely used and well known effective fixity length

model. In general, this model gives good accuracy of results in terms of modal properties and dynamic responses of the structure when stiff soil condition is presented on site [13, 14].

According to the effective fixity length model, the results represent the soil-structure interaction as good as the other complex models. It is a simpler model to use for offshore turbine design applications [13].

1.2.5. Additional Works

Different turbine sizes (i.e. 2MW, 3MW, and 5MW) were compared in the study [15] to analyze them according to two different methods (i.e. combined wind and wave loads, and separate analysis of these two loads). According to this study [15], if the directions of wind and wave load differ slightly, the compared results differ more. Breaking waves are taken into account only in the first method (combined wind and wave load method), therefore, there are great differences between the results of the two methods (analyses under combined load, and separate analyses of wind and wave loads). On the other hand, without the breaking waves, especially 5MW turbine shows a large excitation to the wave forces. That was not checked in that study. Finally, the study suggests that a load case using stochastic wind with periodic wave description should be considered to take into account both the elastic behavior and the nonlinearity of wave kinematics.

On the other hand, according to the study of M. Seidel, large waves must typically be calculated with nonlinear wave theories. REpower 5M was examined as an example in that study. It shows that the influence of wave loading is less pronounced for 5MW turbines than for other turbines [16].

Besides the effect of wave excitations, the cost optimization was also examined in numerous studies. One of the studies of M.B. Zaaijer [41] gives information about the estimation of OWTs cost. The engineering models are compared with the actual project, and the steel weight is considered as the most important cost drive. Without taking the installation costs into account, monopiles and ground base structures (GBS) are compared. And, it is suggested that, steel weight should be multiplied with 2 €/kg and GBS mass

should be multiplied with 0.07 €/kg. According to comparison, the cost of the monopile is less sensitive to the water depth and wave height than the GBS. On the other hand, when the turbine size increases, GBS appears less sensitive depending on the applied costs per kg.

On the other hand, the study [43] compares the different type of OWT foundations in shallow water with OWTs in deep water. In general, monopile foundations are very successful in water depth of 0m-30m for small turbines 2-3 MW due to simple construction and low cost of 2-3 €/kg. Although the steel weight is lesser than monopoles, jacket and tripod structures are cumbersome to weld together and the cost is typically 5-6 €/kg. Because the monopiles are too soft for deeper water (deeper than 30 m), the other type of foundations are more preferable in deep water.

1.3. Objective

The monopile type OWT was designed according to the guidelines. It was realized that although the structural frequency of the OWT is chosen far from the first wave harmonic, the structural response may increase dramatically due to the higher wave harmonics.

The aim of this study is to highlight the effects of higher wave harmonics on the structural response of the OWT that is designed according to the rotor excitations (i.e. 1P and 3P frequencies ranges). Cost optimization study can be considered as the second aim of this thesis. The additional cases that may reduce the cost of the monopile were examined, after the monopile was designed according to stiffness and strength criteria.

1.4. Wind Turbines

1.4.1. Wind energy

Wind energy is the most advanced and commercially viable energy source among the renewable energy resources. Wind power is the conversion of wind energy into a useful form of energy utilizing different devices such as wind turbines and wind mills.

European countries have started to use windmills in the 12th century. The first attempt to produce energy from wind power has started in Denmark in the 19th century, and, finally the electrical energy production has started in 1894. However, because of new energy resources like oil and gas, wind energy has not developed much. The wind energy production has started substantially in 1979 after the world oil crises between 1973 and 1979. These early turbines were small by today's standards, with capacities of 20–30 kilowatt each. Since then, they have increased greatly in size, so wind energy production is common in many countries.

Parallel to the technological improvement, the size of the turbines and the height of towers were increased because of the need for higher wind speed. A large wind farm may consist of a few dozen to several individual wind turbines that cover on a big site having high wind speed. It is necessary that the site to be open area (i.e. flat large areas, mountain, or hill tops), so that to have clean wind (no turbulence). These types of wind farms are called onshore wind farm (Figure 1.1.a). However, onshore wind farms are subjected to many restrictions and objections. Objections are generally due to their negative visual impact and/or noise. On the other hand, restrictions are associated with obstructions of building and/or mountains which cause turbulence in air, or limited availability of land.

Therefore, offshore wind farms (Figure 1.1.b) turn out to be more viable solution. There is higher and constant wind speed, so higher efficiencies on offshore areas. However, OWTs have some disadvantages compared to onshore wind turbines such as increase in foundation, installation, transportation, and maintenance cost. Moreover, the integration power to the central grid is also cumbersome and costly.

The power production of turbines will always be the main criteria for any wind farm project. For a specific site with long-term wind speed measurements, the detailed yearly production calculations and the optimum turbine configuration should be done. A very crude rule of thumb to estimate the total production is 1/3 of the rated turbine output [17]. For example, a 200 MW rated output offshore wind farm (40 efficient 5MW OWTs) would produce 200 x 1/3 x 24 x 365= 584000 MWh/year. An average European household uses 4000 kWh/year, which means the offshore wind farm can supply some 150 000 homes throughout a year [18].

a) b)

Figure 1.1. a) Onshore wind turbine, b) Offshore wind turbine

(www.windenergyplanning.com & www.greentechmedia.com)

According to World Wind Energy Report (2009) of The World Wind Energy Association (WWEA) which is a non-profit organization and acts as a communication platform for all wind energy actors worldwide, world total installed capacity has reached 159 Gigawatt. The growth of the installed capacity is shown figure below.

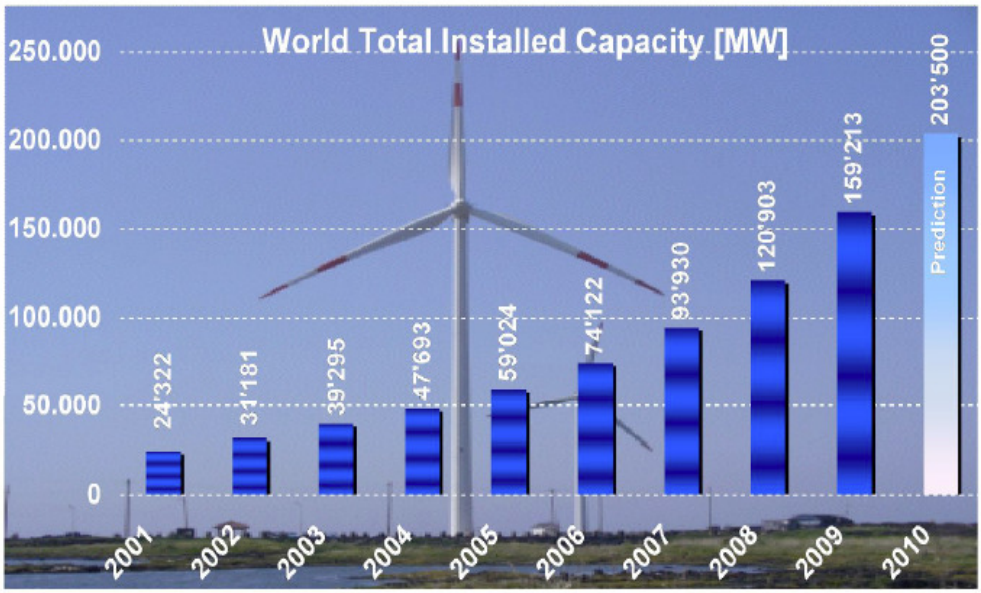

Figure 1.2. Total installed worldwide wind capacity [19]

The growth rate of the wind power is 31.7% in 2009. And, China is the biggest market for wind turbines in that year. The country which has the highest total installed capacity is the USA, followed by China and Germany.

When the growth rate is taken into the consideration, Turkey has the second highest rate in 2009 (Figure 1.3). All wind turbines installed globally by the end of the year 2009 contribute 2 % of the global electricity demand. This energy amount equals the electricity needs of Italy [19].

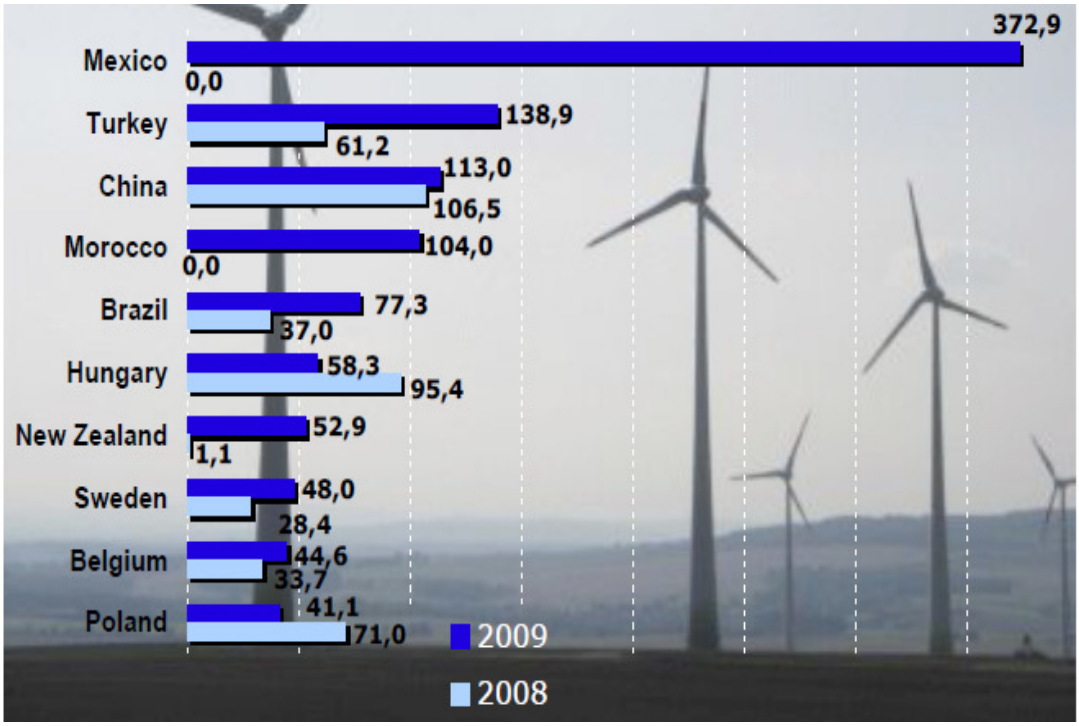

Figure 1.3. Top 10 countries by percent growth rate [19]

On the other hand, offshore wind capacity continued to grow in 2009 (Figure 1.4). Total installed capacity amounted is almost two Gigawatt that is 1.2 % of the total wind capacity worldwide. In Denmark, the largest offshore wind farm installed so far (2009) was in the North Sea: Horns Rev II, which has the capacity of 209 Megawatt [19].

Both in terms of total and additional capacity, Germany (25770 MW / 1880 MW) are still the biggest markets in Europe. Moreover, wind turbine manufacturing industries in Denmark, Germany and Spain are still dominating in many wind markets around the world, and, they seem to be in the leading role in the coming years [19].

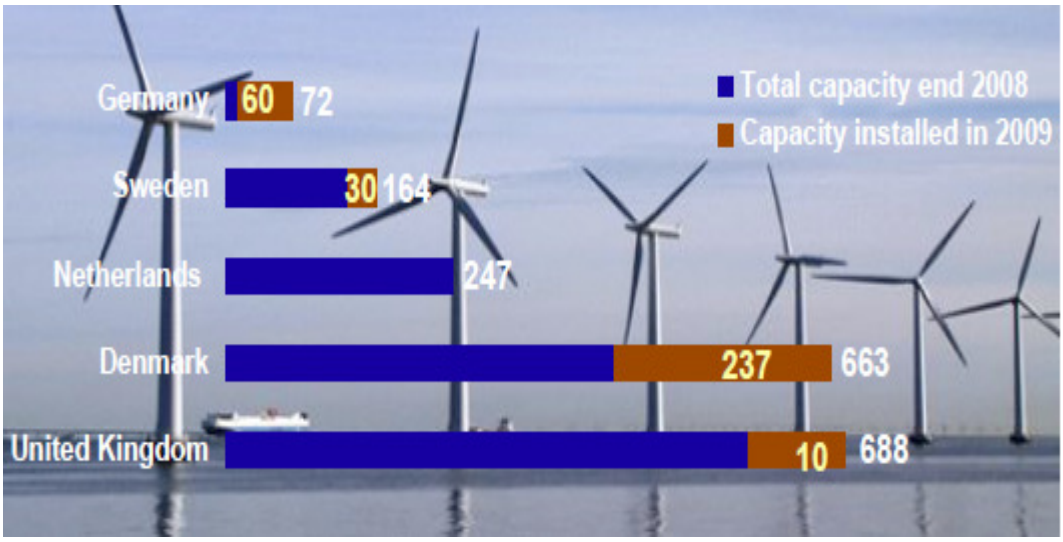

Figure 1.4. Top 5 countries in offshore wind (MW) [21]

1.4.1.1.Wind Energy in Germany. According to the report "Wind Energy Use in Germany – Status 31.12.2009" that was published in DEWI magazine, February 2010, end of the year 2009, a total of 21.164 wind turbines with a rated power of 25.777 MW were installed in Germany (Table 1.1). Apart from reporting new installations, wind turbines can also be replaced with new ones (repowering).

Table 1.1. Potential annual energy yield and installed capacity for Germany [20]

Number of Wind Turbine until 31.12.2009	Installed Capacity until 31.12.2009 (MW)	Potantial Annual Energy Yield (GWh)
21164	25777	46758

By the end of 2009, there were 15 OWTs with a total capacity of 72. Compared to the year of 2008, the average installed capacity per wind turbine has increased slightly by 4.7 % in 2009. And, OWTs with rotor diameters of more than 90 m were erected in same year [20].

Figure 1.5 gives an overview of the shares of the individual wind turbine sizes in the new installations of the year 2009. Compared to the previous year, the share of wind turbines with 1.5-2.0 MW went down. Wind turbines with 2.1 MW and over has increased in 2009. This shows that with the development in wind technology, the turbine sizes and the power production increases.

Apart from size and rated capacity of a wind turbine there are other features; rotor speed, type of control etc. characterize different technologies which are often influenced by the size of a wind turbine.

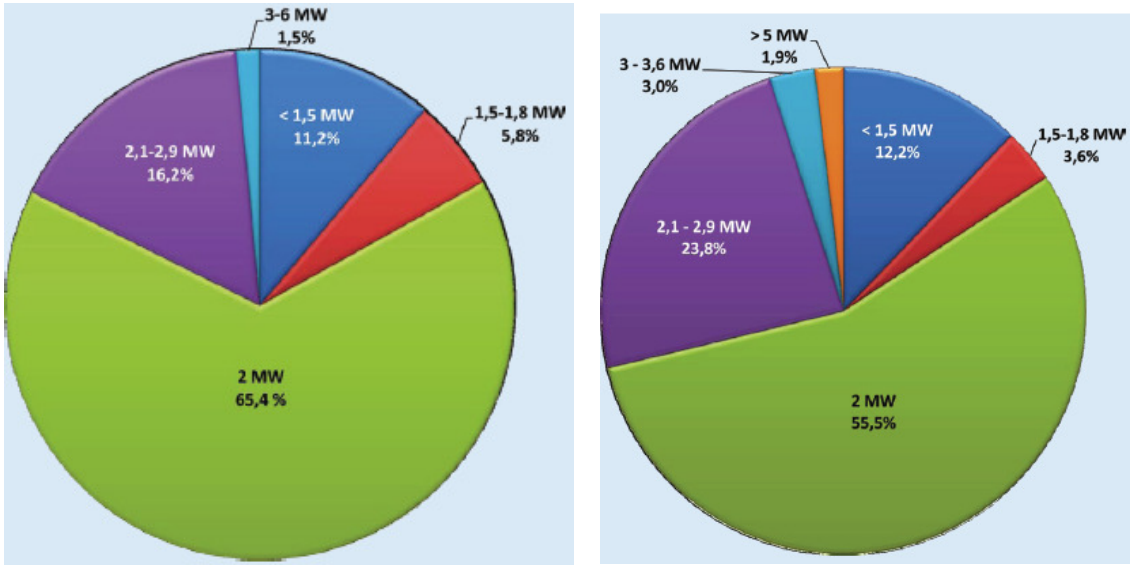

Figure 1.5. Share of individual wind turbine size classes in the newly installed wind turbine in the year 2008 (left) and 2009 (right) [20]

Another interesting point is the hub height of the wind turbines installed in the year 2009. Figure 1.6 shows that approximately 55 % of all wind turbines erected in Germany in 2009 have a hub height of 100 m and less.

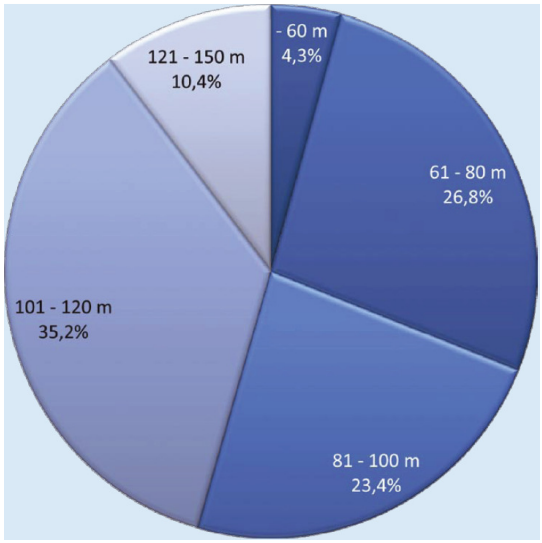

Figure 1.6. Share of the different hub height classes of wind turbines erected in Germany in 2009 [20]

Finally, it is obvious that the size and the installed capacity increased in years. Now, offshore wind energy in Germany has started, and, the first wind turbines have already been erected.

1.4.1.2. Wind Energy in Turkey. Turkey is a fast growing country, both from population and economic aspects. Therefore, energy demand of Turkey is increasing, and, Turkey is one of the fastest growing energy markets of the world in the last years. Today, petroleum is the main source of energy in Turkey, with approximately 50% share in total, and, 90% of which is imported [21].

On February 2001, the privatization of electricity production and distribution has been started. That was also the first step for the foundation of EMRA (Energy Market Regulatory Authority). It was finally established on November 2001, and, the other energy sources have been more important.

Table 1.2. Turkey's renewable energy potential by May 2010 [22]

	Installed Power	Licensed Projects	Targets	Potential
Hydro	14617 MW	27566 MW	30000 MW (2023)	130000000 MWh
Wind	1030 MW	3260 MW	11000 MW (2013) 15000 MW (2015) 20000 MW (2020)	48000 MW
Solar	<1	0	-	380000 MWh
Geotermal	94 MW	164 MW	600 MW (2020)	2000 MW
Biomass-Biogas	87 MW	87 MW	-	-
Renewable / Total Production	20.60%		>25%	

Turkey has one of the biggest wind energy potentials within European countries (more than 20000 MW), but wind farms under operation are still around 1300 MW. However, development is hopeful with more than 2500 MW wind farms under construction. The renewable energy potential and future targets are shown Table 1.2. As it

is seen in the table, the targets show that wind energy is going to be more popular and improving in following years.

1.4.2. Offshore Wind Energy

One of the main reasons for the world-wide increase in offshore wind energy is the higher and more constant wind resource at sea than on land, resulting in higher wind energy production per unit installed. On the other hand, the installation and maintenance cost of the offshore wind farms is higher than that of the onshore wind farms. Design of tower and monopile, or installation and maintenance depend significantly on the marine conditions which set the design limits for the OWT. Therefore, it is very important to have a detailed knowledge of environmental conditions to make offshore wind farms economically feasible. Current knowledge of offshore conditions is very limited compared to conditions on land. Therefore, environmental data from the site may not be accurate enough for the design of the turbine.

1.4.3. Offshore Wind Turbine Types

The OWT development is shown in Figure 1.7 below. The foundation type of a wind turbine mostly depends on the depth of the water.

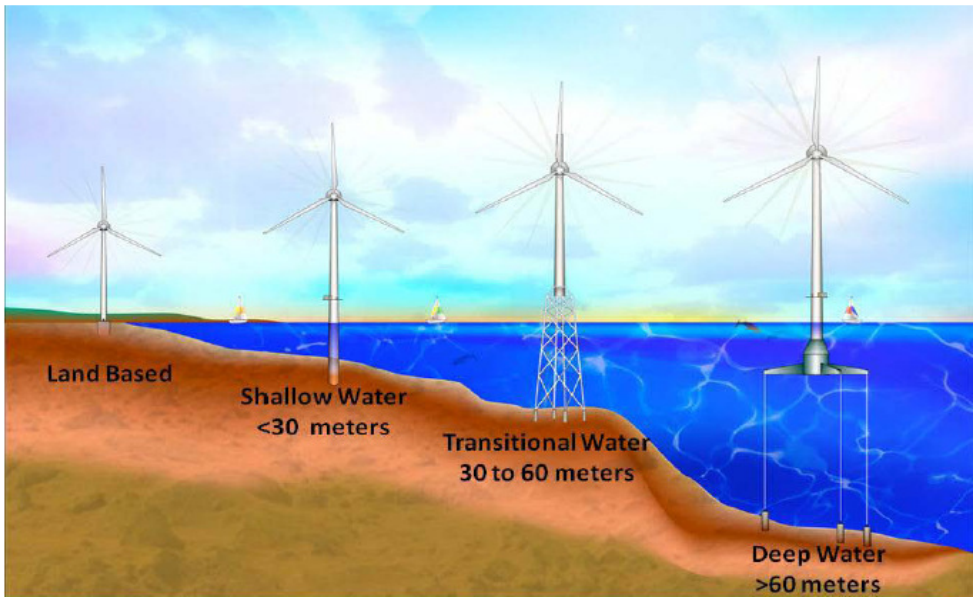

Figure 1.7. The offshore wind energy development [23]

The common foundations that are used for offshore wind projects are shown in the figure below. A monopile consists of steel pile that is driven into the seabed. And, it extends 10 m above water line. At this point there is a transition to the tower which is connected to the monopile either by a bolted flange or with a grouted sleeve connection. The gravity foundation consists of a large concrete or steel base that rests on the seabed. Tripod foundation is generally used in deeper water depths and has not been used on many projects. Jacket type foundations are more common in deeper depths.

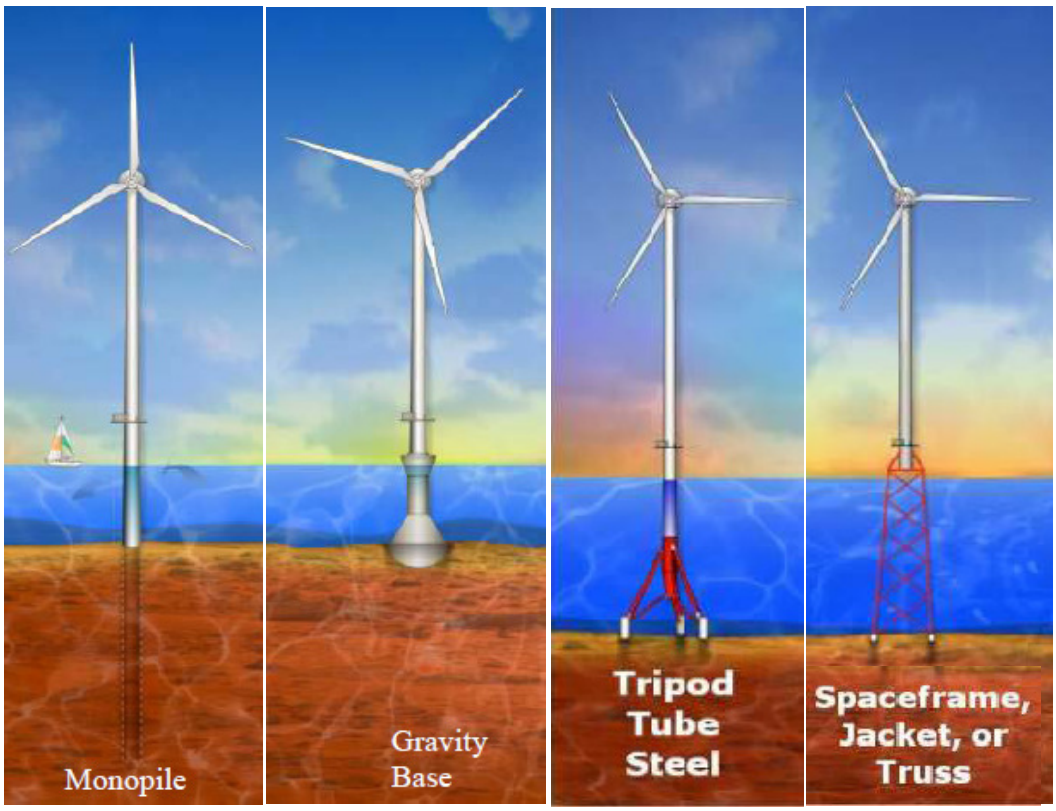

Figure 1.8. Shallow and deep-water foundation technologies [23]

The offshore wind turbines are moving to deeper waters because of the huge energy potential in deep waters. Therefore, the concept of floating OWTs has been started. Nowadays, one of the most commonly used foundation type is monopile. Therefore, monopile type OWT was analyzed in this thesis.

2. DESIGN METHODOLOGY

2.1. General Terminology

An overview of the general terminology for turbine that is used in this thesis is shown in Figure 2.1.

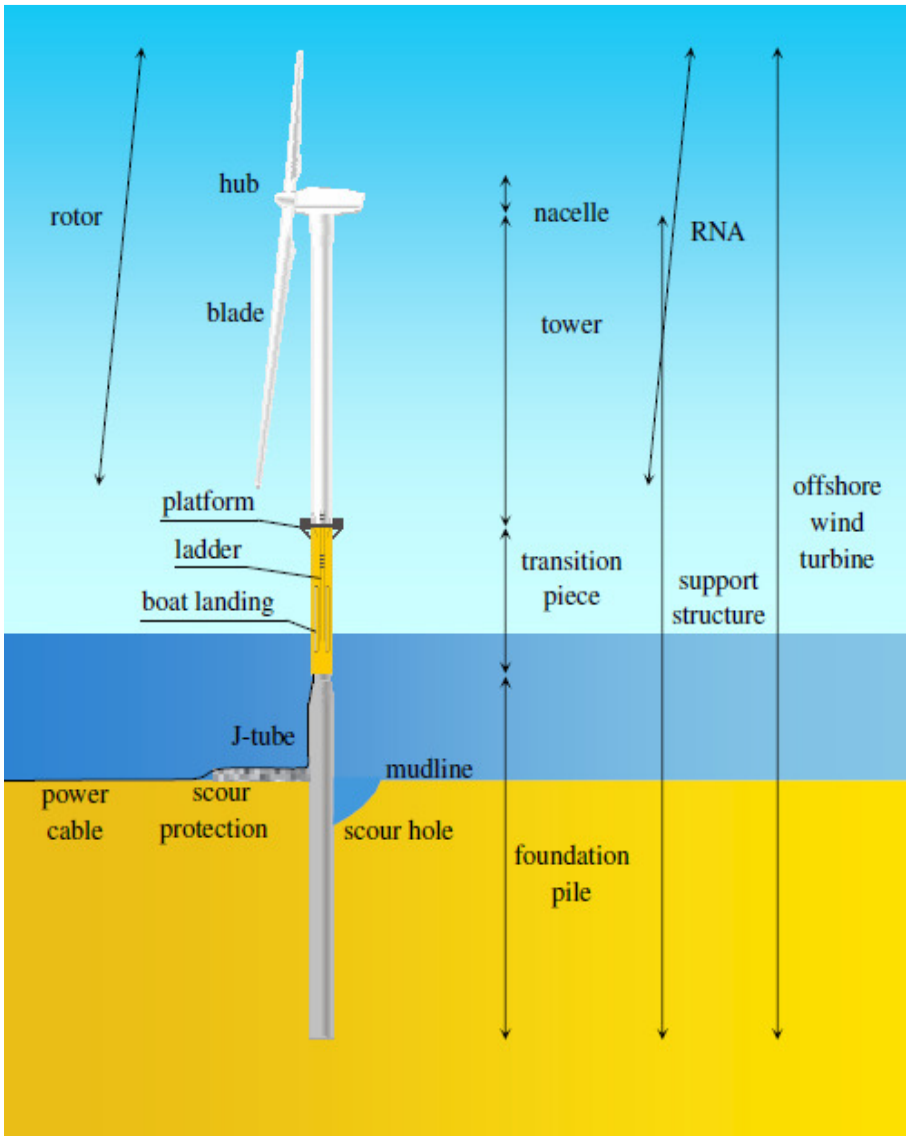

Figure 2.1. Overview of offshore wind turbine terminology [17]

The mechanical part of the turbine called rotor-nacelle assembly and that is shown in Figure 2.2. The energy is produced by the generator in the nacelle as the rotor rotates.

That energy is conveyed by the cables which pass through the tower and monopile and eventually connected to the central grid system.

Figure 2.2. Rotor-Nacelle assembly

(www.noblepower.com/photos/wethersfield-windpark.html)

2.2. Properties of 5 MW Offshore Wind Turbine

NREL's baseline wind turbine aero-elastic model is used in various studies [1]. The same model is analyzed in this thesis. The focus of this study is the support structure and its properties. The gross properties chosen for the NREL 5MW wind turbine, most of which are identical to the REpower 5M, are provided in the Table 2.1.

2.2.1. Blade Structural Properties

The distributed blade structural properties of the NREL 5MW baseline model are based on the structural properties of the 62.6m long LM Glassfiber blade used in the DOWEC project (Dutch Offshore Wind Energy Converter Project). Since the blades in the

DOWEC study are 1.1m longer than the REpower 5M blades, 61.5m blade span is chosen. Table 2.2 summarizes the blade structural properties.

Table 2.1. Gross properties for the NREL 5MW baseline wind turbine model [1]

Rating	5 MW
Wind Regime	IEC 61400-3 (Offshore) Class 1B / Class 6 winds
Rotor Orientation, Configuration	Upwind, 3 Blades
Rotor, Hub Diameter	126 m, 3 m
Hub Height	90 m
Cut-In, Rated, Cut-Out Wind Speed	3 m/s, 11.4 m/s, 25 m/s
Cut-In, Rated Rotor Speed	6.9 rpm, 12.1 rpm
Rated Tip Speed	80 m/s
Overhang, Shaft Tilt, Precone	5 m, 5º, 2.5º
Rotor Mass	110,000 kg
Nacelle Mass	240,000 kg
Tower Mass	347,460 kg

Table 2.2. Blade structural properties [1]

Length (w.r.t. Root Along Preconed Axis)	61.5 m
Mass Scaling Factor	0.04536
Overall (Integrated) Mass	17,740 kg
Second Mass Moment of Inertia (w.r.t. Root)	11,776,047 kg•m^2
First Mass Moment of Inertia (w.r.t. Root)	363,231 kg•m
CM Location (w.r.t. Root along Preconed Axis)	20.475 m
Structural-Damping Ratio (All Modes)	0.0048

2.2.2. Nacelle and Hub Properties

The NREL 5MW baseline model uses the same vertical distance (2.4 m) from the tower-top to the hub height used by the DOWEC study. The nacelle and hub properties are summarized in the Table 2.3 below.

Table 2.3. Nacelle and hub properties [1]

Elevation of Yaw Bearing above Ground	87.6 m
Vertical Distance along Yaw Axis from Yaw Bearing to Shaft	1.96 m
Distance along Shaft from Hub Center to Yaw Axis	5.02 m
Distance along Shaft from Hub Center to Main Bearing	1.912 m
Hub Mass	56,780 kg
Hub Inertia about Low-Speed Shaft	115,926 kg•m^2
Nacelle Mass	240,000 kg
Nacelle Inertia about Yaw Axis	2,607,890 kg•m^2
Nacelle CM Location Downwind of Yaw Axis	1.9 m
Nacelle CM Location above Yaw Bearing	1.75 m
Equivalent Nacelle-Yaw-Actuator Linear-Spring Constant	9,028,320 kN•m/rad
Equivalent Nacelle-Yaw-Actuator Linear-Damping Constant	19,160 kN•m/(rad/s)

Table 2.4. Tower and monopile properties [1]

Tower-Top Height Above MSL	87.6 m
Tower-Base Height Above MSL	10 m
Water Depth (From MSL)	25 m
Tower Base diameter	6 m
Tower Base thickness	0.027 m
Tower Top diameter	3.87 m
Tower Top thickness	0.019 m
Monopile diameter (Constant)	6 m
Monopile thickness (Constant)	0.06 m
Overall (Integrated) Mass	522,617 kg
Young's modulus (E)	210 GPa
Shear modulus (G)	80.8 GPa
Steel density (effective)	8500 kg/m^3
c.g. Location (w.r.t. Mudline Along Tower Centerline)	37.172 m

2.2.3. Support Structure Properties

The support structure properties depend on whether the turbine will be installed in shallow water or deep water. In our case the properties for the shallow water installation is used. The resulting support structure properties are given in the Table 2.4.

The effective density of the steel is considered to be 8500 kg/m^3 rather than the typical value of 7850 kg/m^3 in order to account for paint, bolts, welds, and flanges that are not accounted for in the thickness data [24].

2.2.4. System Dynamics

A wind turbine system has five physical components. These are rotor, generator, transmission, control system and support structure. All of these parts have some effect on the dynamic behavior of the turbine. Therefore, turbine systems should be designed for a complete integrated system.

To understand the modeling dynamics of the structure better, a single degree of freedom (SDOF) mass-spring-damper system is considered (Figure 2.3).

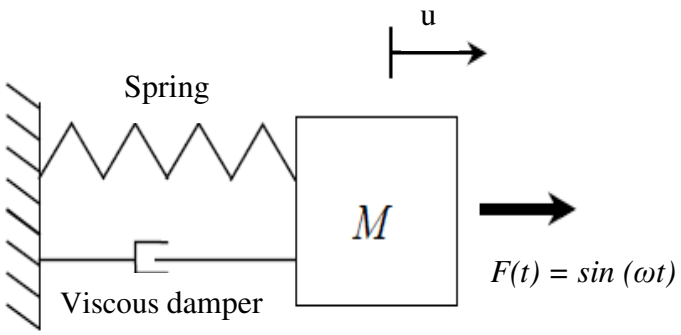

Figure 2.3. SDOF mass-spring-damper system [6]

When an excitation force *(F(t))* is applied to the mass, the magnitude and phase of the response highly depends on the frequency of excitation (ω). Therefore, three response regions can be observed:

- Quasi-static (or stiff) : $f < f_n$ (f_n: natural frequency of the structure)(f : excitation force).
- Resonance : $f = f_n$
- Inertia dominated (or soft) : $f > f_n$

All of the responses are illustrated in Figure 2.4 to Figure 2.6, respectively. The forces are applied with identical magnitudes but with different frequencies. The analytic solutions of the response are presented in Appendix A.

In Figure 2.4, because the displacement of the mass is almost "followed" by the time varying force instantaneously, it is as if the displacement was excited due to a static force. Figure 2.5 shows that the frequency of excitation is close to the system's natural frequency. Therefore, the response is in resonance with the forcing.

Figure 2.6 shows that the frequency of excitation is bigger than the natural frequency, so the mass cannot "follow" the movement. In this case, the inertia of the system dominates the response.

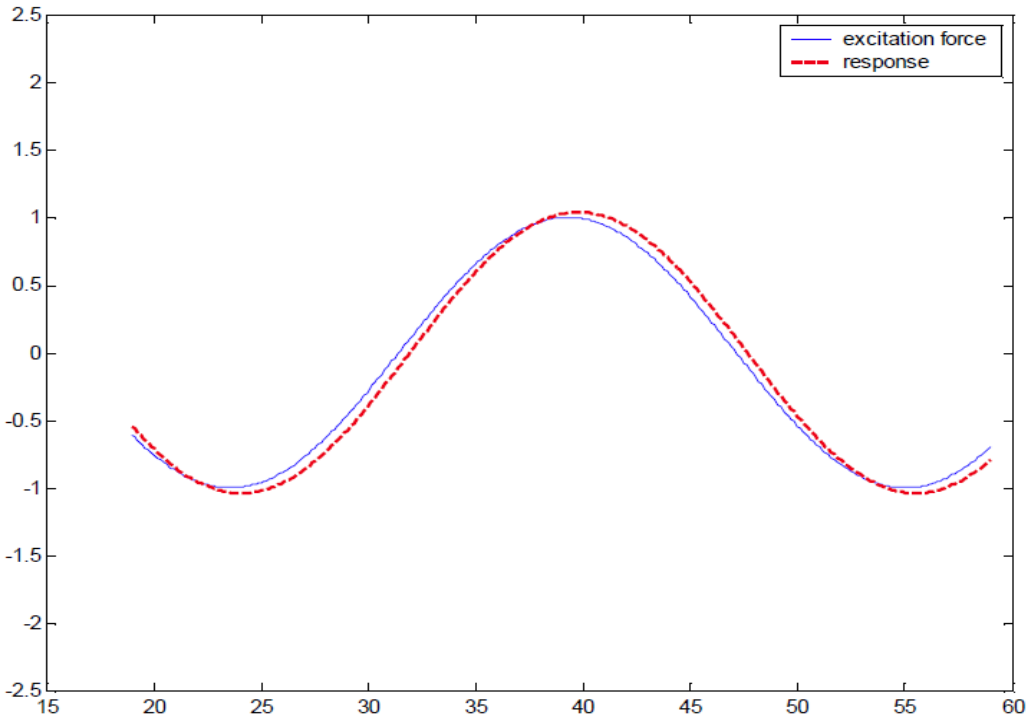

Figure 2.4. Quasi-static response [6]

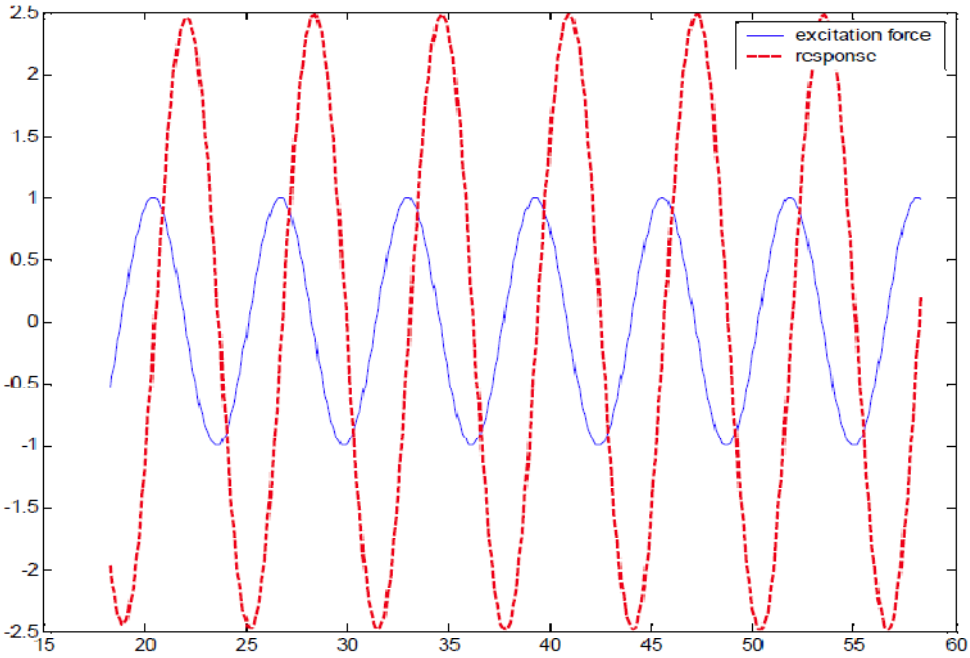

Figure 2.5. Resonant response [6]

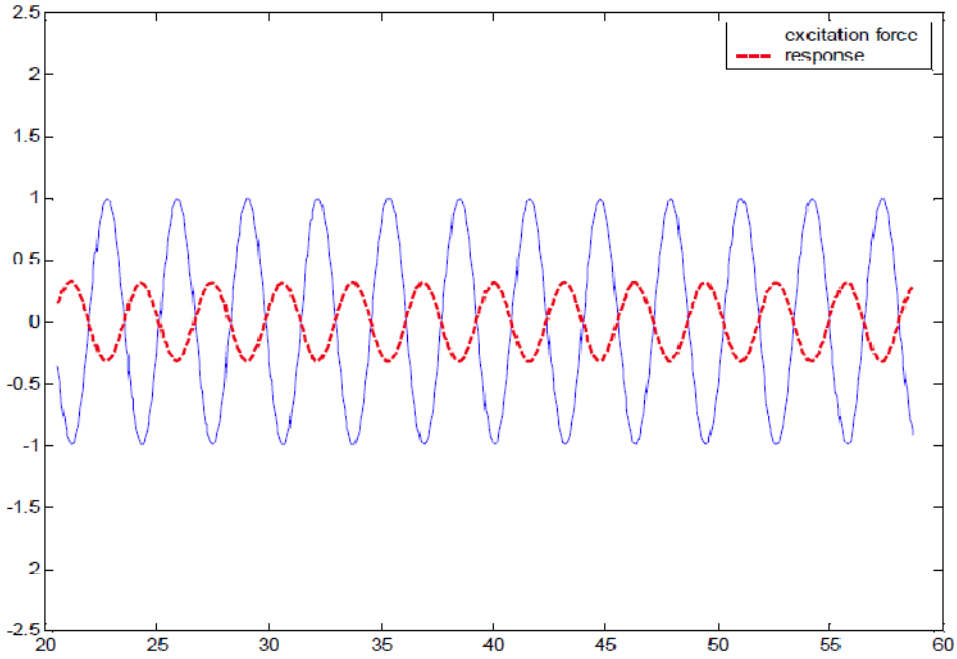

Figure 2.6. Inertia dominated response [6]

The knowledge of the excitation force frequency and the natural frequency is vital for structures where dynamics are expected to be important. In steady state, if a sinusoidal input is applied to a linear system, that system will generate sinusoidal outputs of the same frequency, but differ in magnitude and phase [6]. The magnitude and phase are

summarized in the frequency response function (FRF). Figure 2.7 shows the FRF of the single degree of freedom system.

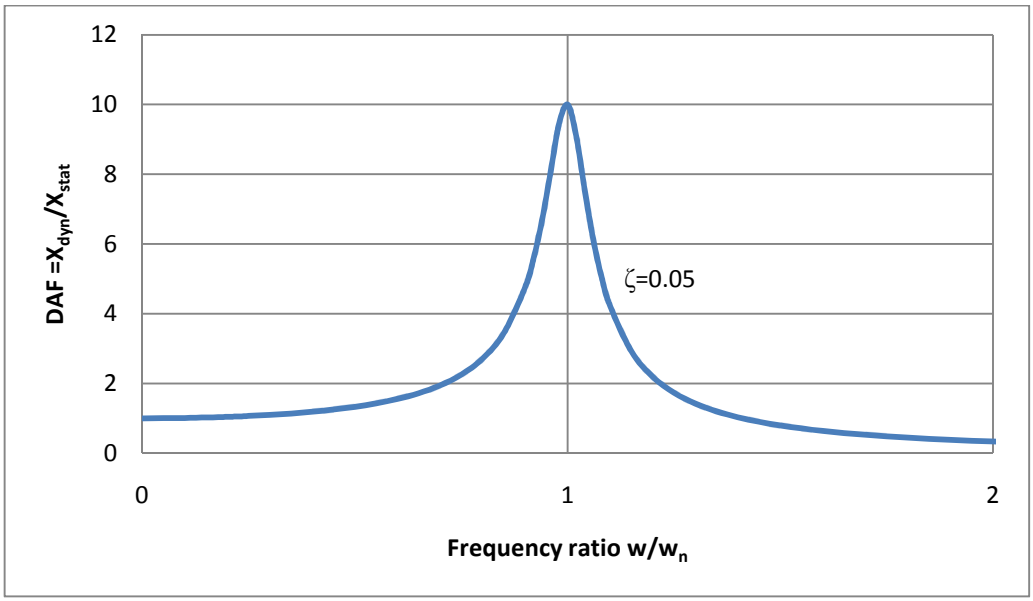

a)

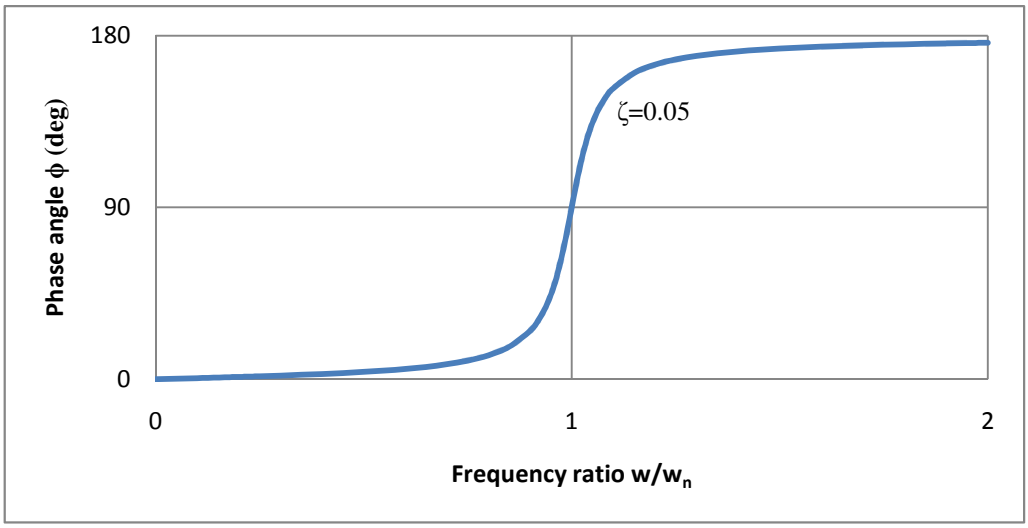

b)

Figure 2.7. Frequency response function (FRF). (a) Magnitude versus frequency, (b) Phase lags versus frequency

The Figure 2.7 (a) was plotted by use of DAF (Dynamic Amplification Factor). DAF (Equation 2.1) is the ratio of dynamic response to the static response. In the preliminary design of OWTs, the DAF is commonly used to account for the effect of dynamic loading [6]. The derivation of the DAF is presented in Appendix A.

$$DAF = \frac{1}{\sqrt{\left(1 - \left(\frac{\omega}{\omega_n}\right)\right)^2 + \left(2 * damping * \frac{\omega}{\omega_n}\right)^2}} \quad (2.1)$$

2.2.5. Cut in and Cut out Speeds

A wind turbine needs a particular minimum wind speed to start operating, typically 3 m/s. This wind speed is called the cut-in speed. The turbine hub continues to rotate more and more from that wind speed until the rated power is reached. The turbine rotation frequency remains constant above rated wind speed 11.4 m/s for the turbine which is considered in this thesis. For very high wind speeds, the turbine shuts down. This happens at the cut-out wind speed, typically 25m/s.

In the design of the OWT, first of all, the excitation frequencies should be examined. The rotor is the most important source of excitation in a wind turbine system. Assuming the turbine has a constant rotational speed. That is called the first excitation (rotor) frequency. Because the masses of blades differ slightly, the center of gravity of the rotor moves with an eccentricity. This frequency is referred as 1P. The second excitation frequency is because of the wind on tower. The wind induces load on the tower, when the blades pass in front of the tower the wind is blocked and the load vanishes at that moment. This happens N_b (the number of rotor blades) times in a full cycle of the hub. This frequency is known as tower shadow, and it is called the blade passing frequency, referred as 3P for a three bladed rotor.

In this thesis, the wind turbine has 6.9 rpm (0.115 Hz) cut in rotor speed and 12.1 rpm (0.202 Hz) rated rotor speed. Therefore 1P and 3P frequencies are in an interval not just a value. These two frequency intervals are shown in Figure 2.8. The horizontal axis represents the frequency in hertz, and the vertical axis has no value.

To avoid resonance, the structure should be designed such that its first natural frequency does not coincide with either 1P or 3P zone. This leaves three possible intervals. These are a very stiff structure with a natural frequency greater than 3P (stiff-stiff), a

structure with a natural frequency between 1P and 3P (soft-stiff), and, a very soft structure with a natural frequency less than 1P (soft-soft) [6].

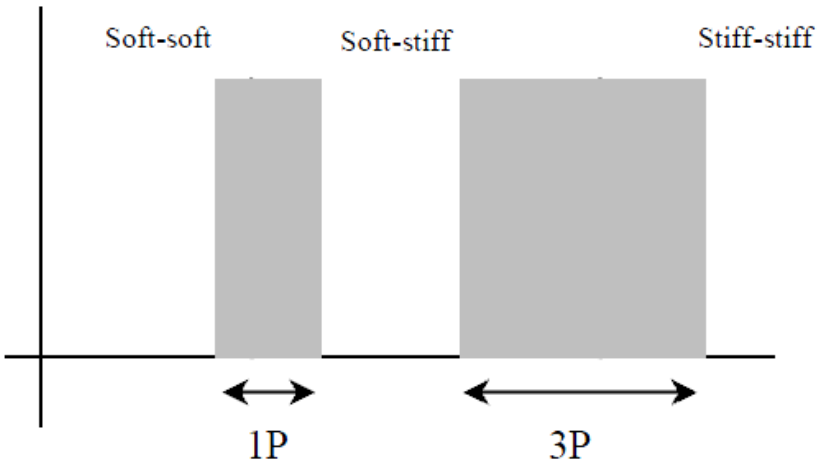

Figure 2.8. Frequency intervals for a turbine system [6]

2.2.6. Campbell Diagram

The main concern of support structure design is to avoid resonance caused by the rotor. If resonance happens, the motion of structure amplifies. It causes significant damages to the structural parts like rotor, blades, and leads to premature fatigue distress in the structure [33].

Figure 2.9 shows the Campbell diagram for the 5 MW turbines analyzed in this thesis. The red and green plot defines the 1P and 3P frequencies for a range of rotor speeds up to the rated rotor speed of the turbine (i.e., the range between the two vertical lines). Resonance conditions occur when structural frequency is in the grey area. The structural frequency should be within three white areas (i.e., from top to bottom, called stiff-stiff, soft-stiff, and soft-soft structural areas).

The structural frequency of the turbine system should be between the frequencies of 0.20 and 0.34 Hz to avoid the resonance condition. The lower end of this frequency range is the most important for the monopile design because lower frequency means more economical system.

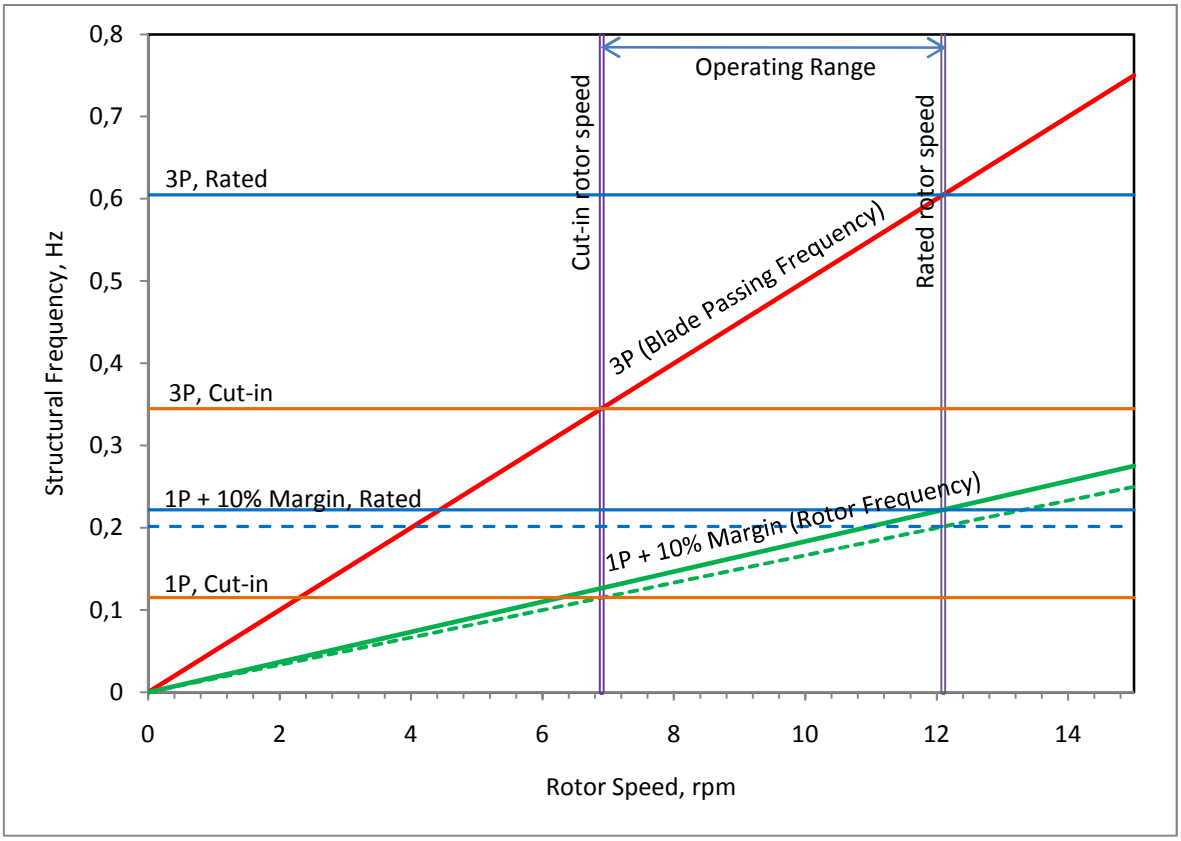

Figure 2.9. Campbell diagram

The structural frequency for resonance avoidance is recommended 5% or more than the rotor frequency provided in Germanischer Llyod (GL). In addition to that, the mass variance in rotor and nacelle causes a variance in the frequency. Therefore, the target structural frequency was selected as 0.22 Hz (i.e. 4.5s period) which is the 10% greater than the rotor frequency of 0.2 Hz (Figure 2.9).

2.3. Loads

The meteorological, the oceanographic and geological conditions at a site have to be considered to calculate the loading on OWTs. The conditions such as water depth, soil conditions, and possible wave heights change significantly for OWTs. The main environmental conditions to be considered for the design of OWTs to prevent the structural damages and operational disturbances of other failures are wind and wave loads (including current and surge). Moreover, in some cases the breaking waves, tides, ice effect, scour effect, ship impact, or earthquake have to be taken into account for design.

Defining wind load is hard because of the stochastic nature of it. And, wind and wave loads never act alone. We have to consider their combined effect while modeling these stochastic loads. Therefore, the FAST (Fatigue, Aerodynamics, Structures, and Turbulence) code was used in this thesis.

The FAST Code is a comprehensive aeroelastic simulator and capable of predicting the extreme loads of wind turbines [25]. The code can model the dynamic response of conventional horizontal axis wind turbines, and, it can also model both the operating (rotating blades) and the parked (stationary blades) conditions [25]. FAST Code defines the time histories of wind and wave forces on structure. It specifically represents the change in blade wind forces caused by motions in the system generated by wave loading on a monopile that is modeled with the tower and turbine.

2.3.1. Wind Loads

The wind speed is the most critical data to calculate both the load contribution to the system and the power potential at the site. The wind is never steady at any site. Because of the stochastic nature of the wind, the wind speed data are collected at a given site. This stochastic data can be defined as appropriate distribution functions. However, for design phase of a turbine, the time history of wind speed should be produced with some software or codes. TurbSim (Turbulence Simulator) Code was used to produce the wind data for this study.

2.3.1.1. TurbSim Code. TurbSim ("Turbulence Simulator" is developed in NREL) is a stochastic, full-field, turbulent-wind simulator. It numerically simulates time series of three-dimensional wind speed vectors at points in a vertical rectangular grid (Figure 2.10).

TurbSim simulation method is a transformation from the frequency domain to time domain producing wind output compatible with other codes. For that, spectra of velocity model and spatial coherence model are defined in the frequency domain, and an inverse Fourier transform produces time series [26].

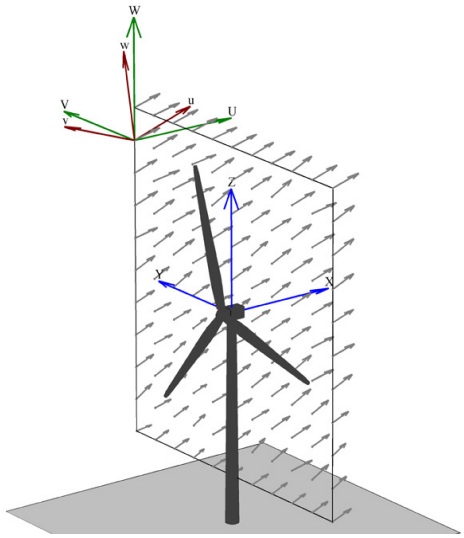

Figure 2.10. Example for TurbSim wind field [26]

The IEC Kaimal Spectral Model was used in this study. IEC 61400-1 3rd ed. defines this model. The velocity spectra of the model were assumed to be invariant across the grid. However, in practice there is small amount of variation in u-component of wind velocity. The spatial coherence was defined in accordance to IEC spectral model, as well. Moreover, the type of the turbulence was Class I Extreme Turbulence Model with medium turbulence intensity, using the 10-minute average wind speed with a recurrence period of 1 year, 50years, or 100 years [26].

Turbsim uses random phase from a distribution model to compute the full field background turbulence. Due to the spatial coherence, a Gaussian distribution of turbulence intensity in the longitudinal wind component is produced by different random seeds [26]. Then, it generates a coherent structure. This coherent structure has a rectangular shape shown in Figure 2.10, and, it has a dimension (bigger than rotor disk) and a location (tower height). For the size, the number of grids and distance between them need to be entered as input.

TurbSim uses empirical values to calculate when and how coherent events (i.e. pieces (sections in time) of a billow (the rise or roll in waves) simulated by using either direct numerical simulation (DNS) or large-eddy simulation (LES)) should be added to the background turbulence [26]. Then, the background wind file was produced by combining the background turbulence with the coherent structure.

2.3.1.2. Distribution of Wind Speed. The variation in wind speed is best described by Weibull distribution function. The Weibull distribution closely mirrors the actual distribution of hourly wind speeds at many locations. On the other hand, for describing turbulent velocity fluctuations about the mean wind speed and dynamic structural response, Gaussian (normal) distribution function is better to use [28]. TurbSim uses Gaussian (normal) distribution function to produce wind data. The graph of Gaussian (normal) distribution function is bell shaped (Figure 2.11) and described with the equation below.

$$\varphi(x;\mu,\sigma) = \frac{1}{\sqrt{2\pi\sigma^2}} e^{-\left(\frac{(x-\mu)^2}{2\sigma^2}\right)} \qquad (2.2)$$

Where;

μ = the mean (location of the peak)

σ^2 = the standard deviation (the measure of the width of the distribution)

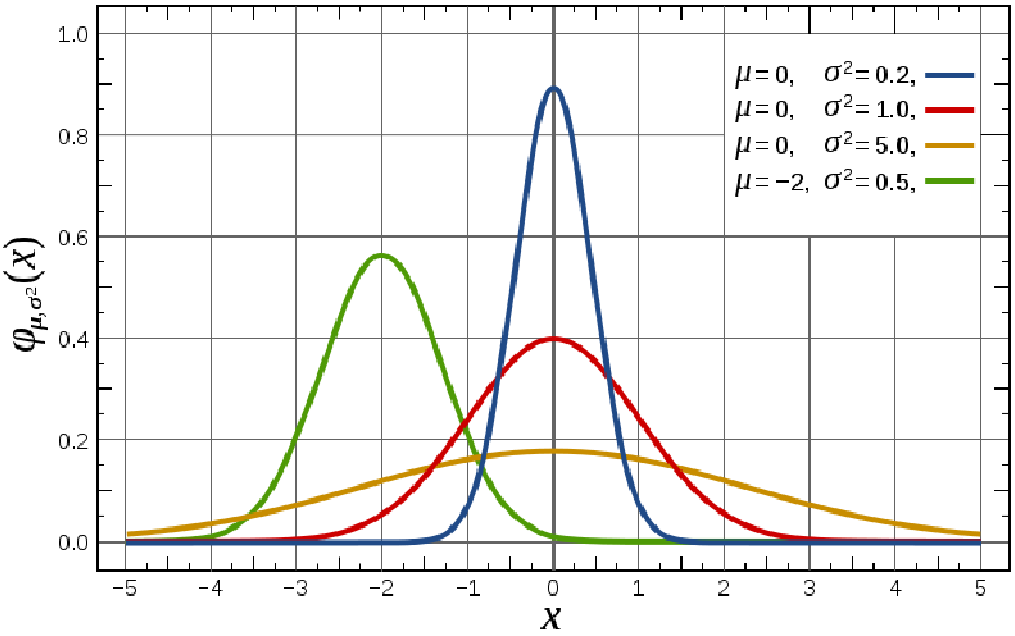

Figure 2.11. Probability density function

(http://www.answers.com/topic/cauchy-distribution)

2.3.1.3. Wind on Blades. As it is mentioned before, stochastic turbulence data (produced by TurbSim code with extreme turbulence model for wind-turbine class 1, according to IEC 61400-1 Edition 3 standard) were applied for a given mean wind velocity at hub-height by using FAST Code.

When wind speed is higher than 3 m/s the blades open up themselves against the wind to operate. When the wind speed reaches 11.4 m/s, the rotational speed of rotor stays constant. This speed is called rated speed. During extreme wind conditions (for mean hub-height wind speeds above 25 m/s) the turbine is positioned as parked (i.e. blades turn off themselves). In other words, the blade rotates along the cord length to the 90^{o} position against the wind so that the exposure to the wind load reduced. The 25 m/s of wind speed is called the cut-out wind speed specified in 5 MW reference wind turbine.

The FAST code takes the wind speed data form TurbSim code, and, applies it on blades by taking the blade condition into account. When the blades coincide with the fluid flow (wind), two main forces (lift and drag) occur. These forces generate the rotation of the rotor and the force to the structural blades and tower.

2.3.1.4. Blade Element Momentum Theory and Element Forces. The blade element momentum (BEM) theory is used to calculate the loads on a turbine. The figure below shows the rotor that slows the wind velocity down (i.e. $V_o > V_{wake}$). When the wind flow passes through the rotor, the axial resulting load on the rotor, F_{ax}, is produced.

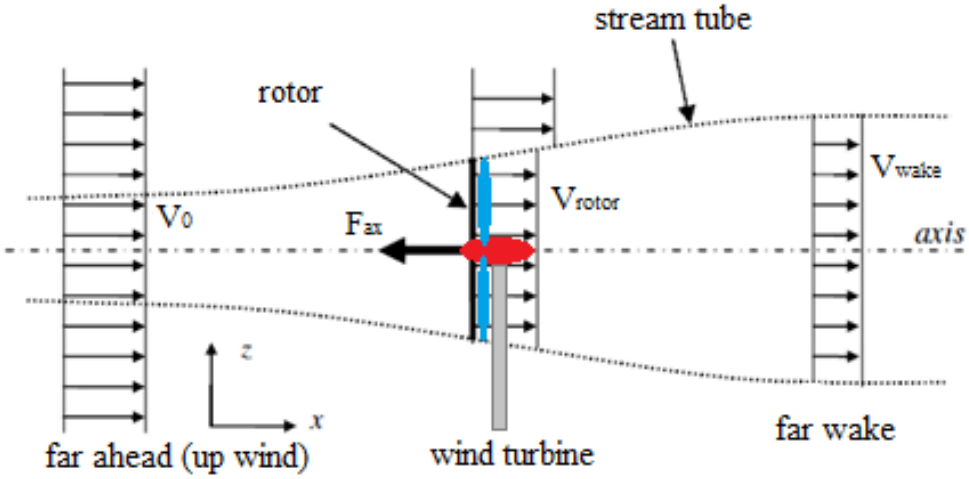

Figure 2.12. Turbine rotor with stream tube [17]

The formula below is used to calculate the load on structure by using Bernoulli [17].

$$F_{ax} = \frac{1}{2} A_{rotor} \rho_{air} V_o^2 * 4a(1-a) \qquad (2.3)$$

Where;

a = induction factor, $a = \frac{V_0 - V_{rotor}}{V_0}$

V_0 = wind velocity, m/s,

V_{rotor}= wind velocity at the rotor, m/s,

ρ_{air} = air density, kg/m^3, (1.225 kg / m^3)

A_{rotor} = area of the rotor disk, m^2.

However, a blade consists of blade elements with their own aerodynamic features. The desired aerodynamic performance of blades is created by a series of airfoil profiles that give shape to the blade. The wind on a blade element can be calculated with an equation below [17].

$$F_{wind} = \frac{1}{2} C_s \rho_{air} A V_{rotor}^2 \tag{2.4}$$

Where;

F_{wind} = wind load, N,

C_s = aerodynamic coefficient (shape), (C_s = 0.7)

A = exposed area, m.

To find the aerodynamic loads on a blade (i.e. lift and drag forces), the relative wind velocity should be introduced. The relative velocity (Equation 2.5) is the combination of wind speed and the rotational speed of the rotor.

$$V_{rel} = \sqrt{V_{rotor}^2 + V_{rot}^2} \tag{2.5}$$

$$V_{rotor} = V_0(1 - a) \;\; and \; V_{rot} = \Omega . r$$

Where;

V_{rel} = relative wind speed at a blade section, m/s,

V_{rotor} = wind velocity at airfoil, m/s,

V_{rot} = linear rotation speed at a blade section, m/s,

Ω = angular rotation speed, rad/s,

r = distance of blade element to axis of rotation, m.

The airfoil profile that is exposed to the relative wind velocity is shown in Figure 2.13 below.

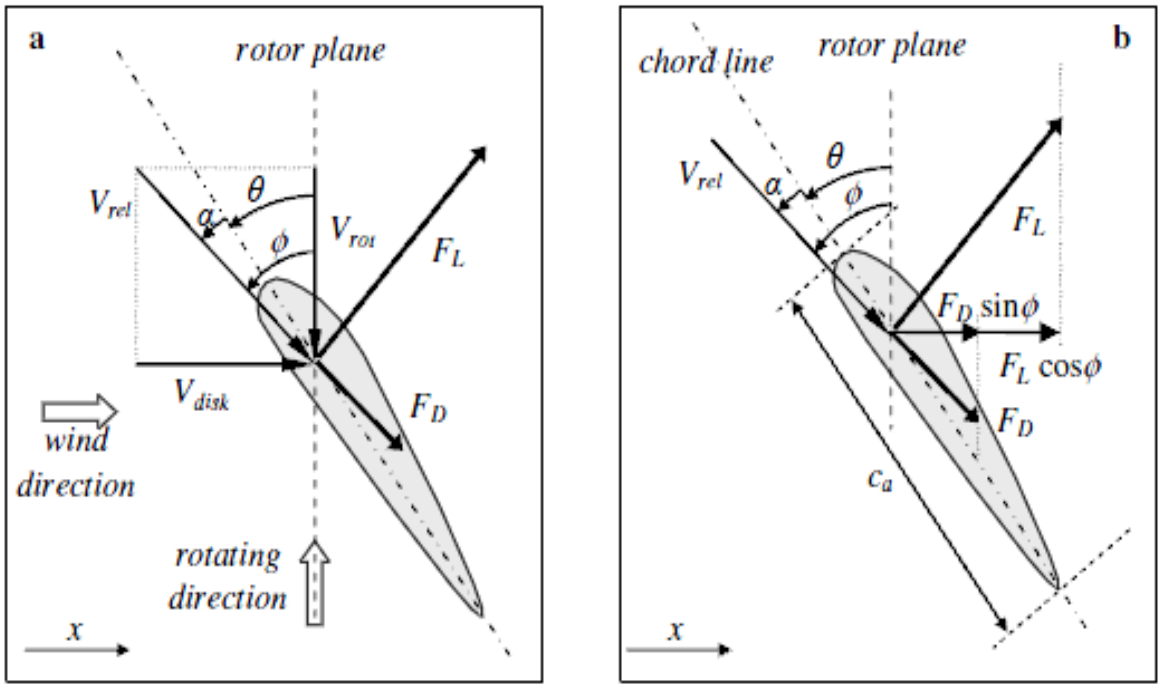

Figure 2.13. a) Lift and drag load on a blade element b) resulting loads in the x direction [17]

According to the figure, F_L and F_D shows the lift and drag forces respectively. And, these forces can be introduced in the Equation 2.6.

$$F_L = \frac{1}{2} C_L(\alpha_a) \rho_{air} V_{rel}^2 c_a \Delta r \qquad F_D = \frac{1}{2} C_D(\alpha_a) \rho_{air} V_{rel}^2 c_a \Delta r \qquad (2.6)$$

Where;

F_L =aerodynamic lift, N,

F_D =aerodynamic drag, N

$C_L(\alpha)$ =aerodynamic lift coefficient,

$C_D(\alpha)$ =aerodynamic drag coefficient,

ρ_{air} = mass density of air, kg/m^3,

c_a = airfoil chord length, m,

Δr = radial length of blade element, m,

α_a = angle of attack, deg,

θ = pitch angle, deg,

φ = angle of inflow, deg.

Lift and drag forces depends on the coefficient C_L and C_D. They also depend on the cross section of blade, and the wind strikes to the blade angle, α. They cannot be calculated by hand, they are measured experimentally in wind tunnels [29].

The total axial load in x direction for 3 blades is,

$$F_{ax} = 3 * \sum_{r\,root}^{r\,tip} F_{x,r} \tag{2.7}$$

Where;

F_x = axial load on blade, N, ($F_x = F_L cos\varphi + F_D sin\varphi$).

2.3.1.5. Wind on Tower. The FAST Code does not take the wind load on tower into the account. This force was calculated independently according to the Equation 2.8 mentioned in API RP-2A. This static force should be added to the aerodynamic loads obtained by FAST.

$$F = \frac{\rho_{air}}{2} V_0^2 C_s A \tag{2.8}$$

Where;

V_0 = Wind velocity, m/s,

C_s = Aerodynamic shape coefficient (0.5 for cylindrical sections),

ρ_{air} = mass density of air, kg/m^3,

A = the projected area of the tower facing the coming wind.

Moreover, wind is influenced by the ground surface at altitudes up to 100 meters. In general, the more pronounced the roughness of the earth surface is; the more the wind will be slowed down. Water surface is smoother than earth surface, and will have less influence on the wind. Wind speed varies with height above ground. This is called wind shear. Equation 2.9 shows the description of the wind profile.

$$V_2 = V_1 \left(\frac{h_2}{h_1}\right)^{\alpha} \tag{2.9}$$

Where;

V_1 = Wind speed at height h_1, m/s,

V_2 = Wind speed at height h_2, m/s,

α = the coefficient for roughness of ground (It is often stated that α = 1/7 = 0.14 for open sites).

2.3.2. Wave Load

One of the most important environmental loading is wave loading for design of an offshore structure. The wind on sea surface generates the motion of the water (the waves) that causes the forces on the structure. The time-history of wave forces along the depth of the monopile was required for coupled dynamic analyses. These forces can be determined by idealization of the wave surface profile, and the wave kinematics.

Generally, in ocean engineering, Airy wave theory (by George Biddell Airy) is often applied to model the random sea states. The theory gives a linear description of the wave kinematics and dynamic. This linear theory is usually used to get quick estimate of wave characteristics and their effect without amplitude dispersion, and, it is limited to low-amplitude waves [27].

However, most of the real waves are not linear and they have complex periodic features. For nonlinear description of the wave kinematics and dynamic, 5^{th} order stokes waves are used for FAST Code analyses in this study. Stokes' wave theory (by George Gabriel Stokes) can describe the weakly nonlinear and dispersive waves [27]. The detailed

information about the wave theories is presented in Appendix B. Moreover, to calculate the drag and inertia forces on the monopile, the relative velocity form of the Morrison equation (Equation 2.10) was used in FAST Code calculations.

$$F = \underbrace{\frac{1}{2}C_D\rho A(u-\dot{q})|u-\dot{q}|}_{\text{Drag Force}} + \underbrace{C_A\rho V(\frac{\delta u}{\delta t}-\ddot{q})}_{\text{Inertia Force}} + \underbrace{\rho V\frac{\delta u}{\delta t}}_{\text{Froude-Krylov force}} \quad (2.10)$$

Where;

A = the projected area, m,

V = the displaced volume of the cylinder per unit length, m^3,

q = the displacement degree of freedom of tower/monopile node, m,

u = the water particle velocity, m/s,

C_A = the normalized hydrodynamic-added-mass coefficient;

The inertia coefficient $C_M = 1+C_A$

C_D = the normalized viscous drag coefficient

$\dot{q}$ = the particle velocity, m/s,

$\ddot{q}$ = the particle acceleration, m/s^2.

However, in SAP 2000 calculations, the structural cylinder is assumed to be stationary. Therefore the Morrison equation becomes;

$$F = \frac{1}{2}C_D\rho Au|u| + C_M\rho V\frac{\delta u}{\delta t} \quad (2.11)$$

The drag and inertia coefficients that are applicable to evaluate monopile with FAST analyses are as follows:

$$C_D = 1.03$$

$$C_M = 1.30$$

In fluid dynamic, the Morison equation is a semi-empirical equation for the inline force on a body in oscillatory flow. Traditionally, the Morison equation is used to determine the wave loads in the design of offshore structures.

2.3.2.1. Extreme Waves, Non-linear Wave Theories. The maximum wave for the site must be known to determine the extreme wave loads on a structure. When long-term measurements of wave heights are available, a distribution curve (i.e. Rayleigh Distribution) can be fitted through the maximum values and extrapolated to find the 50 and 100 year return period maximum wave height. It is also possible that the maximum wave height is limited by to the breaking wave limit due to reduced water depth at the site [17].

To calculate the wave forces on the structure, it is needed to be described that the non-linear features of these extreme waves. Three wave parameters determine which wave theory to apply in the design. These are the wave height (*H*), the wave period (*T*) and the water depth (*d*). There parameters are used to define three non-dimensional parameters that determine ranges of validity of different wave theories [44].

Wave steepness parameter:

$$S = 2\pi \frac{H}{gT^2} = \frac{H}{L_0} \tag{2.12}$$

Shallow water parameter:

$$\mu = 2\pi \frac{d}{gT^2} = \frac{d}{L_0} \tag{2.13}$$

Ursell parameter:

$$U_r = \frac{H}{{k_0}^2 d^3} = \frac{1}{4\pi^2}\frac{S}{\mu^3} \tag{2.14}$$

Where, L_0 and k_0 are the linear wave length and wave number corresponding to wave period *T*.

The range of application of the different wave theories are given in the Figure 2.14. The x component is corresponded with the shallow water parameter, and y component is corresponded with wave steepness parameter. According to the wave data for Massachusetts site in the Table 2.5, three cases were considered for the support structure design. These cases were presented in the Table 2.5 and plotted on the Figure 2.14.

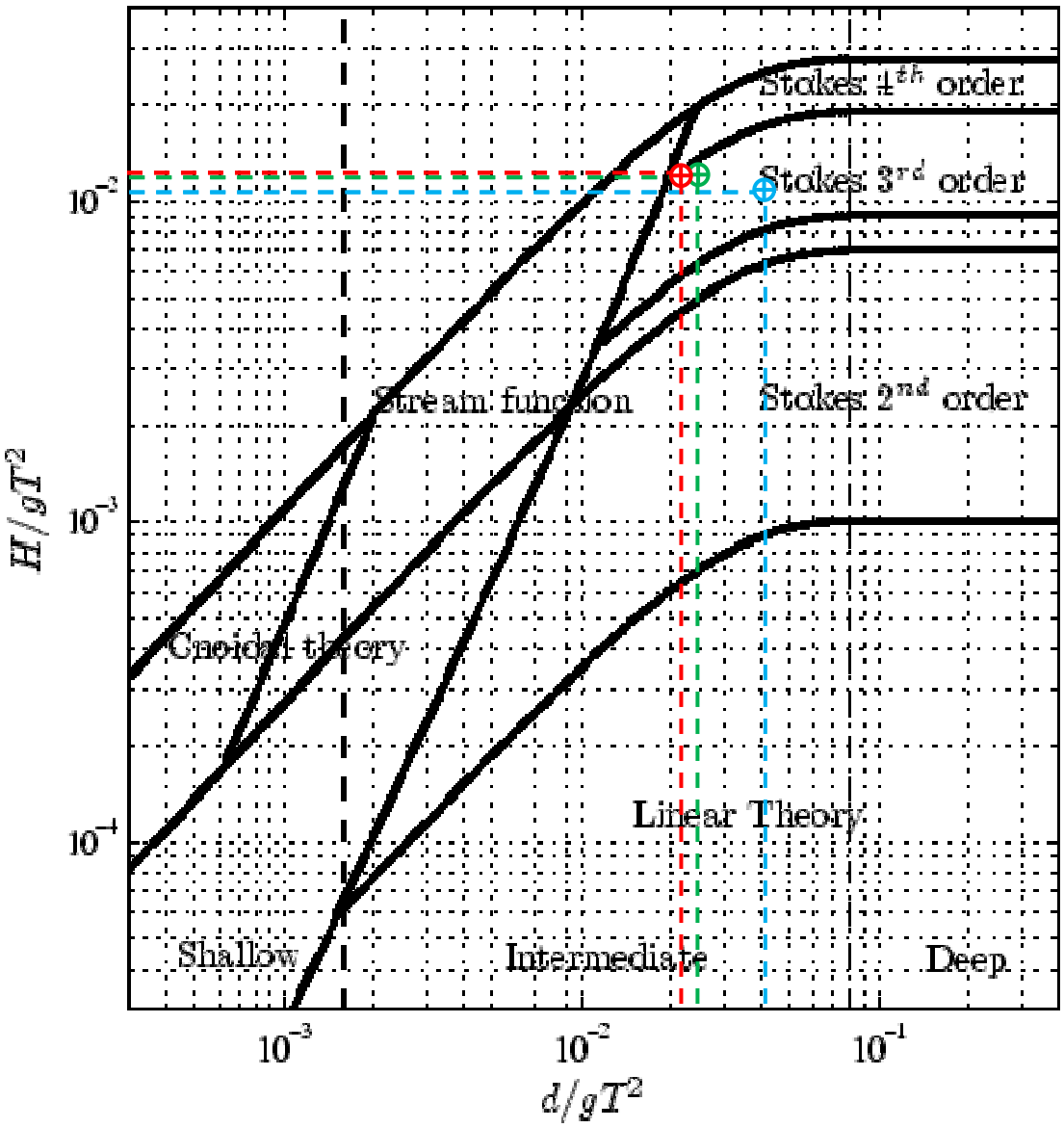

Figure 2.14. Regions of validity for various wave theories (Le Mehaute (1976)) [45].

Table 2.5. Maximum values of wave data for Massachusetts site.

Case	H_{max} (m)	T_{max} (sec)	$H/(gT^2)$	$d/(gT^2)$
1 – Operating Case	7.17	8.37	0.0104	0.0364
2 – Extreme Case (50 years)	14.1	10.9	0.0121	0.0214
3 – Extreme Case (100 years)	15.7	11.4	0.0123	0.0196

All the cases were fitted to the Stokes' wave theory. Therefore, 5th order Stokes' wave theory will be used for the determination of wave surface profile and the wave kinematics.

2.3.2.2.Wave Spectrum. The surface of the sea is reduced to a single point. The surface of elevation is measured in time as it runs through this point. This time varying signal can be transformed to an energy density spectrum (i.e. wave spectrum). Some characteristic parameters can be defined from both the spectrum and the time series. The relations between time domain and spectral parameters are given below.

The spectral moment M_n of general order n is defined as

$$M_n = \int_0^\infty \omega^n S(\omega) d\omega \tag{2.15}$$

Where, n = -1, 0, 1, 2,..

Significant wave height: $H_s = 4\sqrt{M_0}$ (2.16)

Mean zero crossing period: $T_z = \sqrt{\frac{M_0}{M_2}}$ (2.17)

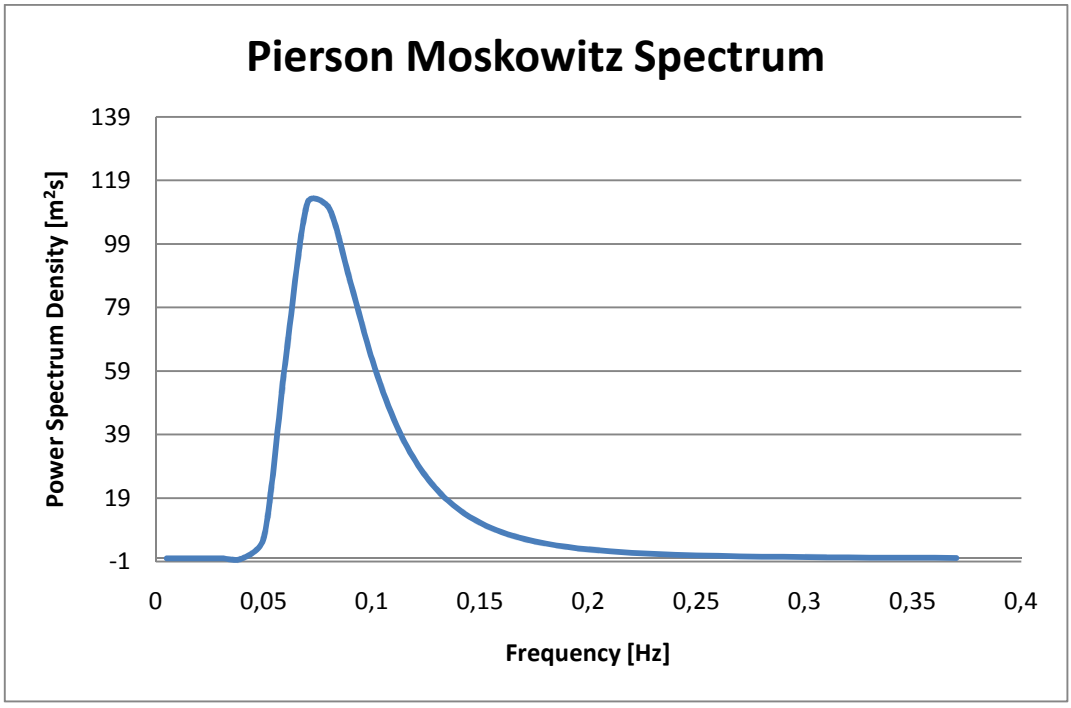

Figure 2.15. Pierson Moskowitz Spectrum for H_s = 3.99 m and T_z = 6.97sec.

Frequently used spectral shape is the Pierson-Moskowitz (PM) (1964) wave spectrum. Both spectra are describing wind sea conditions. They are reasonable for the

most severe sea states. The spectrum describes the sea surface elevation due to the wind speed for a fully developed sea at infinite fetch. The spectrum description was adjusted to have H_s and T_z as input,

$$S_{PM}(f) = \frac{H_s^2}{4\pi T_z^4 f^5} \exp\left(-\frac{1}{\pi}(fT_z)^{-4}\right) \tag{2.18}$$

Where,

f = wave frequency (1/T), Hz.

Figure 2.15 shows a plot of the PM spectrum for the parameters H_s and T_z that are taken from the first case of the Massachusetts site (i.e. H_s = 3.99 m and T_z = 6.97 sec).

2.3.2.3. The Joint Probability Density Function (JPDF). The JPDF applicable to wave height and period was first developed and revised by Longuet-Higgins (1983) [47]. Longuet-Higgins formulates the distribution of wave amplitude a and wave period T for a narrow banded wave spectrum as,

$$f(r,n) = \frac{2}{\sqrt{\pi}\nu}\left(1+\frac{\nu^2}{4}\right)\left(\frac{r}{n}\right)^2 exp\left\{-r^2\left[1+\left(1-\frac{1}{n}\right)^2\frac{1}{\nu^2}\right]\right\} \tag{2.19}$$

Where,

r = dimensionless wave amplitude, $\frac{a}{\sqrt{2M_0}}$,

n = dimensionless wave period, $\frac{T}{T_{mean}}$,

a = H / 2, m,

T_{mean} = $2\pi\frac{M_0}{M_1}$, sec,

ν = $\sqrt{\frac{M_0 M_2}{M_1^2} - 1}$

Figure 2.16 shows the contour curves of the joint probability density function given in Equation 2.19 for ν = 0.4. Moreover, Figure 2.17 shows the conditional probability density of wave period T at fixed values of the wave height H for the three cases examined in this thesis. The calculation to produce the figure below was presented in Appendix C.

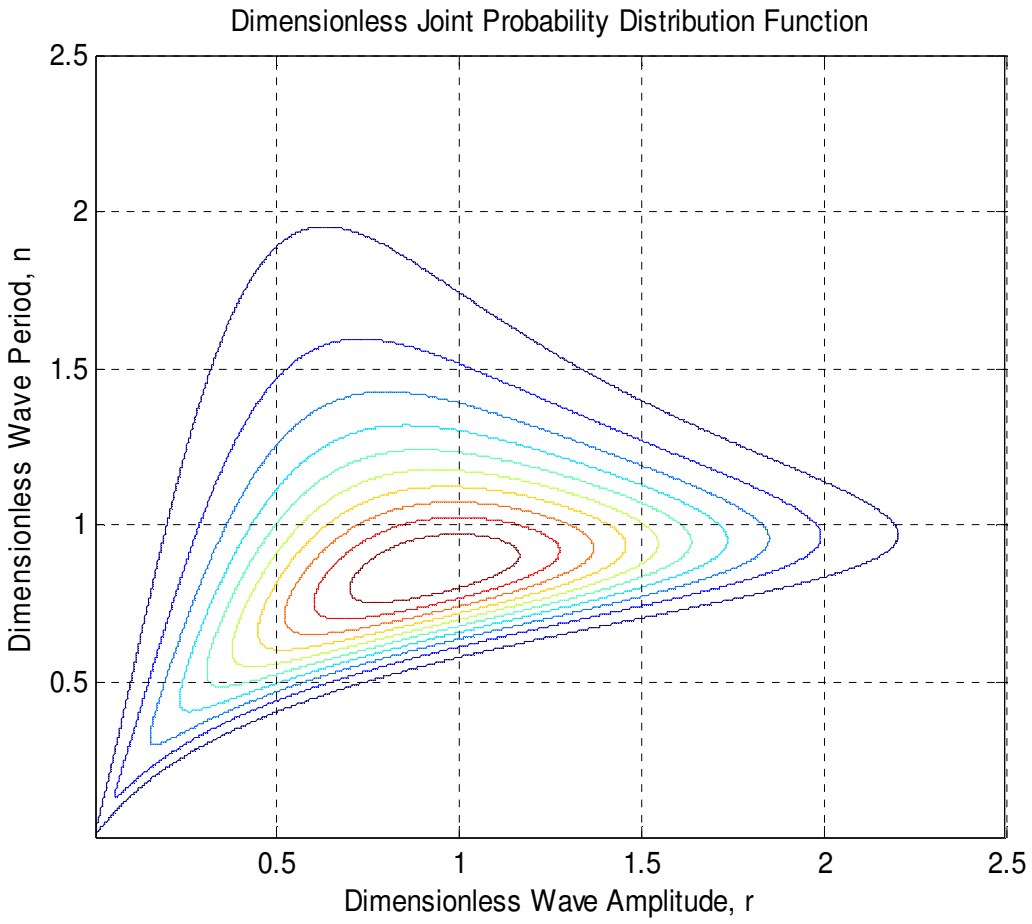

Figure 2.16. Contours of dimensionless joint probability density function

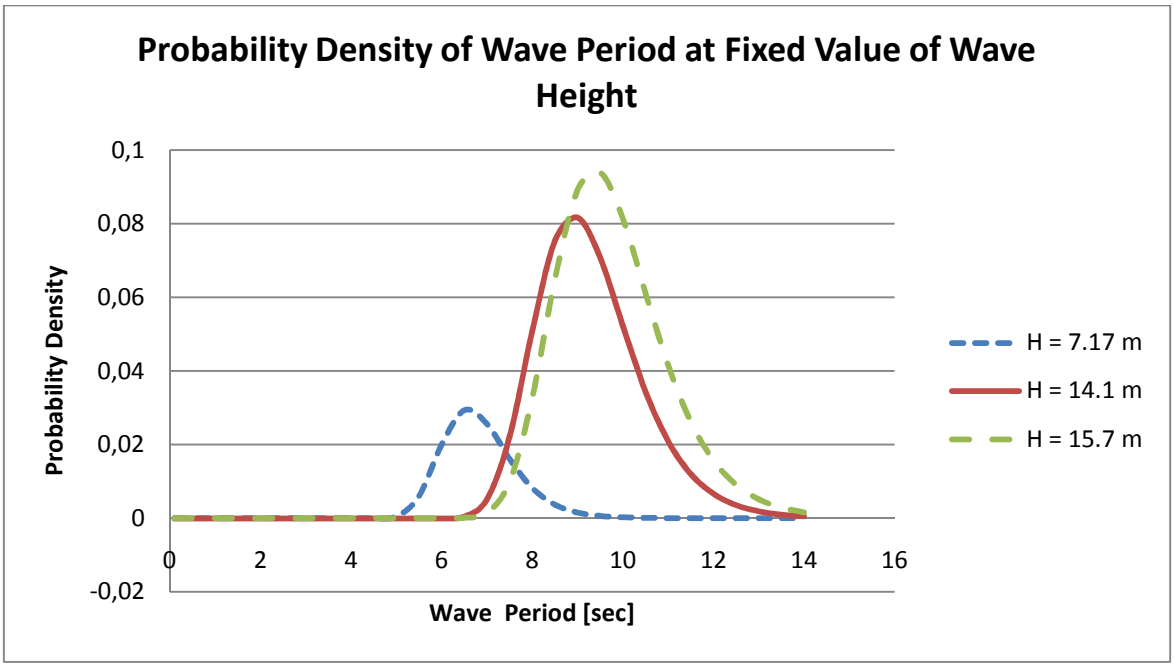

Figure 2.17. Probability density of wave period T at a fixed values of the wave height H.

2.3.2.4. Breaking waves. Wave breaking may take place due to shallow water. In other words, the wave breaking is water depth-dependent. Calculations for wave breaking level and load can be determined by any offshore standards [i.e. 30, 31].

In general, waves are assumed to break when wave height (H)/water depth (d) >0.78 [17]. At an offshore wind farm site, the probability of breaking wave needs to be assessed (i.e. sites with a steep sea floor slope, at sandbanks or rocky outcrops). In our site, the breaking waves occur at 15.8 m of wave height; therefore, it is not taken into account for analysis in this thesis.

2.3.2.5. Current. Current modeling can be preceded in accordance with i.e. [30, 31, or 32]. Currents are important for the design of offshore structures. There are two types of current which are wind (storm) generated and tidal generated currents. For extreme wave conditions, the current profile should be taken into account. The profile gives the speed and the direction of the current at specified elevation and site.

2.3.2.6. Tides. Tides can be classified into two categories. The first one is astronomical tides such that the moon causes an increase or a decrease in water level. The second one is storm surges such that during a storm, combined effect of wind and barometric pressure differential causes the surges (tides) [28].

2.3.3. Other Loads

Besides the main design loads (wind and wave load), there are some other important loads that should be considered for design of offshore structures, and, in some sites they may not be considered for design. The design loads, such as ice load, ship impact, scour or earthquake, are not taken into account in this study.

2.3.3.1. Ice Load. Although the ice loads is not a part of this study they will often be a design driver for some sites. Ice loads may be calculated by the references [30, 32]. For determination of direction and magnitude of the ice loads, the contact area, size and shape of the structure and mechanical properties of ice should be taken into account. The direction of moving ice can be considered as the same direction of wind load.

2.3.3.2. Ship impact. Ship impact load can be considered as variable functional loads. Design of OWTs for such impact load can be carried out as Ultimate Limit State (ULS) analyses [30]. However, there is also accidental limit state which is not possible to protect the structure against the damage. Therefore, there are some measures that are considered to reduce the risk of damage [32].

2.3.3.3. Earthquake. Typically, offshore structures in seismic regions are designed for two level of earthquake intensity (i.e. the ductility level and the strength level earthquakes). The ductility level earthquake is defined for the maximum possible earthquake at site. And, the structure is designed for inelastic response and for reserve strength to avoid collapse. On the other hand, strength level earthquake is defined for reasonable likelihood earthquake of not being exceeded during the structure's lifetime (recurrence interval ~ 200 - 500 years). And, the structure is designed to respond elastically [28].

2.3.3.4. Scour. Foundation of a wind turbine has to be designed in account with the possible scour effect around the foundation at the level of seabed. This scour may happen due to climatic or seasonal change. And, if it is necessary for stability reasons, scour protection can be applied around the foundation (pile) [32]. However, scour effect is not considered for this study.

2.4. Guidelines and Design Loads

It is important that the design of an offshore structure should be in accordance with the guidelines. The International Electrotechnical Commission (IEC) has developed guidelines (IEC 61400-1, and IEC 61400-3) only for the requirements of OWTs. These guidelines are commonly used within Europe. Other than that, because Germany and Denmark are two of the leading countries, two classification societies (i.e. Germanischer Lloyd (GL), and Det Norske Veritas (DNV) [30]) also developed the design guidelines specifically for OWTs [7].

On the other hand, U.S. doesn't have guidelines specifically for OWTs. The American Petroleum Institute (API) recommended the standard, API RP-2A, for fixed offshore structures. Guidelines such as IEC 61400-3 and API RP-2A include similar design

requirement for wave loading conditions. However, for extreme environmental design condition, the IEC uses 50-year return period storm, and, API PR-2A uses a 100-year return period storm [7].

The storm conditions in both guidelines (API RP-2A and IEC 64100-3) were considered in this study for Massachusetts site. The site is one of the most feasible offshore sites in the US. And, there have been some feasibility studies for the site to build an offshore wind farm. It is hard to get all environmental time-history data for the site, however, the MMI report [33] gives the parameters for the site that are needed for design. These design parameters are presented on Table 2.5.

Table 2.6. Wave and wind data for Massachusetts site [33]

#	Case	Return Period		W_s 10m, 1hr (m/s)	W_s 90m, 10 min (m/s)	H_{max} (m)	T_{max} (sec)	Surge (m)	Current (m/sec)
		Max. Wave	Wind Speed						
1	Operating Case	1	<1	10.99	11.4	7.17	8.37	0.159	0.146
2	50 years RP Case	50	50	40.42	42.98	14.1	10.9	0.945	0.381
3	100 years RP Case	100	100	45.29	48.35	15.7	11.4	1.172	0.441

According to the table, it is required to find a method to determine design parameters for 50-year and 100-year return period cases, because it is almost impossible to have 100-year period of data for a particular site. Traditionally, data are collected for 1-2 year periods to determine design parameters for extreme conditions.

2.4.1. Determination of Return Period of 50 and 100-year Wind Speed

Wind loads are one of the important loads affecting offshore structures. It is known that wind is random in nature, so its properties must be defined statistically. Wind data were analyzed statistically using Gumbel method (Appendix D). The same method can be used for measured wave records. Appendix D also gives an example of the return period for maximum annual wind speed of Alaçatı (onshore) in Turkey.

2.5. Design Criteria

There are two basic design criteria for the conceptual offshore turbine design in this thesis:

- The operating frequency of the turbine should not interfere with the vibration characteristics of the support structure.
- All members should be sufficiently strong to resist the environmental load effects taking place in operating and storm conditions.

In addition, all the structural components should be sufficiently strong to resist the load effects during the installation. Furthermore, fatigue life of structural members should not be less than their life time. However, because the structural frequency is assumed to be well separated from the rotor frequencies, this is not considered in this study.

2.5.1. Stiffness

As it is mentioned before, the support structure must be designed to avoid resonance due to the rotor. For that reason, the Campbell diagram was introduced and the target structural frequency was selected as 0.22 Hz.

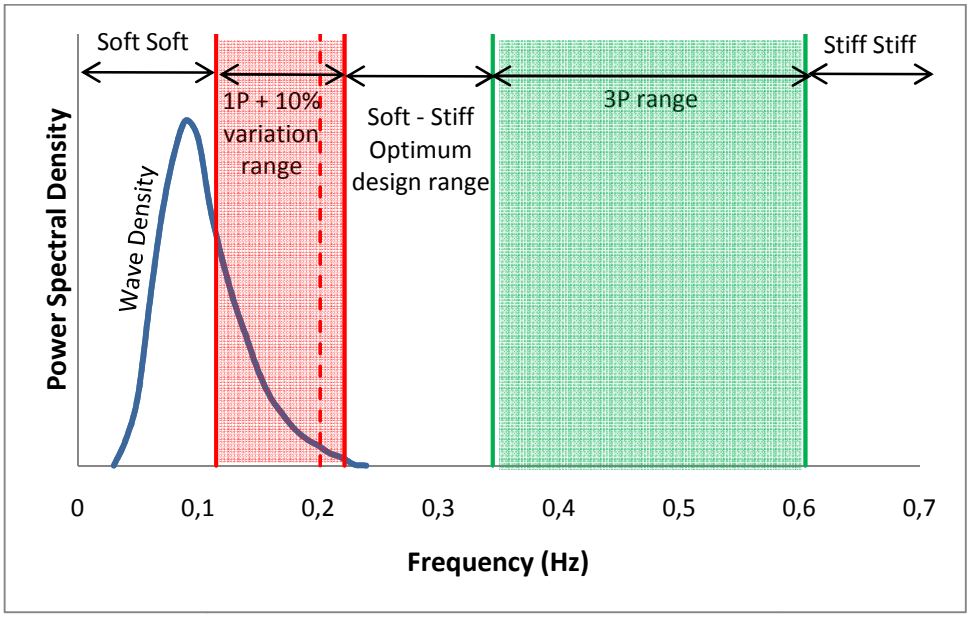

Figure 2.18. Typical excitation range of an offshore wind turbine

2.5.1.1. Stiffness Check. Traditionally, the OWTs are designed such that the first structural frequency does not coincide with the excitation frequencies. The excitation ranges, 1P and 3P, and the realistic normalized power spectra for hydrodynamic excitation are illustrated in Figure 2.14.

2.5.2. Strength

For structural design of foundation systems, all members should have sufficient strength against environmental loads both in storm and operating conditions. The design codes for wind turbines gives many rules on the strength requirement. Although the monopile and the tower composed of many interior parts that should be checked for strength requirement, only the monopile section which is the most important and most costly part was checked according to guidelines. In general, API RP-2A [31] was used for strength check of monopile in this study.

The allowable compression stress, F_a, (API RP2A Eq.3.2.2-1), the allowable bending stress, F_b, (API RP2A Eq.3.2.3-1), and, the allowable shear stress, F_v, (API RP2A Eq.3.2.4-4) for cylindrical members should be determined based on the equations below.

$$F_a = \frac{\left[1 - \frac{\left(\frac{Kl}{r}\right)^2}{2C_c^2}\right] * F_{y,new}}{\frac{5}{3} + \frac{3\left(\frac{Kl}{r}\right)}{8C_c} - \frac{\left(\frac{Kl}{r}\right)^3}{8C_c^3}} \tag{2.20}$$

$$F_{y,new} = \text{Smaller}\,(F_{xe}; F_{xc}) \tag{2.21}$$

$$F_{xe} = \frac{2CEt}{D} \tag{2.21a}$$

$$F_{xc} = F_y * \left[1.64 - 0.23 * (\frac{D}{t})^{\frac{1}{4}}\right] \tag{2.21b}$$

$$F_b = \left[0.72 - 0.58\frac{F_y D}{Et}\right] * F_y \quad (2.22)$$

$$F_v = 0.4 * F_y \quad (2.23)$$

Where;

F_y = yield strength, MPa, (in the thesis F_y = 250 MPa),
E = Young's Modulus of elasticity, MPa, (in the thesis E = 210,000 MPa),
D = outside diameter, m, (in the thesis D = 6.2 m),
t = wall thickness, m, (in the thesis t = 0.062 m),
K = effective length factor, Section 3.3.1d in API RP2A (in the thesis K = 1),
l = unbraced length, m, (in the thesis l = 160 m, where moment is zero),
r = radius of gyration, m, (in the thesis r = 2.17 m),
C = critical elastic buckling coefficient, (in the thesis C =0.6),

$$C_c = \left(\frac{2\pi^2 E}{F_{y,new}}\right)^{\frac{1}{2}}$$

Then, the maximum beam shear stress, f_v, for cylindrical members is,

$$f_v = \frac{V_{tr}}{0.5 * A} \quad (2.24)$$

Where;

V_{tr} = the transverse shear force, MN,
A = the cross sectional area, m^2, (in the thesis A = 1.20 m^2).

Shear requirement condition should be checked so that it is safe or not.

$$f_v < F_v \quad (2.25)$$

Compression capacity requirement condition,

$$f_a < F_a \quad (2.26)$$

It should be checked so that it is safe or not.

Finally and most importantly, combined axial compression and bending should be checked according to API RP2 (Equation 2.27).

$$\frac{f_a}{0.6F_y} + \frac{\sqrt{f_{bx}^2 + f_{by}^2}}{F_b} \leq 1.0 \qquad (2.27)$$

Where;

f_{bx} and f_{by} = the computed bending tensile stresses, $f_b = \frac{M*y}{I}$, MPa.
I = inertia of the section, $I = \pi(d_{out}^4 - d_{in}^4)/64$, m^4.

2.5.3. Drivability

In addition to stiffness and strength requirement for the turbine design, it is also required to consider the constructability of the system. The loads during fabrication, transportation or installation phases, and the availability of equipments required for transportation and installation could be considered as the limitations for constructability. Among these limitations, pile drivability is specifically important for design of monopile in this thesis.

Many different guidelines suggest some ratio for monopile diameter and thickness to avoid the local buckling during the installation. The monopile D/t ratio of 100 is taken to be constant throughout this study.

2.6. Summary of Methodology

The methodology applied for the design of an OWT is summarized as a flowchart in Figure 2.15 below.

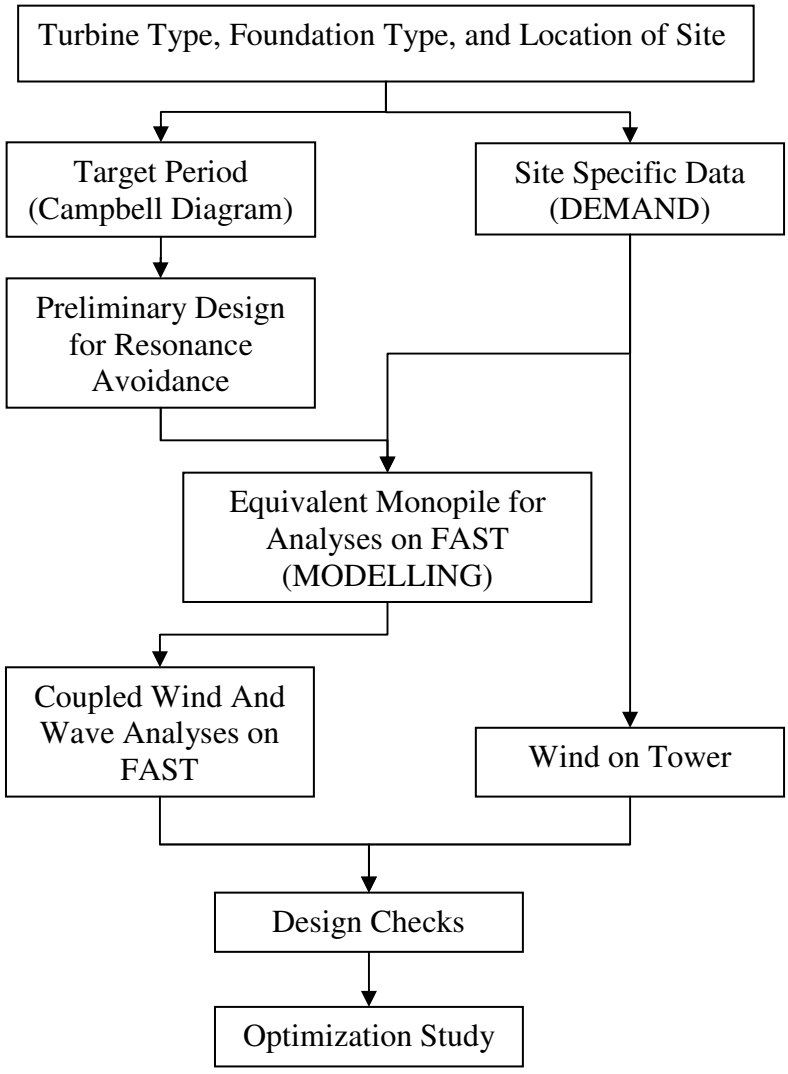

Figure 2.19. Methodology flowchart

3. ANALYSIS

3.1. Modeling

3.1.1. Soil Data

The site is located south of Massachusetts and Rhode Island between Martha's Vineyard and Block Island. The water depth at the site was assumed to be 25 meters.

The monopile is the most basic of configuration in OWT foundations. It is a large single pile that has a penetration depth that provides the necessary mudline fixity to resist the large overturning moments caused by wind and wave loads.

Figure 3.1 shows that the uniform soil strength profile of a clay site where the shear strength linearly increases from 12 kPa to 120 kPa at the top 4-meter portion and then remains constant below that.

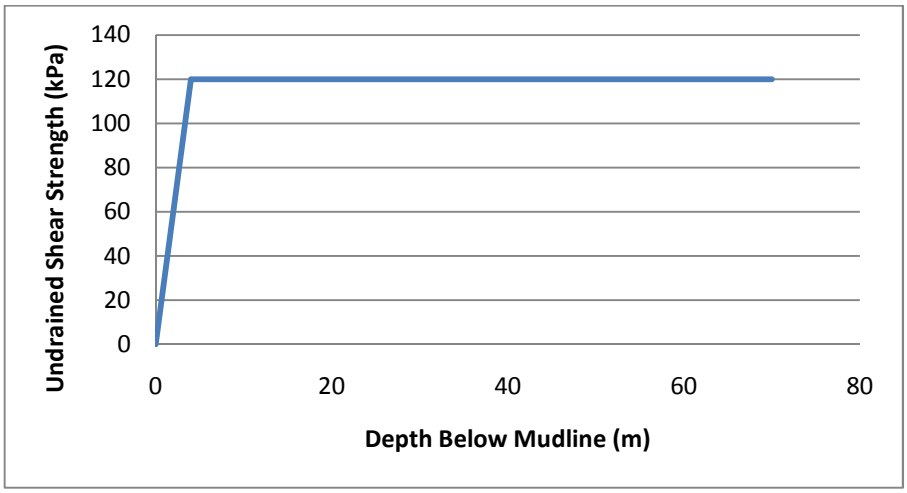

Figure 3.1. Soil strength profile [33]

The monopile model was developed with soil springs to capture the soil-structure interaction properly. Soil-pile interaction was represented explicitly using soil springs to model with the lateral bearing (p-y), shaft friction (t-z) and end bearing (q-z) reaction of the soil. These springs were distributed along the pile as shown in Figure 3.2 below. The

vertical springs along the pile are referred as t-z springs whereas the spring at the bottom tip is referred as Q-z spring.

3.1.2. Soil Spring Calculations

The soil spring properties were developed based on the formulations recommended by API RP2A. In the force-displacement curves, the lateral (p-y) and vertical (t-z) springs at the first 4 meters portion of the monopile under mudline were assumed to be the same (66 kPa). Below that, the soil profile is uniform. These give two different spring properties (i.e. above and below the 4 meters under the mudline). And, both parts were assumed to be constant. The springs were assigned as one meter away from each other (Figure 3.2).

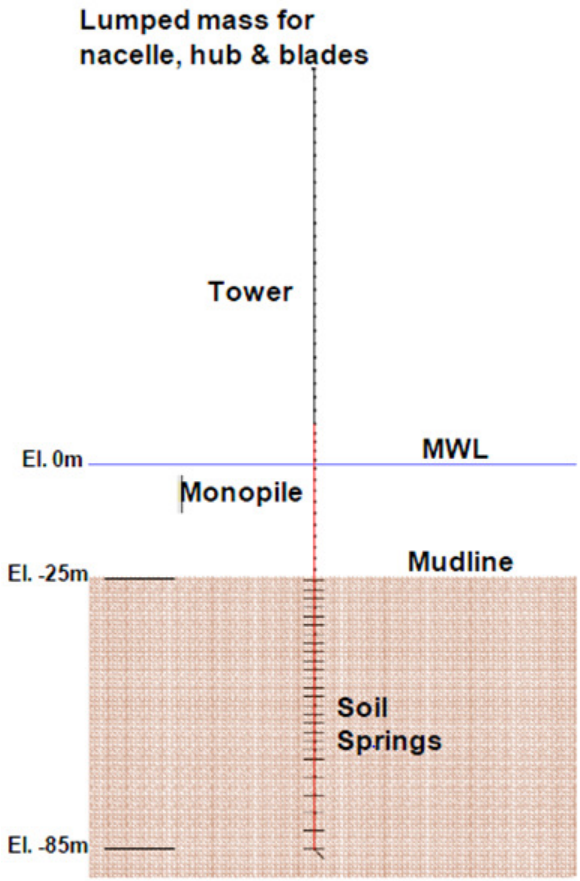

Figure 3.2. Soil spring model [33]

The following section shows how to find the soil stiffness recommended by API RP2A [31].

3.1.2.1. Soil Reaction for Laterally-Loaded Pile. Firstly, lateral bearing (p-y) capacity for soft clay was calculated. The ultimate unit lateral bearing capacity of soft clay p_u has been calculated according to the formula given [31].

$$p_u = 3c + \gamma X + J\frac{cX}{D} \tag{3.1}$$

$$p_u = 9c \quad for\ X \geq X_R \tag{3.2}$$

Where;

p_u = ultimate resistance, kPa,

c = undrained shear strength for undisturbed clay soil samples, kPa,

D = pile diameter, mm,

γ = effective unit weight of soil, MN/m^3,

J = dimensionless empirical constant with values ranging from 0.25 to 0.5 determined by field testing,

X = depth below soil surface, mm,

X_R = depth below soil surface to bottom of reduced resistance zone, mm.

$$X_R = \frac{6D}{\frac{\gamma D}{c} + J}$$

Table below shows the lateral bearing capacity distribution of the site.

Table 3.1. The ultimate unit lateral bearing capacity calculations

X (mm)	c (kPa)	D (mm)	γ(MN/m3)	J	X_R	p_u (kPa)
10	12	6000	8	0.5	8.998875	108
1000	39	6000	8	0.5	29.23812	351
2000	66	6000	8	0.5	49.46599	594
3000	93	6000	8	0.5	69.6825	837
4000	120	6000	8	0.5	89.88764	1080
5000	120	6000	8	0.5	89.88764	1080
6000	120	6000	8	0.5	89.88764	1080
∞	120	6000	8	0.5	89.88764	1080

Secondly, load-deflection (p-y) curves for soft clay are obtained. Because of the non-linear nature of the lateral soil resistance-deflection relationship for piles in soft clay, API RP2A recommends the p-y curves for the short-term static load case that can be generated from the following table:

p/p_u	y/y_c
0.00	0.0
0.50	1.0
0.72	3.0
1.00	8.0
1.00	∞

Where;

p = actual lateral resistance, kPa,

y = actual lateral deflection, mm,

$y_c = 2.5\ \varepsilon_c\ D$, mm,

ε_c = strain which occurs at one-half the maximum stress on laboratory undrained compression tests of undisturbed soil samples (Table 3.2).

Table 3.2. Laboratory undrained compression tests of undisturbed soil samples [35]

Consistency of Clay	Undrained Shear Strength (kPa)	ε_c
Very soft	>12	0.02
Soft	12-24	0.02
Medium	24-48	0.01
Stiff	48-96	0.006
Very Stiff	96-192	0.005
Hard	>192	0.004

The spring constant can be calculated as,

$$k = (p/y)\ xD\ x1\text{m} = p/(y/D)\text{x}1\text{m}$$

The p-y curves are presented in the figure below for Massachusetts site.

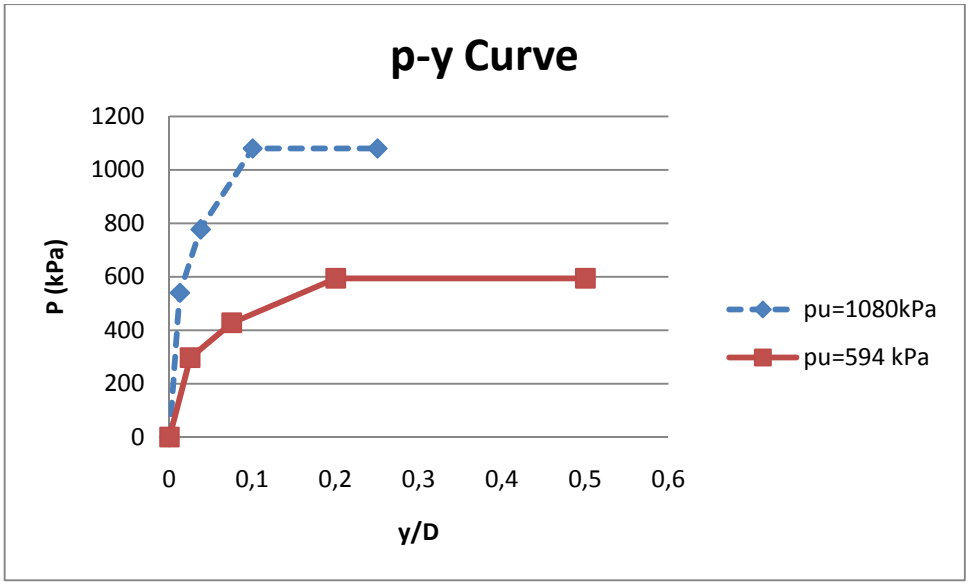

Figure 3.3. Load-deflection (p-y) curve for Massachusetts site

The dashed curve shows p-y curve of first portion (under the 4 meter depth of penetration) of the monopile under mudline. When $y / D = 0.025$, $p = 658.8$ kPa.

The solid curve shows p-y curve of second portion (above the 4 meter depth) of the monopile under mudline. When $y / D = 0.05$, $p = 362.34$ kPa.

Therefore, $k_1 = 26352$ kN/m

$k_2 = 7246.8$ kN/m

3.1.2.2. Soil Reaction For Axially-Loaded Piles. The pile foundation should be designed to resist the static and cyclic axial loads. The axial resistance of the soil is provided by a combination of axial soil-pile adhesion or load transfer along the sides of the pile and end bearing resistance at the pile tip.

The plotted relationship between mobilized soil-pile shear transfer and local pile deflection at any depth is described by using a *t-z* curve. Similarly, the relationship between mobilized end bearing resistance and axial tip deflection is described using a *Q-z* curve [31].

In the absence of more definitive criteria, API RP2A recommends the following *t-z* curves for clays. The axial load transfer (t-z) curve is explained below.

z/D	t/t_{max}
0.0016	0.30
0.0031	0.50
0.0057	0.75
0.0080	0.90
0.0100	1.00
0.0200	0.70 to 0.90
∞	0.70 to 0.90

Where;

z = local pile deflection, mm,

D = pile diameter, mm,

t = mobilized soil pile adhesion, kPa,

t_{max} = maximum soil pile adhesion or unit skin friction capacity computed according to the Equations 3.3 and 3.4 below, kPa.

For piles in cohesionless soils, the shaft friction, *f*, in kPa may be calculated by the equation:

$$f = Kp_0 \tan \delta \tag{3.3}$$

Where;

K = coefficient of lateral earth pressure
(the ratio of horizontal to vertical normal effective stress),

p_o = effective overburden pressure, kPa,

δ = friction angle between the soil and pile wall.

For piles in cohesive soils, the skin friction, *f*, in kPa at any point along the pile may be calculated by the equation.

$$f = \alpha . c \tag{3.4}$$

Where;

α = a dimensionless factor,

c = undrained shear strength of the soil at the point.

The factor, a, can be computed by the equations:

$$\alpha = 0.5\,\psi^{-0.5} \psi \leq 1.0 \tag{3.5}$$

$$\alpha = 0.5\,\psi^{-0.25} \psi > 1.0 \tag{3.6}$$

With the constraint that, $\alpha \leq 1.0$,

Where;

$\psi = c/p'_o$ for the point in question,

p'_o = effective overburden pressure at the point in question, kPa.

Finally, the t-z curves are shown in Figure 3.4 below for the Massachusetts site.

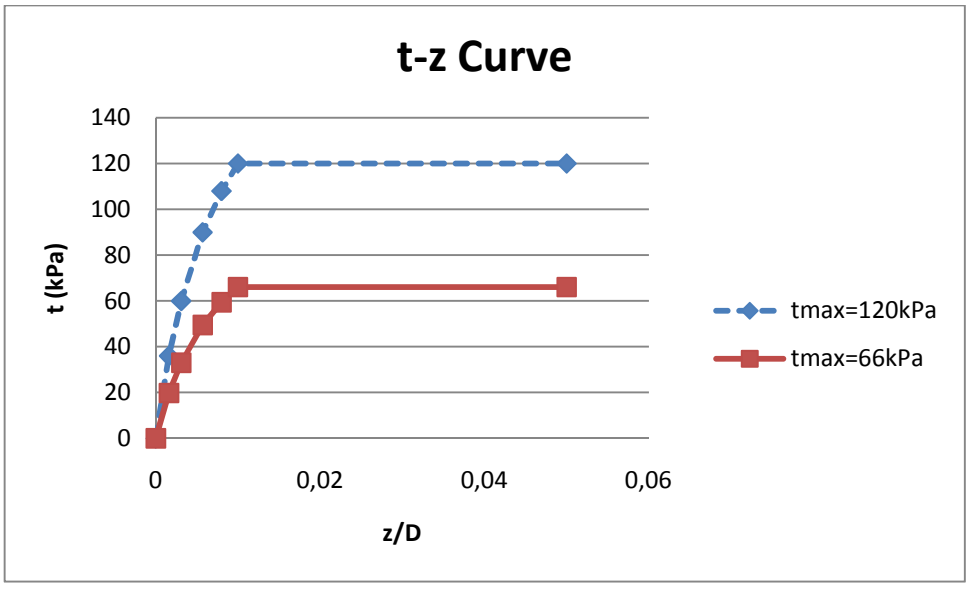

Figure 3.4. Axial load transfer (t-z) curve for Massachusetts site

The spring constant can be calculated as,

$$k = (t/z)\, xD\ x1\text{m} = t\ /(z/D)\ \text{x1m}$$

The dashed curve shows t-z curve of first portion (under the 4 meter depth of penetration) of the monopile under mudline. When z/D = 0.01, t = 120 kPa.

The solid curve shows t-z curve of second portion (above the 4 meter depth) of the monopile under mudline. When z/D = 0.01, t = 66 kPa.

Therefore, k_1 = 12000 kN/m
k_2 = 6600 kN/m

3.1.2.3. Tip-load - Displacement (Q-z) Curve. In the absence of more definitive criteria, API RP2A recommends the following curve for both sands and clays.

z/D	Q/Q_p
0.002	0.25
0.013	0.50
0.042	0.75
0.073	0.90
0.10	1.00

Where;

z = axial tip deflection, mm,
D = pile diameter, mm,
Q = mobilized end bearing capacity, KN.
Q_p = total end bearing, kN, $Qp = q\,Ap$, (Q_p= 30000kN for the site [33])
q = unit end bearing capacity, kPa,
A_p = gross end area of pile, m^2.

And, finally the Q-z curve is shown in the figure below for the Massachusetts site.

The spring constant can be calculated as, $k = Q/z$.

The curve shows Q-z curve at the bottom head of the pile.

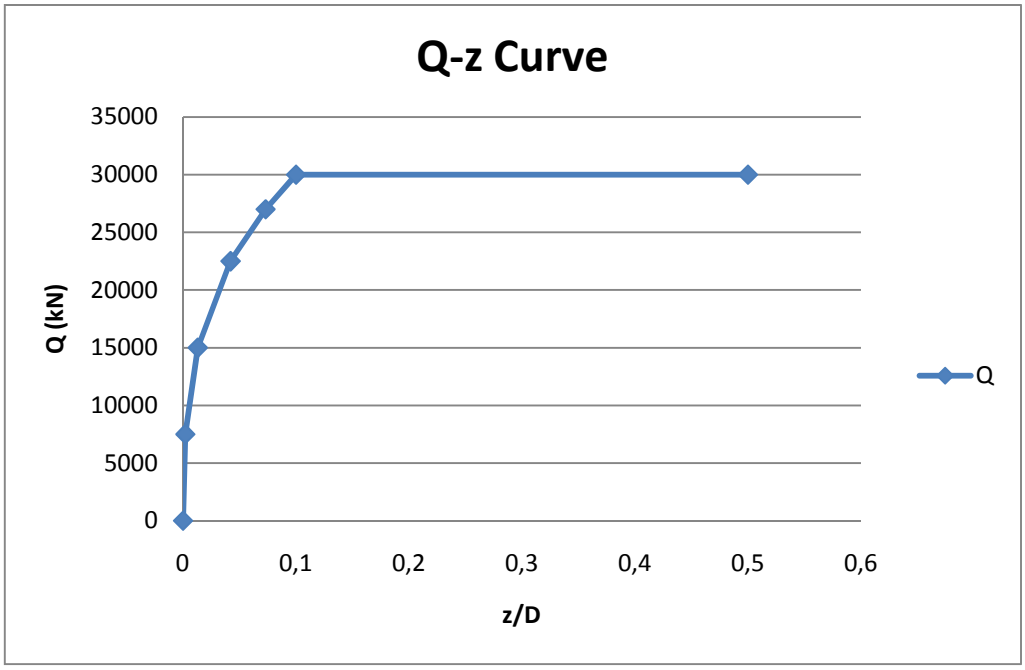

Figure 3.5. End bearing (Q-z) curve for Massachusetts site

When z/D = 0.1, and D = 6m, then z = 0.6m, and Q = 30000 kN.

$$k = 30000\text{kN}/0.6\text{m}$$

Therefore, k_1 = 50000 kN/m.

3.1.2.4. Summary. The spring constants (k) were divided two part k_1 and k_2. k_1 represents the spring constant below 4 m under mudline, and k_2 represents the spring constant between 0 m - 4 m (the spring properties are assumed to remain constant in that section).

The soil springs to model the lateral bearing (p-y) reaction of the soil were found as: k_1 = 26352 kN/m, and, k_2 = 7246.8 kN/m.

The soil springs to model the shaft friction (t-z) reaction of the soil were found as: k_1 = 12000 kN/m, and, k_2 = 6600 kN/m.

The soil springs to model the end bearing (Q-z) reaction of the soil was found as: k_1 = 50000 kN/m.

3.1.3. Foundation Models

The general model for pile foundations is a finite element model with soil springs ('py', 'tz' and 'Qz' curves) to represent the pile–soil interaction. It is called distributed spring model (Figure 3.6). However, because the FAST Code is not capable of analyzing the distributed spring model, a simpler foundation model was obtained. Effective fixity length approach is one of the commonly used simple foundation model. The other common foundation model for wind turbines is a single rotation spring model at the mudline. It is also known as coupled spring model. These two models will be explained in details in following section.

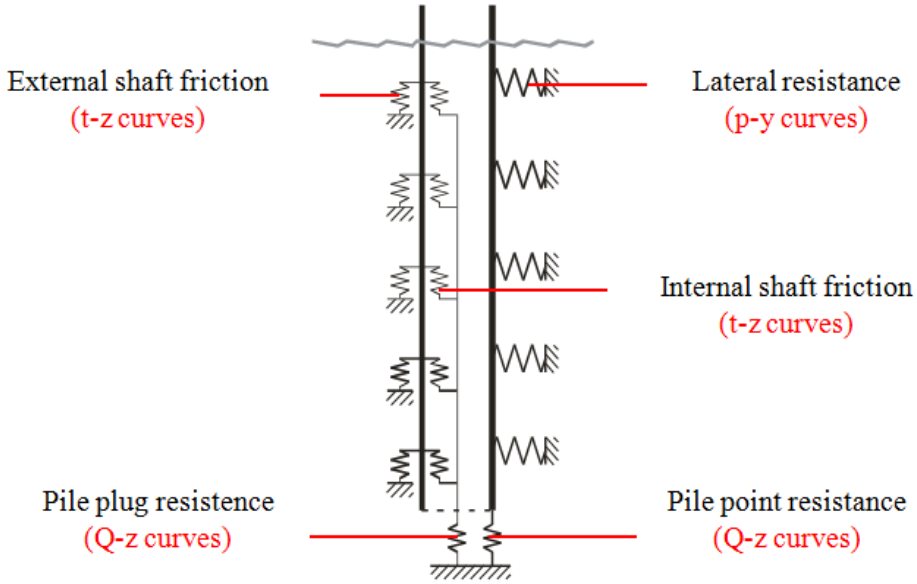

Figure 3.6. Distributed spring model [36]

3.1.3.1. Effective Fixity Length Approach. In this model the clamping effect of the soil is replaced by rigid clamping of the pile at an effective depth below the seabed (Figure 3.7) [14].

For offshore structures, analysis of Barltrop [37] leads to an effective fixity length values between 3.5 and 8 times the pile diameter below the mudline depending on the soil conditions. On the other hand, analysis of Kühn [38] proposes the values between 3.3 and 3.7 times the pile diameter for OWTs on monopile foundations. In our case effective fixity length is 3.8 times the pile diameter.

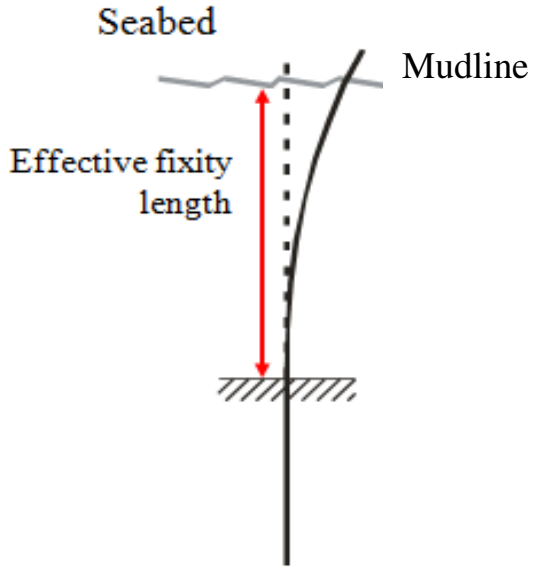

Figure 3.7. Effective fixity length [36]

The distributed spring model was used as reference model for the structural frequency and the deflections under applied point loads. The deflections (u and φ) can be found under applied loads (i.e. lateral force and overturning moment).

The following equations could be applied to find effective fixity length and effective Young's modulus.

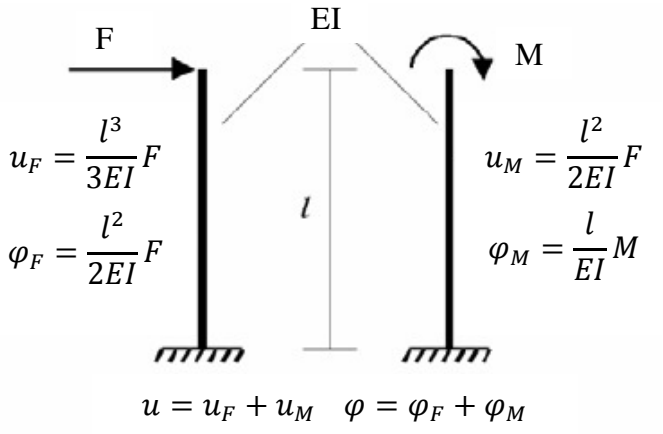

Figure 3.8. Effective fixity length calculation [13]

$$\frac{l^3}{3EI}.F + \frac{l^2}{2EI}.M = u \tag{3.7a}$$

$$\frac{l^2}{2EI}.F + \frac{l}{EI}.M = \varphi \tag{3.7b}$$

By combining the equation 3.7a and 3.7b together, the fixity length, L_f can be found from the equation 3.8. And, *EI* values can be calculated either from equation 3.9a or 3.9b. Therefore, the fictive bending stiffness E_f can be found from the equations below.

$$\frac{l}{3}.\frac{2.l.F + 3.M}{l.F + 2.M} - \frac{u}{\varphi} = 0 \tag{3.8}$$

$$EI = \frac{F.l^3}{3.u} + \frac{M.l^2}{2.u} \tag{3.9a}$$

$$EI = \frac{F.l^2}{2.\varphi}.+\frac{M.l}{\varphi} \tag{3.9b}$$

3.1.3.2. Coupled Spring Approach. In this model, the coupled stiffness of the pile head is simplified to independent springs for each relevant degree of freedom (Figure 3.9). The springs are illustrated only for the lateral translation and the rotation. The spring stiffness of the coupled spring model can be determined from the stiffness matrix using the reference model.

Two load cases were applied to the reference model at mudline level to obtain the stiffness matrix below.

$$\begin{bmatrix} k_{u,F} & k_{u,M} \\ k_{\varphi,F} & k_{\varphi,M} \end{bmatrix} \begin{bmatrix} u \\ \varphi \end{bmatrix} = \begin{bmatrix} F \\ M \end{bmatrix} \tag{3.10}$$

$$F_1 = k_{u,F}.u_1 + k_{u,M}.\varphi_1 \tag{3.11}$$

$$M_1 = k_{\varphi,F}.u_1 + k_{\varphi,M}.\varphi_1 \tag{3.12}$$

$$F_2 = k_{u,F}.u_2 + k_{u,M}.\varphi_2 \tag{3.13}$$

$$M_2 = k_{\varphi,F}.u_2 + k_{\varphi,M}.\varphi_2 \quad (3.14)$$

The stiffness values ($k_{u,F}$ & $k_{u,M} = k_{\varphi,F}$ & $k_{\varphi,M}$) were found from the equations so that the simplified model has the first structural frequency similar with the reference model.

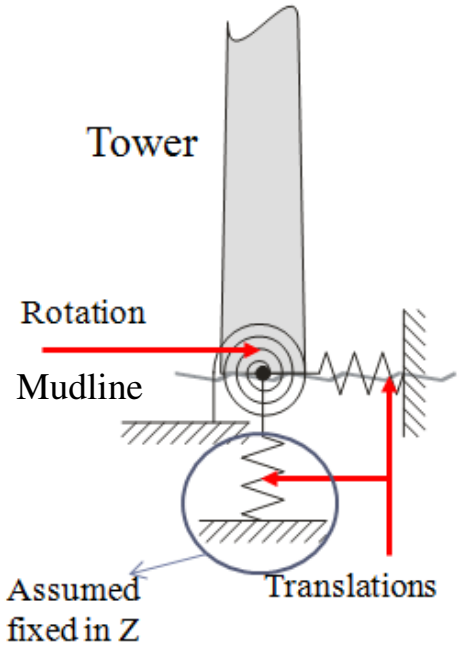

Figure 3.9. Coupled Spring Model [36]

3.1.4. Foundation Analysis

The reference model was set up on SAP 2000 v14, and, the loads are applied on the structure at 10 meters above the water surface shown in the Figure 3.10 below.

When the wind speed in 50-year storm case (42.98 m/s) was taken into account, the applied loads (Force = 350 kN and Moment = 27 MNm) were calculated and applied to the bottom of the tower.

The soil springs were applied as found in the section 3.1.2. After the system was analyzed in SAP 2000, the mode shapes (Figure 3.11), structural frequency and the deflections (u and φ) at applied load level were found. The results are given in the following sections.

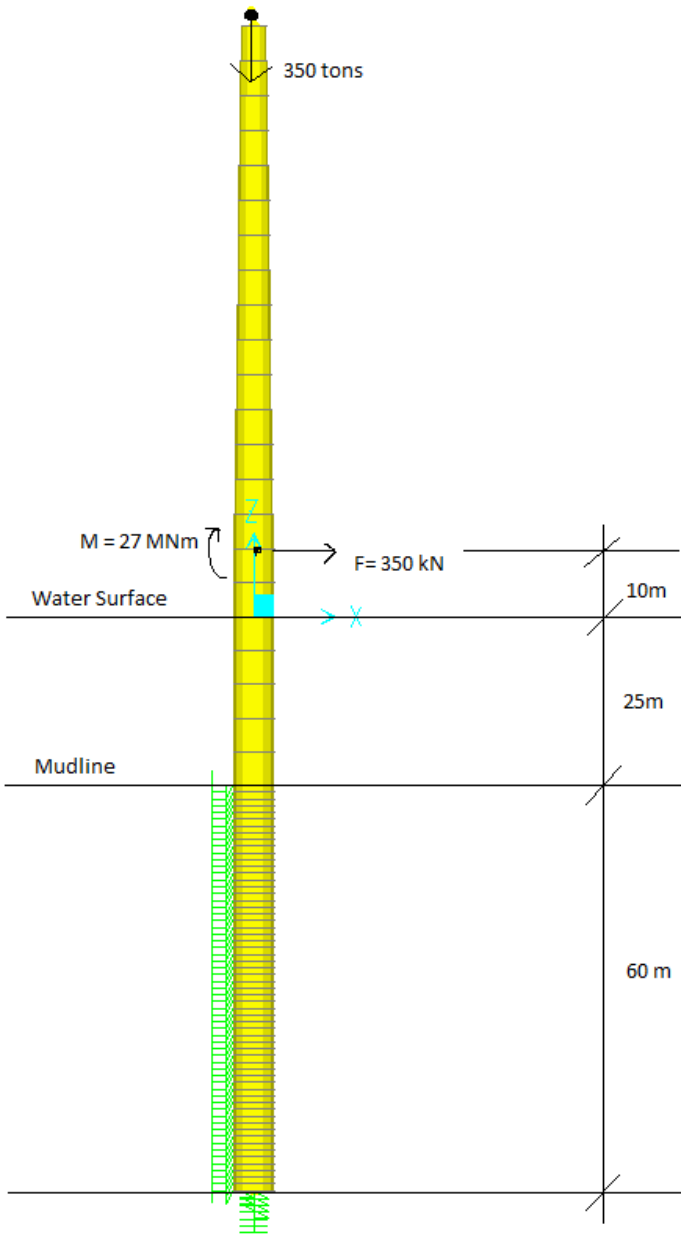

Figure 3.10. SAP 2000 wind tower model and loads

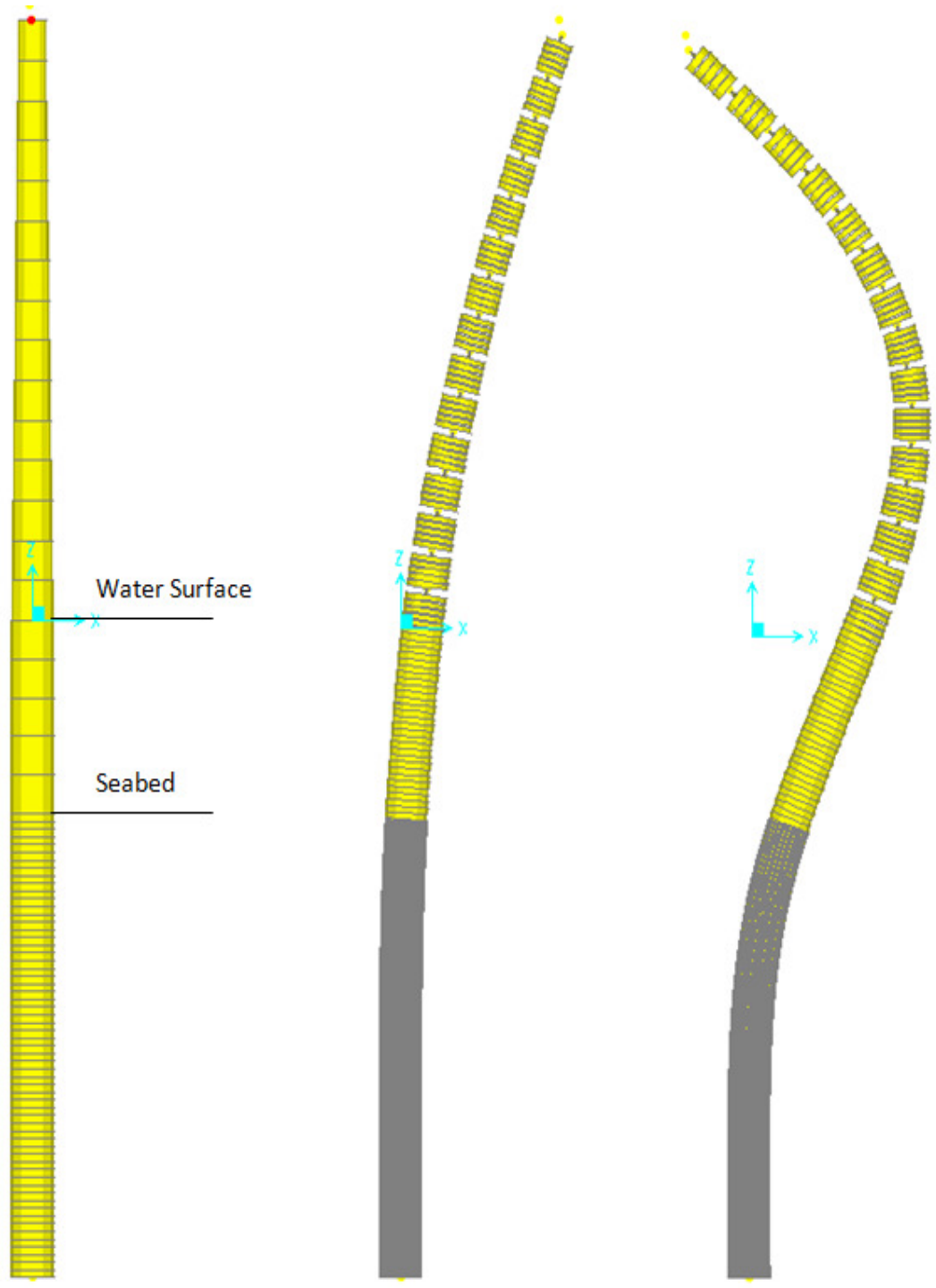

(a) (b) (c)

Figure 3.11. Mode shapes of monopile (SAP 2000) (a) Distributed spring model, (b) First mode, (c) Second mode

3.1.4.1. Effective Fixity Length Model Calculations. The deflections under the applied load are presented in the table below by using the SAP 2000 model.

Table 3.3. Deflection results of the effective fixity length model

	Load (kNm & kN)	u (m)	φ (deg)
Moment	27000	0.04291	0.0015
Force	350	0.02195	0.000556
Total		0.06486	0.002056

The Young's modulus, E, of the monopile is 210000 MPa and the moment of inertia, I, is equal to 4.9387 m^4.

Therefore, according to Equation 3.8,

$$\frac{l}{3}.\frac{2.l.F+3.M}{l.F+2.M}-\frac{u}{\varphi}=\frac{l}{3}.\frac{2xlx350+3x27000}{lx350+2x27000}-\frac{0.06486}{0.002056}=0$$

The roots of the equation gives, L_1 = 57.83 m and L_2 = -126.23 m.

Moreover, according to Equation 3.9b,

$$E_fI=\frac{F.l^2}{2.\varphi}.+\frac{M.l}{\varphi}=\frac{350x57.83^2}{2x0.002056}+\frac{27000x57.83}{0.002056}=1044097304\ kNm^2$$

$$E_f=\frac{1044097304\ kNm^2}{4.9387\ \mathrm{m}^4}=211375\ MPa$$

In conclusion, it was found that the effective length, L_f, was 57.83 m including the 10 meters of monopile part above water surface. And, effective Young's modulus, E_f, was 211375 MPa.

3.1.4.2. Coupled Spring Model Calculations. In this case, two load cases were applied to

the mudline level of the reference model, and, the deflection results are presented table below.

Table 3.4. Deflection results of the coupled spring model for two load case

		Load (kNm & kN)	u (m)	φ (deg)
Case 1	Moment	27000	0.00638	0.0005884
	Force	350	0.00173	0.00008264
	Total		0.00811	0.000671
Case 2	Moment	35000	0.00826	0.0007627
	Force	430	0.00213	0.0001015
	Total		0.01039	0.0008642

According to equations 3.11 to 3.14;

$$F_1 = k_{u,F}.u_1 + k_{u,M}.\varphi_1 \overset{\text{so}}{\Rightarrow} 350 = k_{u,F}\text{x}0.00811 + k_{u,M}\text{x}0.000671$$

$$M_1 = k_{\varphi,F}.u_1 + k_{\varphi,M}.\varphi_1 \overset{\text{so}}{\Rightarrow} 27000 = k_{\varphi,F}\text{x}0.00811 + k_{\varphi,M}\text{x}0.000671$$

$$F_2 = k_{u,F}.u_2 + k_{u,M}.\varphi_2 \overset{\text{so}}{\Rightarrow} 430 = k_{u,F}\text{x}0.01039 + k_{u,M}\text{x}0.0008642$$

$$k_{u,M} = k_{\varphi,F}$$

By using these four equations and four unknowns, the stiffness matrix was founded as,

$$k_{u,F} = 377042\,\frac{\text{kN}}{\text{m}},\ k_{\varphi,M} = 89013106\,\frac{\text{kN}}{\text{m}}, \& \ k_{\omega,M} = k_{\varphi,F} = -4035486\,\frac{\text{kN}}{\text{m}}$$

3.1.4.3. Foundation Models Comparison. Using the distributed spring model as reference model, the other two simpler models were calculated and presented in the figure below.

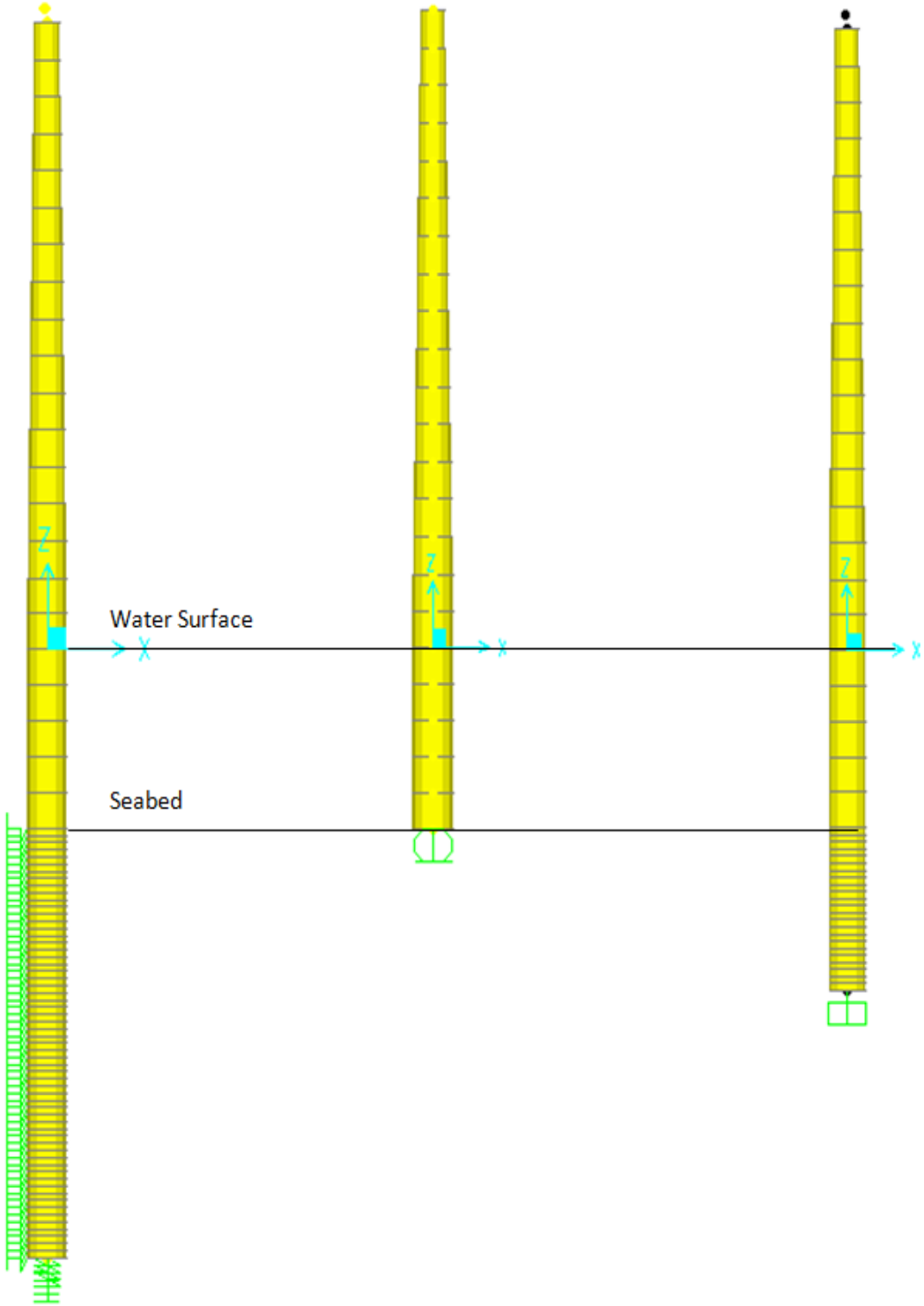

(a) (b) (c)

Figure 3.12. Foundation models (a) Distributed spring model, (b) Coupled spring model, (c) Effective fixity length model

After the foundation models were obtained, the first natural structural periods were compared in the table below.

Table 3.5. First natural structural period comparison between three foundation models

Model	Structural Period (s)	Percent Change (%)
Distributed Spring	4.34	0.00
Effective Length	4.36	0.46
Coupled Spring	4.34	0.00

As it is shown in table above, there is less than 1 % difference in the first structural periods between all three foundation models. And, because effective fixity length model is less complicated then the other two models, it was used for the calculation in this thesis.

Moreover, it is confirmed that the structural period in FAST Code is 4.5 sec (target period) for this model because of the reasons such as explicit modeling of blades.

3.1.5. Equivalent Monopile Properties For Fast Analyses

The FAST program is limited to the modeling of fixed monopile support structure configurations. For monopiles, the program represents the supporting structure both in terms of applied wind and wave load, and more importantly, in terms of the structural vibration characteristics, that affect the resulting turbine wind loads. Any support structure requires an equivalent representation to capture at least the first mode of vibration, wave drag, and inertial loading.

An equivalent fixed base monopile was chosen to match the desired structural period for each case study by changing depth of fixity and also calibrating the system damping. The equivalent representation of the monopile is illustrated in Figure 3.13. And, the model is called effective fixity length model. It was concluded that the effective length under water surface, L was taken 48 m and Young Modulus, E was taken 210 GPa for FAST Code analyses [33].

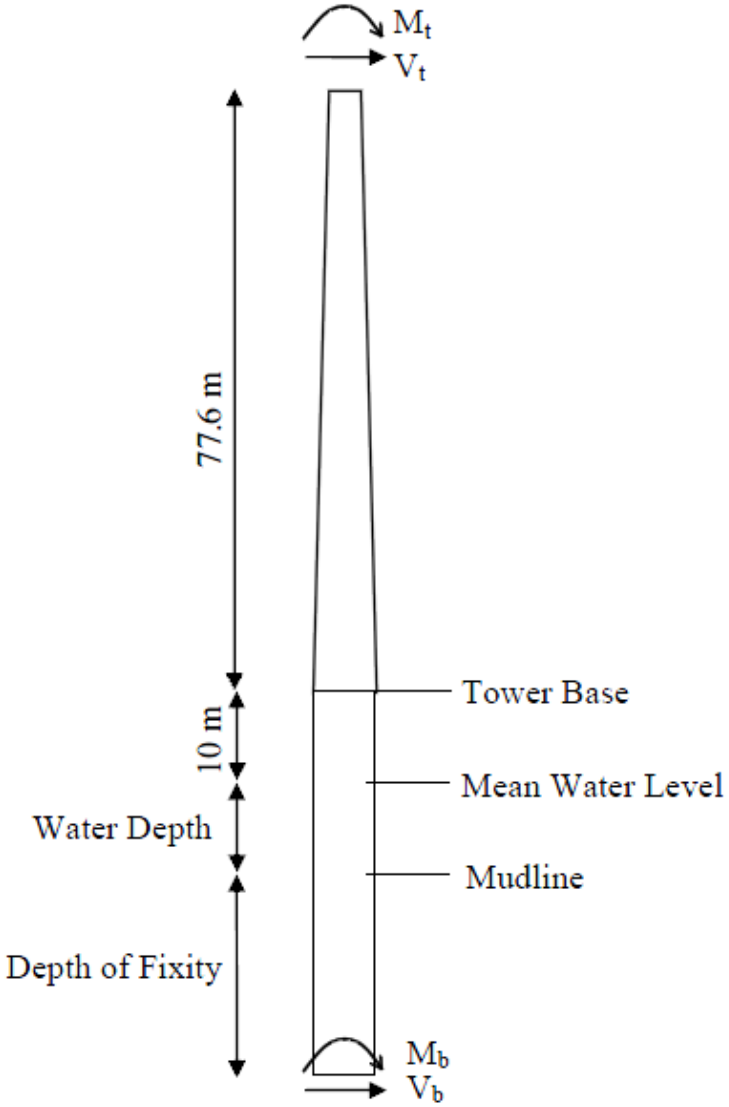

Figure 3.13. Effective fixity length model representation [33]

3.2. Demand

For different storm conditions, each load case was defined with a combination of maximum wave height with current and surge, and average wind speed. A sensitivity study was performed to assess the effect of variation of wind turbulence. For that, a number of simulations were performed to obtain a converged estimate of the maximum structural response.

For each storm conditions, ten different stochastic simulations of turbulent wind flow were performed. The maximum overturning moment and base shear values were

extracted from each simulation. The mean of these maximum values were used for design and capacity analysis.

3.2.1. Wind Data

Three different combinations for wind and wave data were specified for the site. Ten simulations were performed for each case. It was determined that 10 simulations provide a stable representation of the wind force (Section 3.2.1.3).

The maximum force and moment component for the monopile were obtained for each case in the form of a time-history series; namely, base shear and over-turning moment ("BS', V_b and "OTM", M_b). These components were recorded for 10 simulations. The mean of these maxima were used for the strength check of the structure.

3.2.1.1. Wind on Blades. Wind loads on blades are crucial for the design of the structure. It is needed to have wind speed data to find the load.

The main feature of wind speed is its mean; however, the mean wind speed is not plausible to use as a constant value that acts on the rotor area to obtain the response of the structure, because the wind speed that acts on structure in its lifetime is higher than the mean wind speed. Therefore, stochastic wind speed data is needed.

3.2.1.2. Comparison of Constant and Stochastic Wind Data. The comparison was made for a mean wind speed of 49.47 m/s. One stochastic simulation was produced by TurbSim Code for the mean wind speed, shown in Figure 3.14 below.

The loads for the two cases that were applied to the top of the tower is shown in time domain (Figure 3.15). Both of the time history data were modified as slightly increasing load at the beginning to eliminate the instant load effect on the structure.

After time history loads (from FAST Code) were applied to the top of the structure in SAP 2000 v14 software. The results of base shear (BS) and over turning moment (OTM)

at 4m below mudline were shown in Figure 3.16 and Figure 3.17, respectively. The reason to take the results at 4 meters below the mudline will be explained in the section 3.2.2.

The maximum values of the time domain results are summarized in Table 3.6.

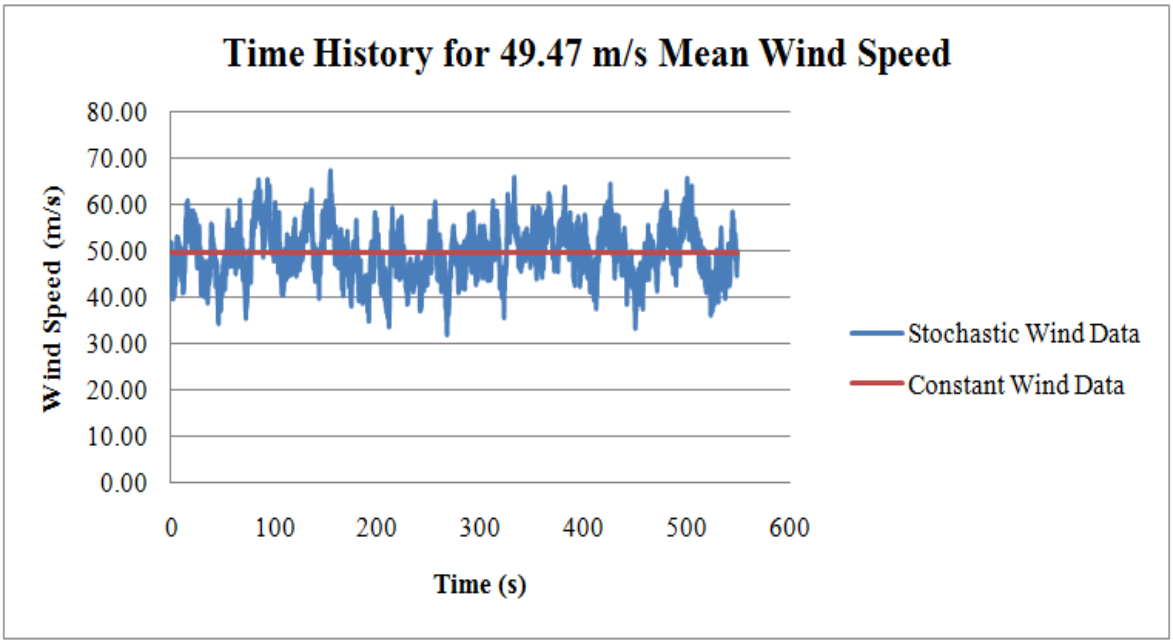

Figure 3.14. Time domain record of stochastic and constant wind speed (W_s = 49.47 m/s)

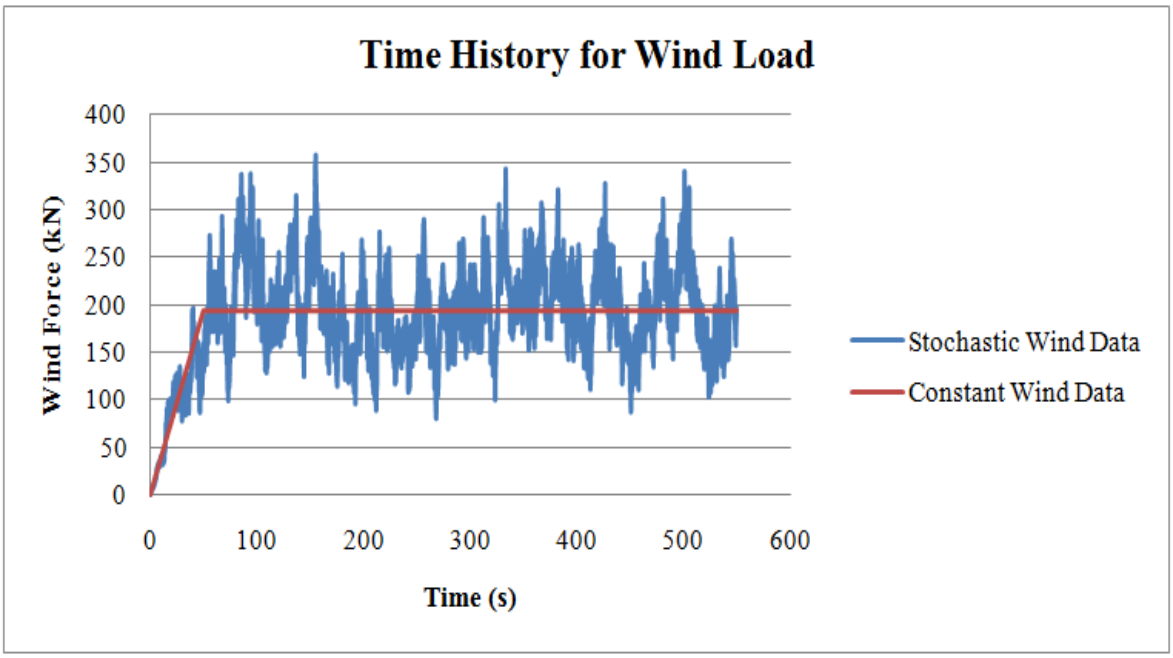

Figure 3.15. Time domain record of stochastic and constant wind load (W_s = 49.47 m/s)

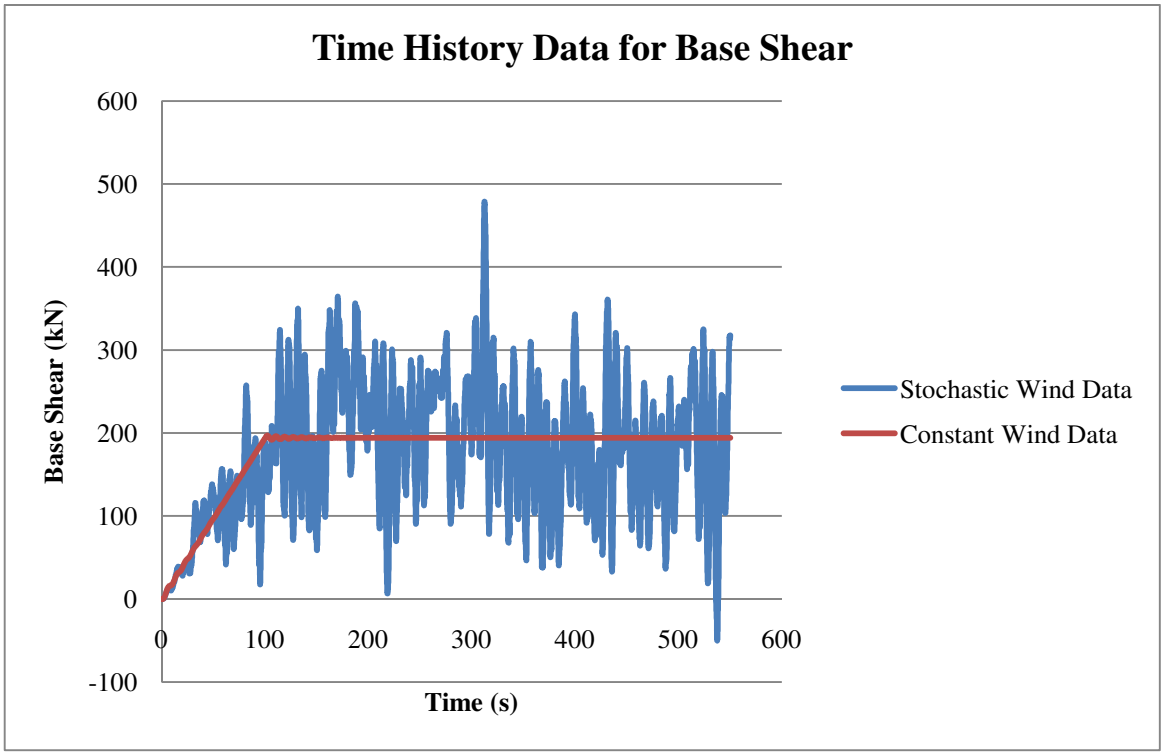

Figure 3.16. Time domain record of base shear under stochastic and constant wind speed data

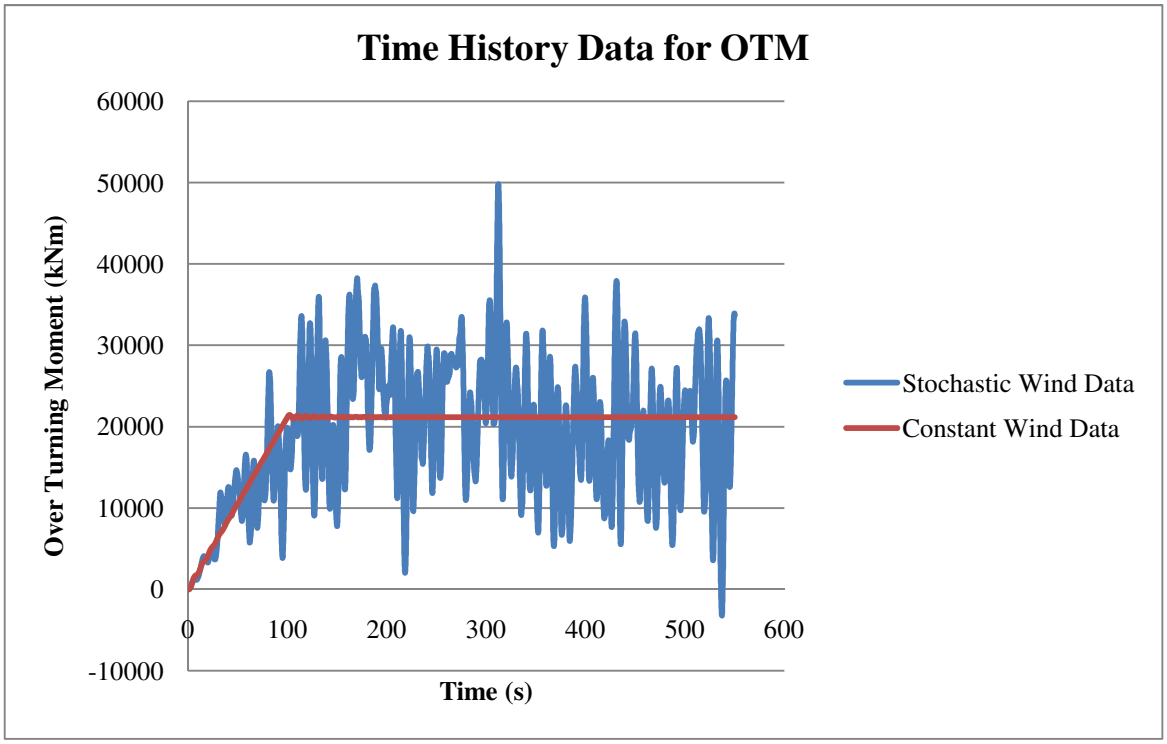

Figure 3.17. Time domain record of overturning moment under stochastic and constant wind speed data

Table 3.6. Comparison of the maximum values in time domain records

Maximum Values in SAP 2000 Results			
Stochastic BS (kN)	Constant BS (kN)	Stochastic OTM (kNm)	Constant OTM (kNm)
478.8	197.0	49796.3	21418.5

As it is shown in the table, the analysis results for stochastic wind speed data were more than twice of the results for constant wind speed data. This explain the main motivation to use software such as FAST which can analyze the structure under stochastic loading.

3.2.1.3. Study on Sensitivity of Load Results. Due to the stochastic nature of the turbulent wind load, there was a variation in the maximum of the BS and OTM results. Therefore, the load analyses should be performed for more than one simulation. For each simulation, the maximum base shear and overturning moment are obtained. The mean of these maximum values is used for the strength check of the structure.

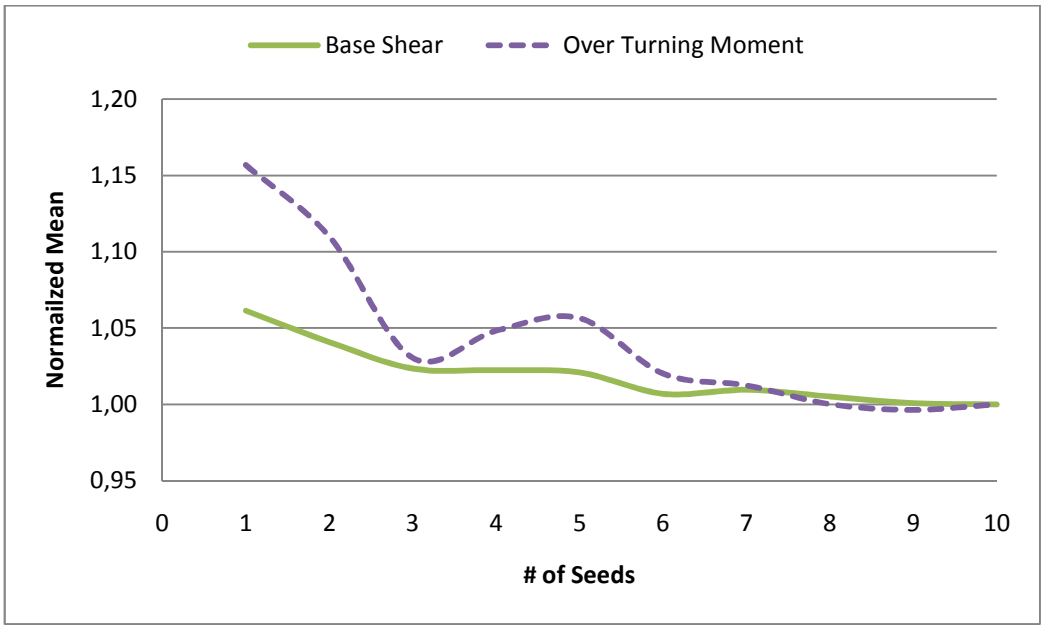

Figure 3.18. Sensitivity analyses results

For example, Figure 3.18 shows the sensitivity analysis result for 10 simulations. The mean wind speed was chosen as 20 m/s. On the other hand, maximum wave period

was 13.85 sec and maximum wave height was 10 meters. It can be observed that the variation is 15% for overturning moment, and after fifth simulation the variation drops to be 5%. Because the level of variation can be considered significant, 10 simulations were decided to perform to achieve the acceptable level of accuracy.

3.2.1.4. Wind on Tower. The wind on tower is calculated according to Section 2.3.1.5, and the results shown in the table below. The calculation of wind load on tower is presented in Appendix E in tabular form for each design case. These values were added to the design data founded in FAST Code.

Table 3.7. Summary of wind load on the tower

Case	BS (kN)	OTM (MNm)
Operating	13.4	1.00
50-year Storm	195.4	14.7
100-year Storm	247.2	18.8

3.2.2. Wave Data

Some analyses were performed to verify the wave force formulation included in FAST. The time-histories of base shear and overturning moment were generated with FAST and SAP 2000 and compared. Both FAST Code and SAP 2000 software finds the wave force on monopile based on the Morrison equation which uses stokes wave theory.

SAP 2000 offshore module was applied to the structural model that was found by the effective fixity length approach (Section 3.1.3.1). The effect of the wave on monopile was calculated for the 100-year storm case.

The wave velocity profile is shown in the Figure 3.19 and maximum wave height was found as 37.08 meters. It was obvious that the wave has positive direction velocity when the wave height is higher than the sea surface (Figure 3.19a), and, it has negative direction velocity the wave height is lower than the sea surface (Figure 3.19b). That gives the positive force and negative force respectively.

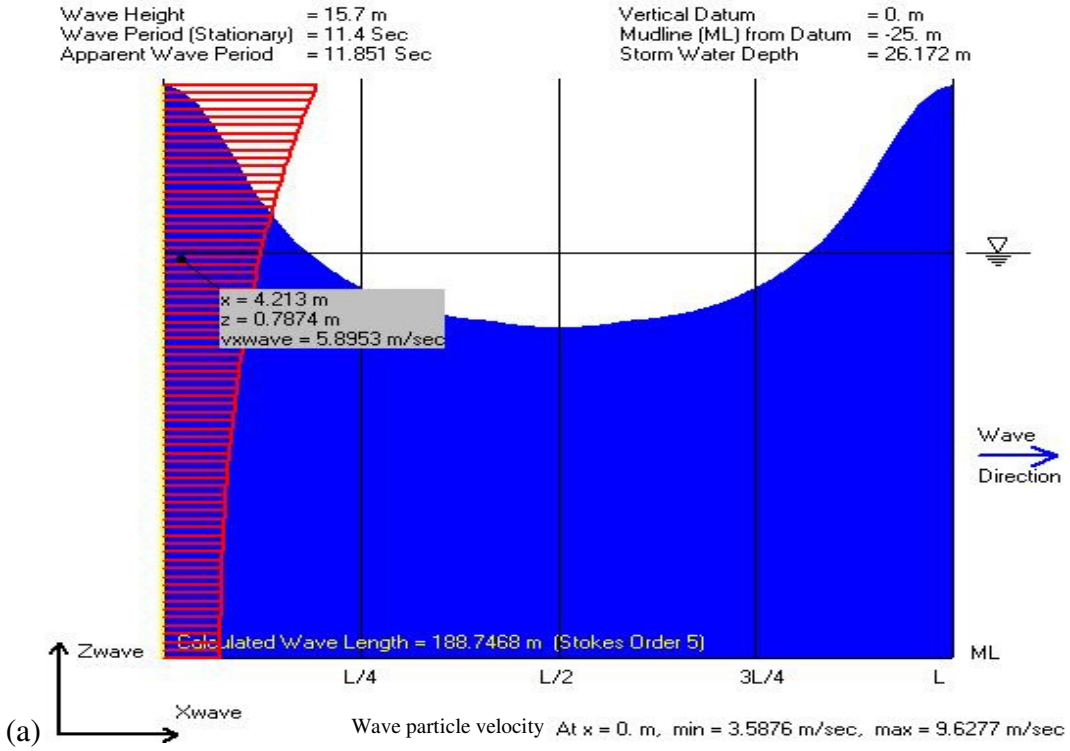

(a)

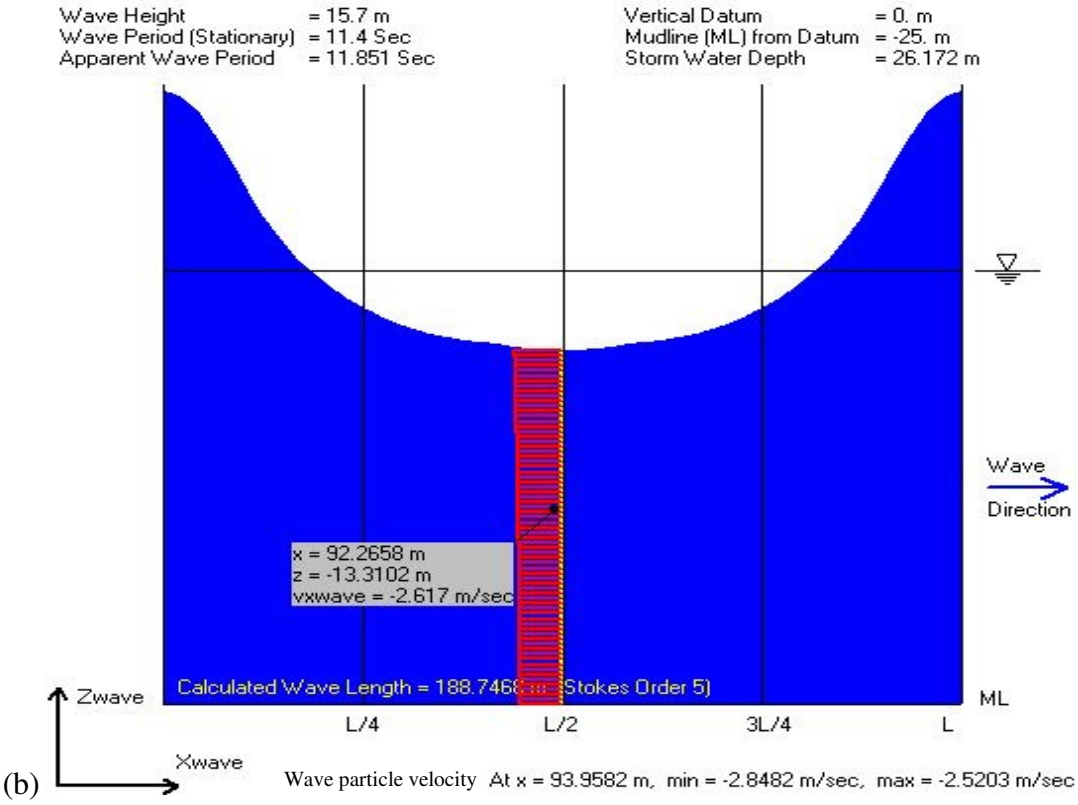

(b)

Figure 3.19. 100 years storm case wave velocity profiles, (a) Wave velocity profile at the beginning of its period, (b) Wave velocity profile at the mid-period

The monopile was modeled in the SAP 2000 software for wave load only. The results are shown in the table below.

Table 3.8. Element forces at base level in the SAP 2000 model

Output Case	Axial kN	Shear kN	Moment MN-m
100-year storm	1264	5135	229

In addition to that, the base level moment in the Table 3.8 should be modified because maximum moment is obtained at a level closer to mudline. To find the point where the maximum moment happens, the full spring model (the reference model) was used with combined wave and wind loads (Figure 3.20) so that the OTM results that were found from both softwares can be modified. Wind loads that were applied to tower top (the moment is equal to 4727 kNm and shear is equal to 652 kN) were taken from the FAST analysis.

According to Figure 3.20, the maximum moment occurs at 4 m below the mudline. Moreover, the effective fixity length of the model was 48 meters from water surface. Therefore, 48m – 25m - 4m = 19m is the moment arm. It was used to find the amount of the OTM that should be extracted from the base OTM from the result.

By using the Table 3.8 and the result from the Figure 3.20, the base shear and the over turning moment of SAP model were modified for 100 years return period storm case as;

Base Shear = 5135 kN

Overturning Moment = $M_3 – L$ x V_2 = 228840 -19 x 5135 = 131275 kNm.

Afterwards, the FAST Code analysis was carried out under the wave load only. The Code gave Base Shear = 4955 kN and Overturning Moment = 230800 kNm at base level. Therefore, modified OTM = 136655 kNm in the code.

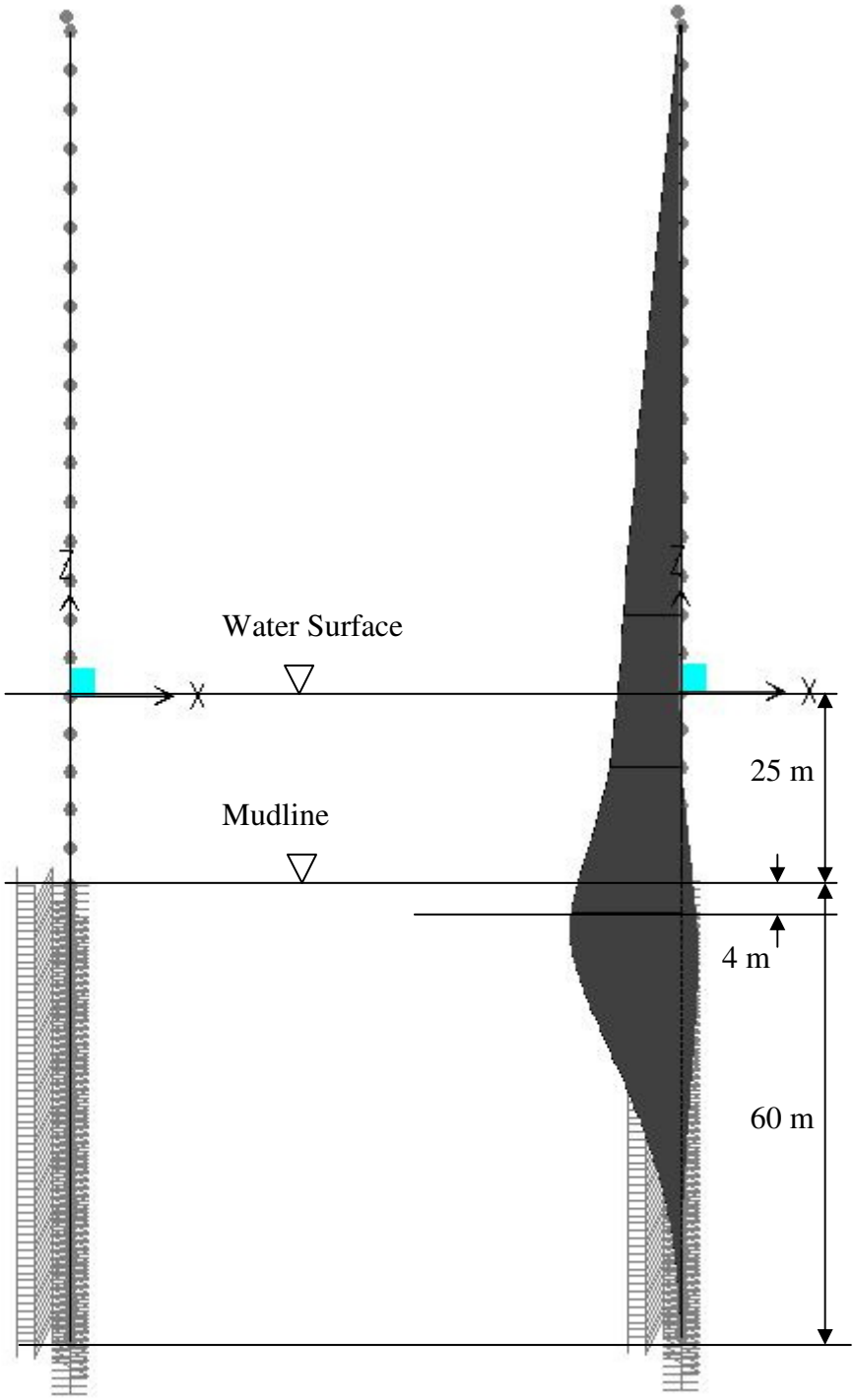

Figure 3.20. Moment distribution of tower and monopile under combined wave and wind load

The comparison of the final results is shown in Table 3.9. And, there is a slight difference (less than 4 %) between the results. It can be concluded that the results obtained from the two softwares compared well.

Table 3.9. Comparison of the results

	BS (kN)	OTM(kNm)
FAST	4955	136655
SAP 2000	5135	131275
Percent variation (%)	-3.6	3.9

3.2.3. Design loads

The design loads for three cases are presented in the following sections.

3.2.3.1. Operational Speed Case. Ten stochastic wind speed seeds were performed for operational speed case for the site and average of the resultant forces was obtained. The Figures 3.21 below shows two different seeds to compare how the wind speed changes.

Maximum wind speed in the first wind seed is 17.94 m/s, and, the wind speed in the second seed reaches 21.13 m/s. This is expected because of the stochastic nature of the wind.

Moreover, Figure 3.22 shows one of the load time histories on monopile at operating speed case for seed number five.

The result of the analyses for ten seeds is shown in the Table 3.10. The results of the base shear and over turning moment for the monopile were taken from 4 meters below the mudline.

According to the Table 3.10, the maximum percentage change of wind speeds is about 18% (i.e. the speeds differ from 17.94 m/s to 21.13 m/s), the maximum percentage

change in OTM is about 10% (i.e. the OTM results differ from 123.3 MNm to 136.0 MNm), and the maximum percentage change in BS is about 8% (i.e. the BS results differ from 2149 kN to 2323 kN).

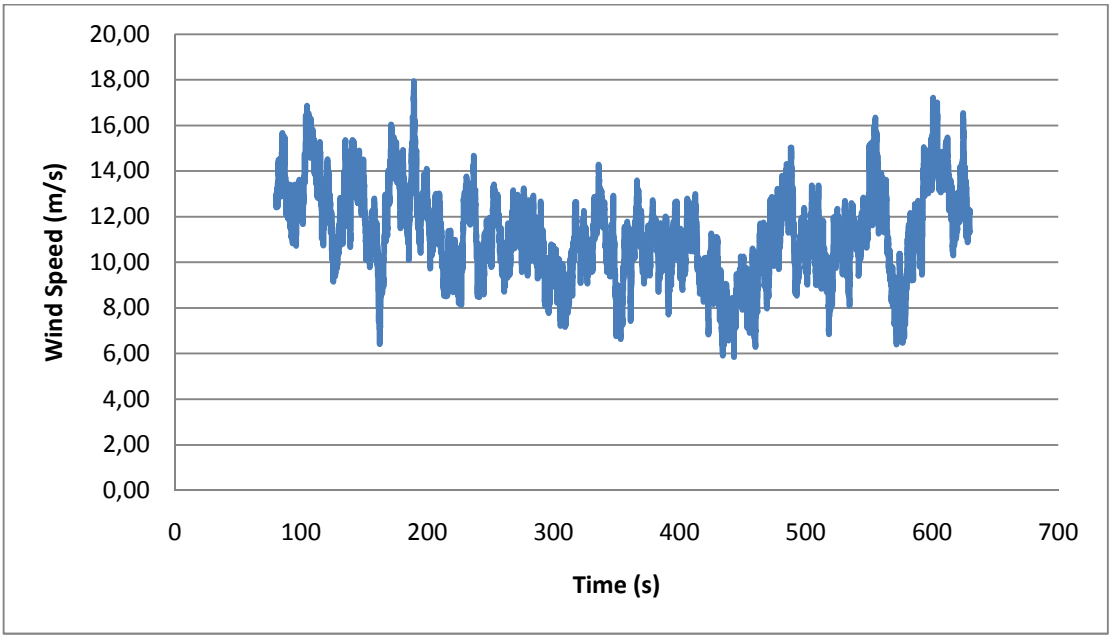

(a)

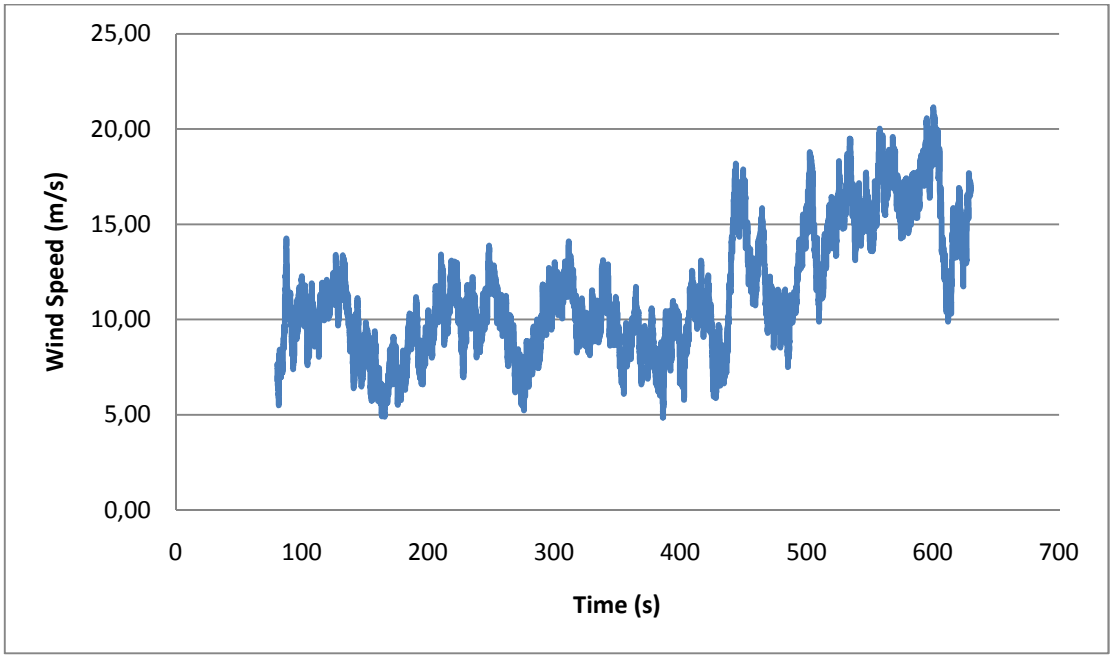

(b)

Figure 3.21. Wind speed seeds for operational speed case in Massachusetts site ($W_{s,average}$ =11.4 m/s), (a) Fourth wind speed seed (b) Seventh wind speed seed

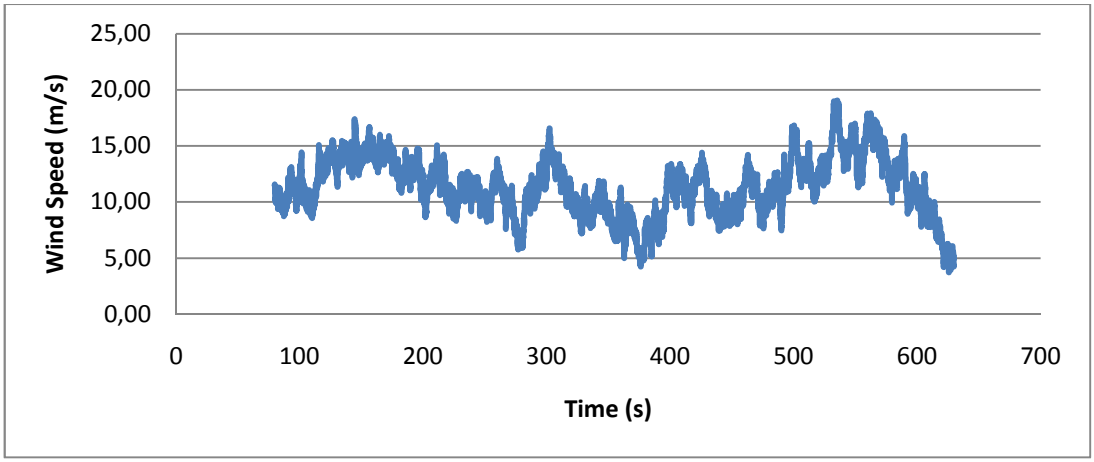

(a)

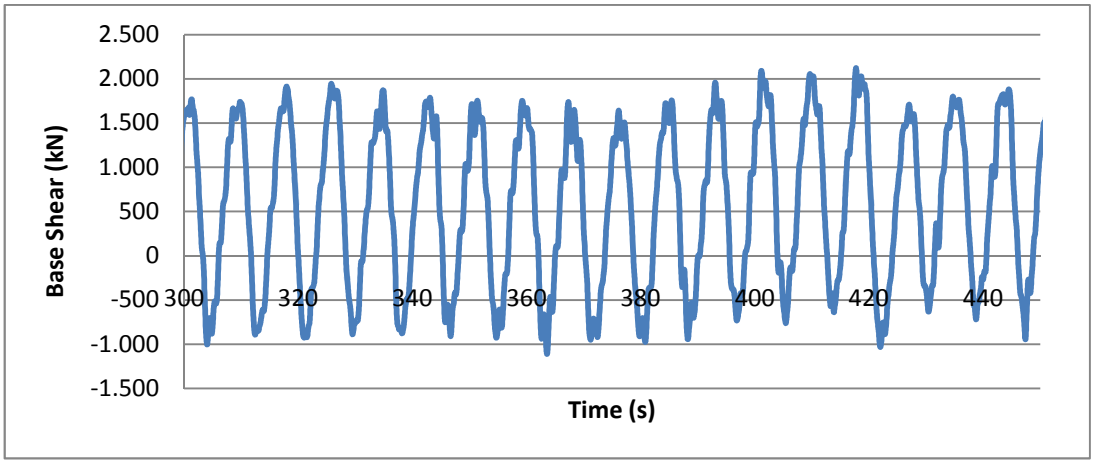

(b)

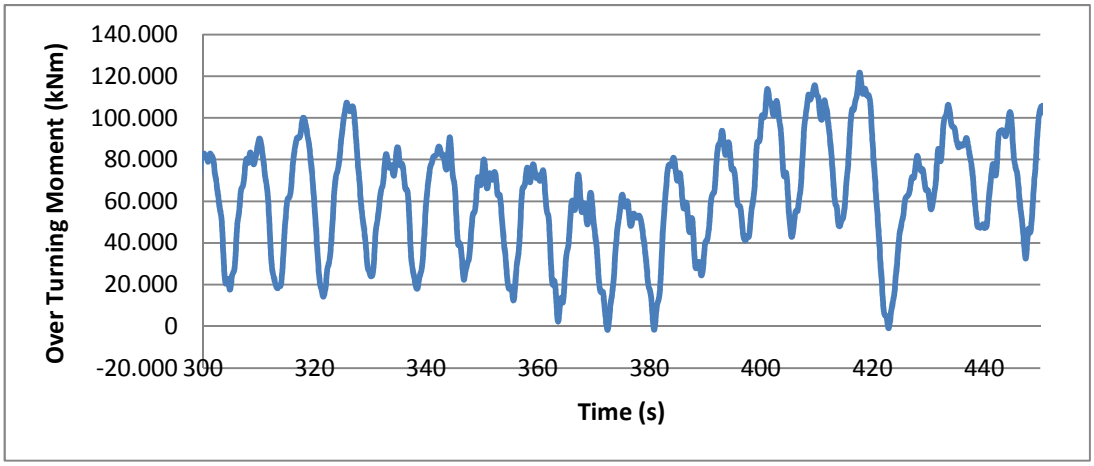

(c)

Figure 3.22. Time history data for operating speed case - seed number five, (a) Wind speed, (b) Base shear, (c) Over turning moment

Table 3.10. Maximum analysis results on structures for operational speed case

Seed	Wind Speed (m/s)	Base Shear (BS) (kN)	Overturning Moment (OTM) (MN·m)
1	20.0	2181	131.1
2	18.6	2196	127.9
3	18.36	2233	130.9
4	17.94	2323	136.0
5	19.05	2226	123.3
6	19.83	2262	134.8
7	21.13	2251	124.8
8	19.9	2227	127.8
9	19.03	2199	125.3
10	18.84	2149	130.0
Average		2225	129.2

3.2.3.2. 50-year Return Period Case. Ten stochastic wind speed seeds were performed for 50-year return period storm case for the site, and, the average of the resultant forces was obtained. The Figure 3.23 below show two different seeds to compare how the wind speed changes.

Maximum wind speed on the first wind seed is 62.83 m/s on the figure above. On the other hand, the wind speed in the second seed reaches 58.22 m/s.

Moreover, Figure 3.24 shows one of the load time histories on monopile at 50-year return period storm case for seed number four.

The result of the analyses for ten seeds is shown in the Table 3.11. The results of BS and OTM for the monopile were taken from 4 meters below the mudline.

According to the Table 3.11, the maximum percentage change of wind speeds is about 10% (i.e. the speeds differ from 57.3 m/s to 62.8 m/s), the maximum percentage

change in OTM is about 4% (i.e. the OTM results differ from 133.1 MNm to 138.7 MNm). and, the maximum percentage change in BS is about 1% (i.e. the BS results differ from 4024 kN to 4071 kN).

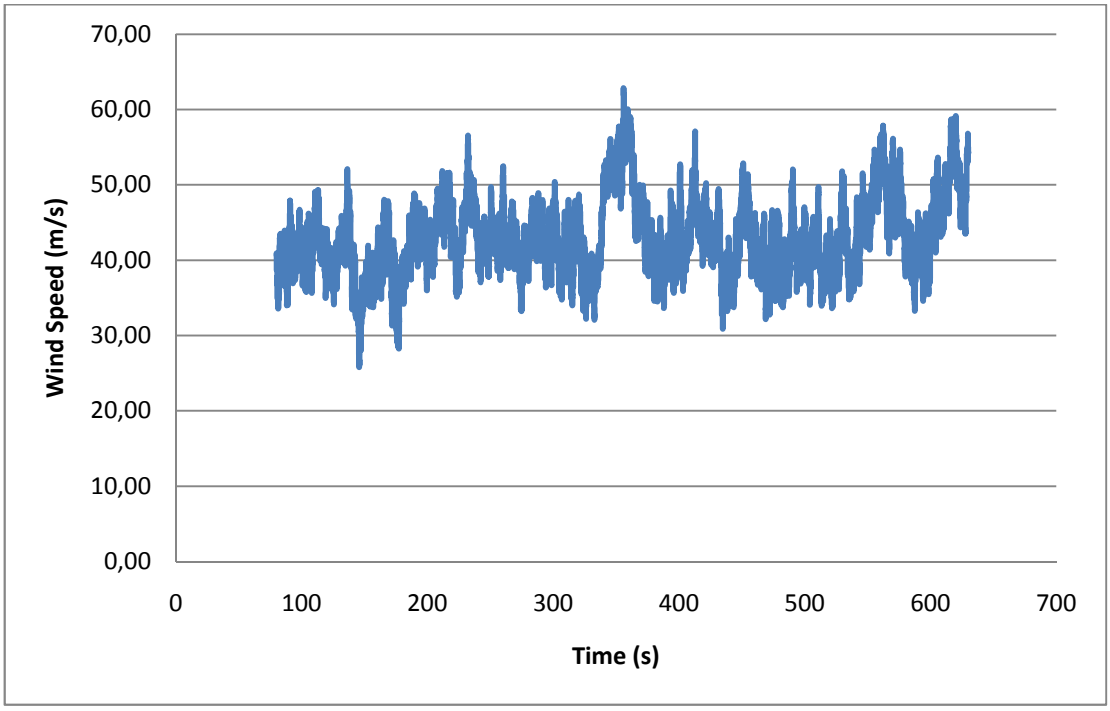

(a)

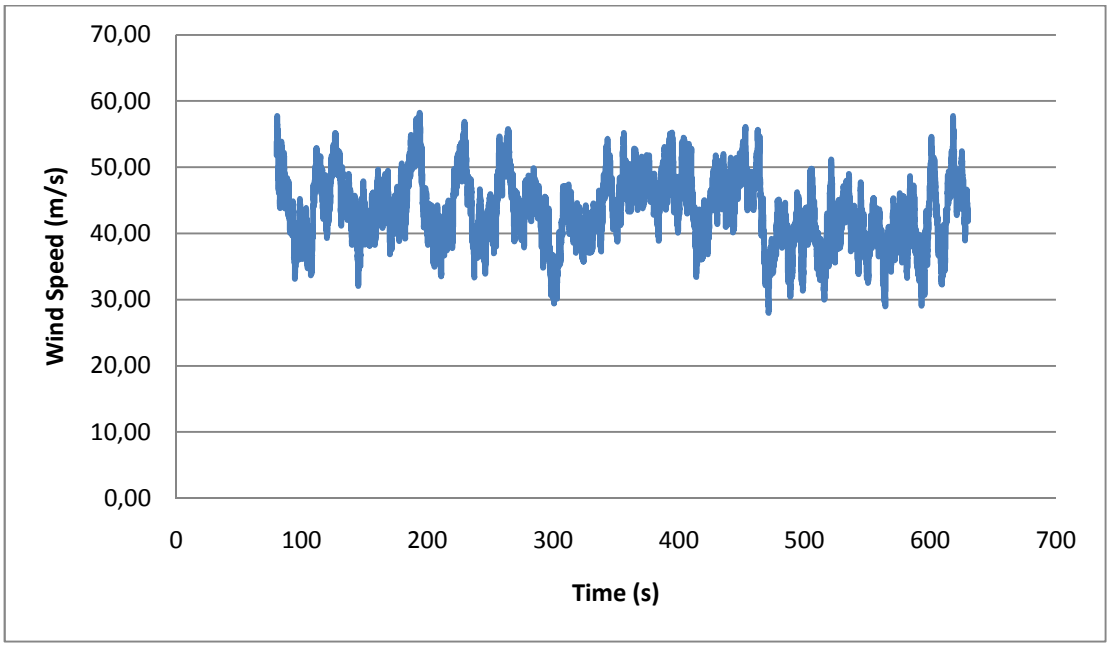

(b)

Figure 3.23. Wind speed seeds for 50-year return period storm case ($W_{s,average}$ =42.98 m/s) (a) Second wind speed seed (b) Seventh wind speed seed

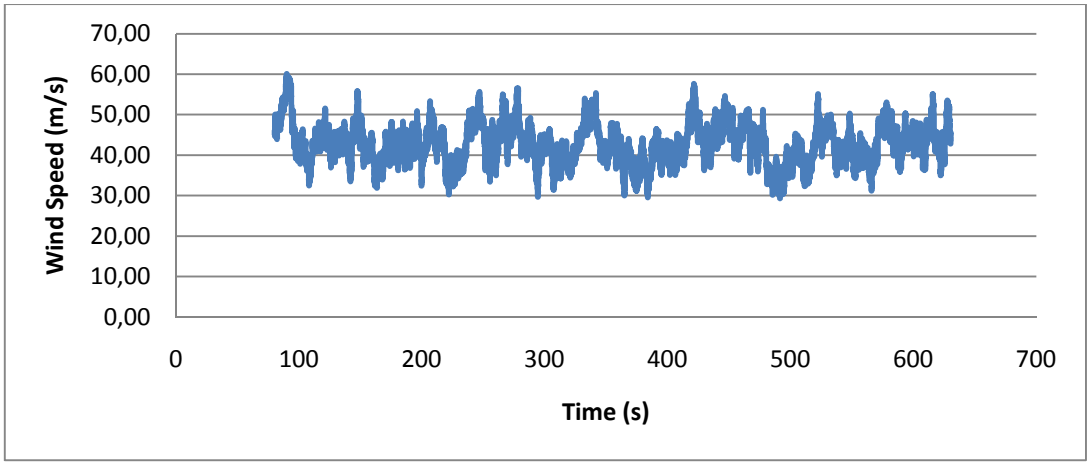

(a)

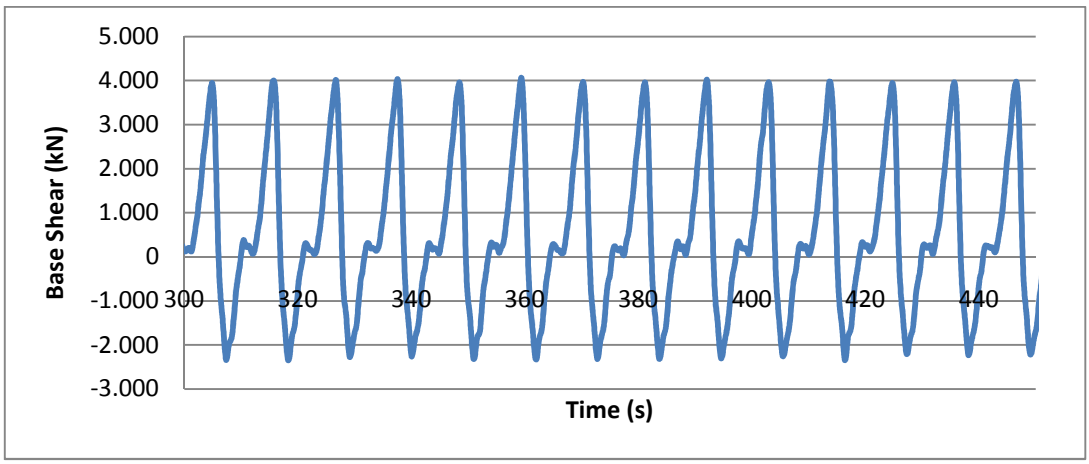

(b)

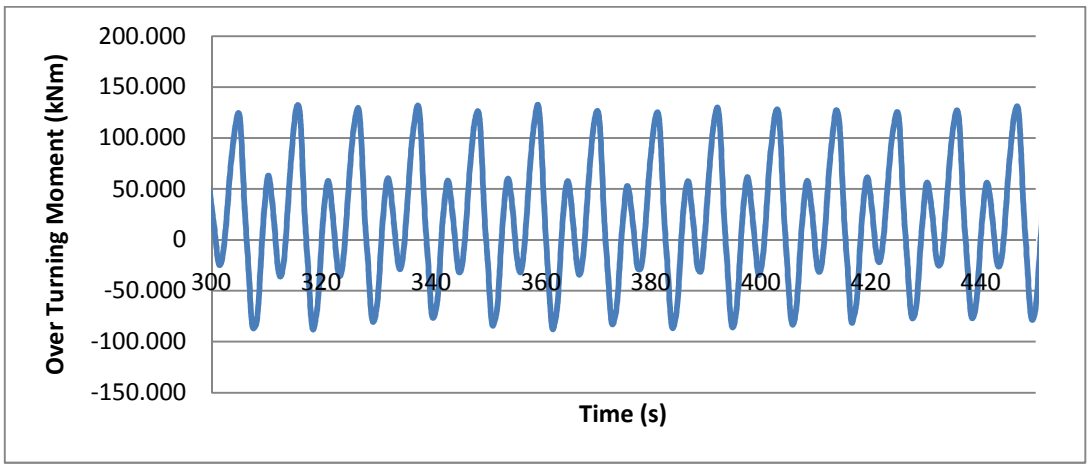

(c)

Figure 3.24. Time history data for 50-year return period storm case - seed number four, (a) Wind speed, (b) Base shear, (c) Over turning moment

Table 3.11. Maximum analysis results on structures for 50-year return period storm case

Seed	Wind Speed (m/s)	Base Shear (BS) (kN)	Overturning Moment (OTM) (MN·m)
1	59.1	4067	137.2
2	62.8	4057	137.0
3	58.7	4045	136.5
4	60.0	4071	138.7
5	57.6	4056	135.8
6	58.2	4036	135.4
7	57.5	4035	136.4
8	57.3	4044	135.9
9	58.7	4045	137.7
10	58.3	4024	133.1
Average		4048	136.4

3.2.3.3. 100-year Return Period Case. Ten stochastic wind speed seeds were performed for 100-year return period storm case, and, the average of the resultant forces was obtained. The Figure 3.25 below show two different seeds to compare how the wind speed changes.

Maximum wind speed on the first wind seed is 62.93 m/s on the graph above. On the other hand, the wind speed in the second seed reaches 69.11 m/s.

Moreover, Figure 3.26 shows one of the load time histories on monopile at 100-year return period storm case for seed number four.

The result of the analyses for ten seeds is shown in the Table 3.12. The result of the base shear and over turning moment for the monopile were taken from 4 meters below the mudline.

According to the Table 3.12, the maximum percentage change of wind speeds is about 10% (i.e. the speeds differ from 62.9 m/s to 69.11 m/s), the maximum percentage

change in OTM is about 4% (i.e. the OTM results differ from 156.9 MNm to 162.9 MNm). and, the maximum percentage change in BS is about 1% (i.e. the BS results differ from 5126 kN to 5171 kN).

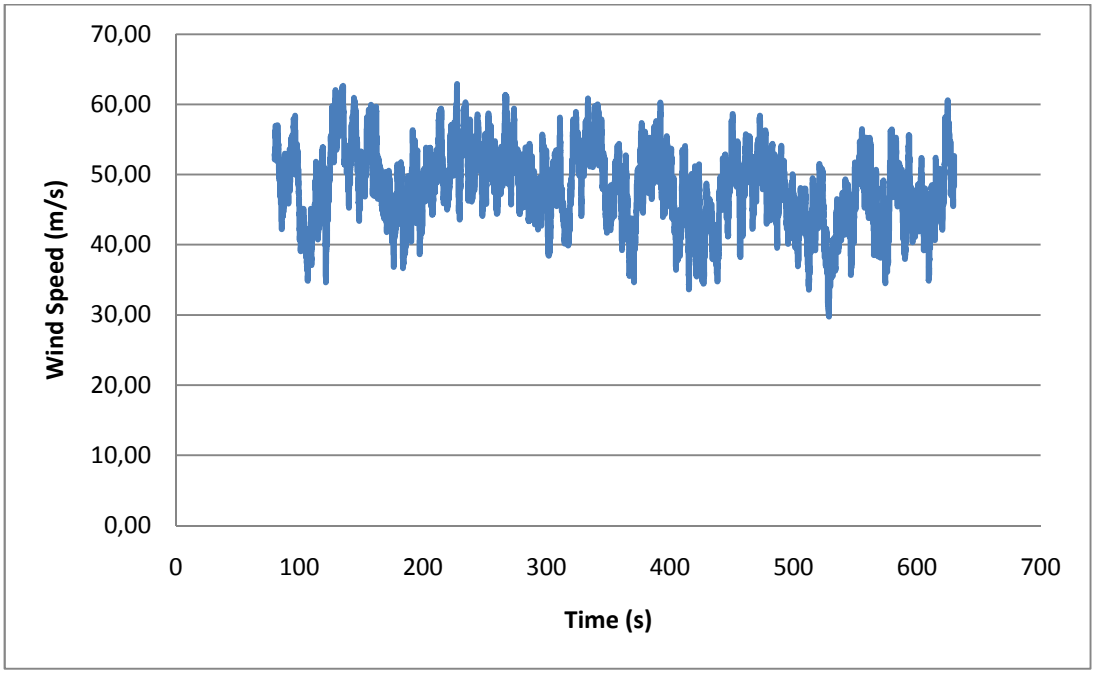

(a)

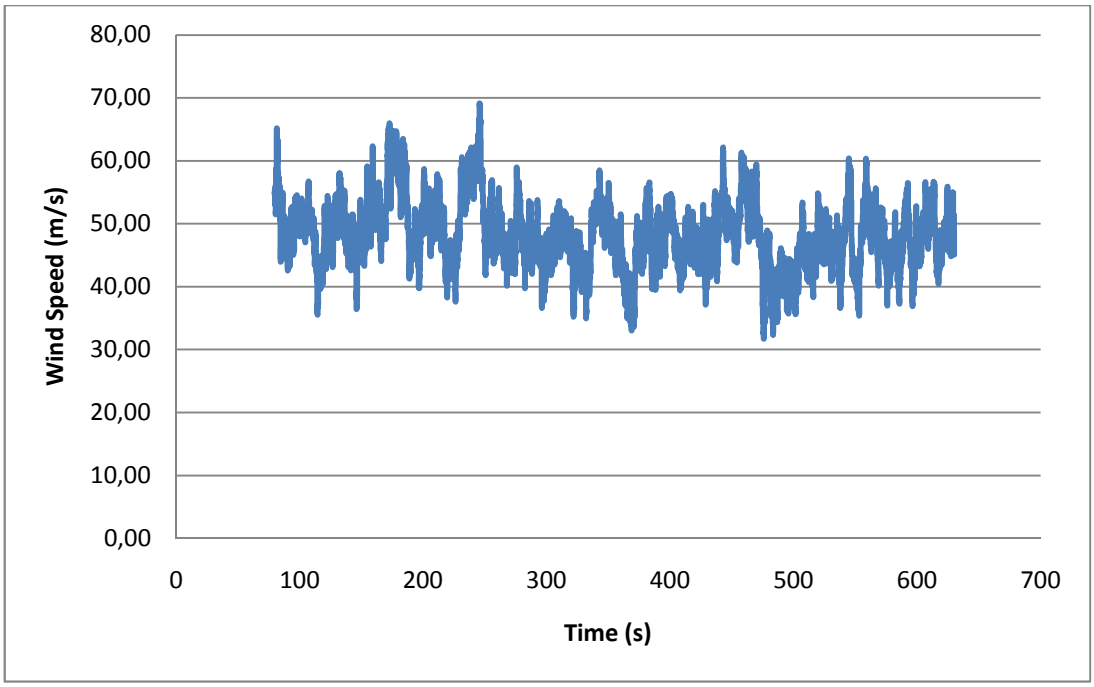

(b)

Figure 3.25. Wind speed seeds for 100-year return period storm case ($W_{s,average}$ = 48.35 m/s) (a) Third wind speed seed (b) Fifth wind speed seed

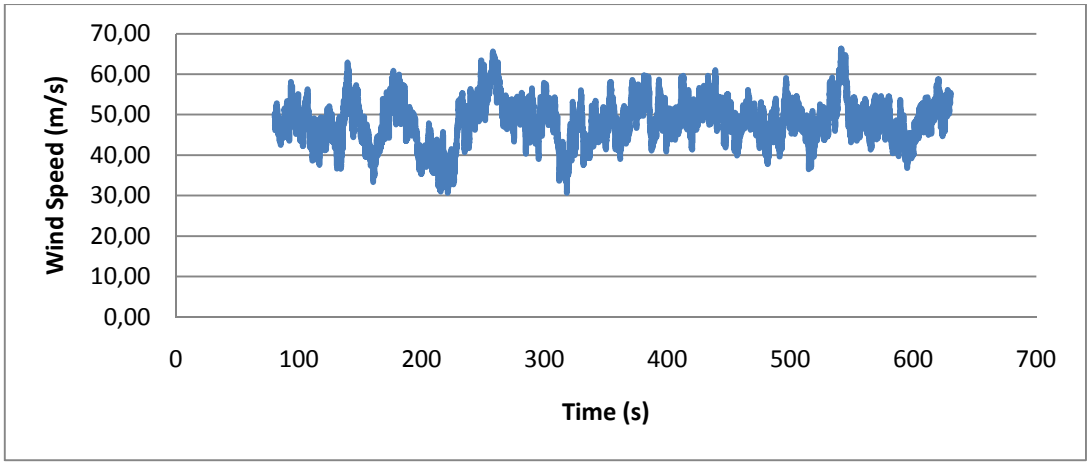

(a)

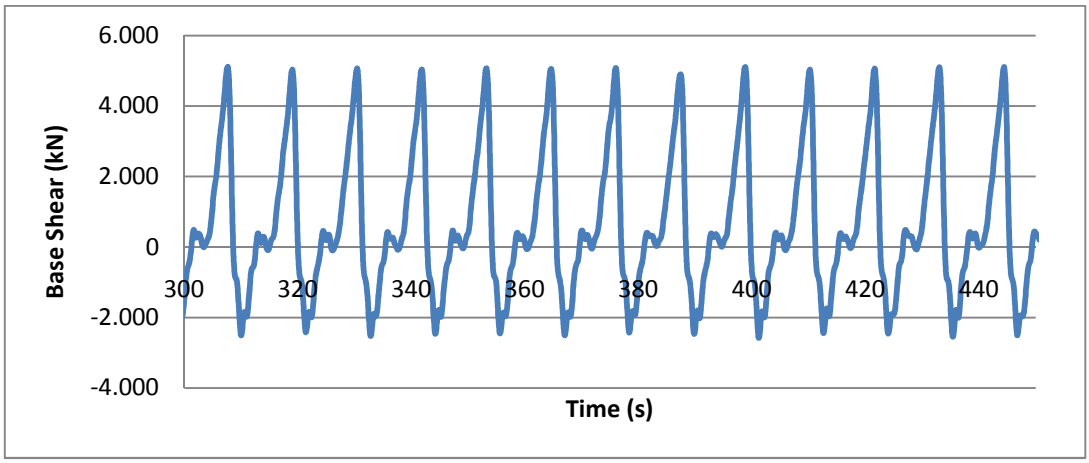

(b)

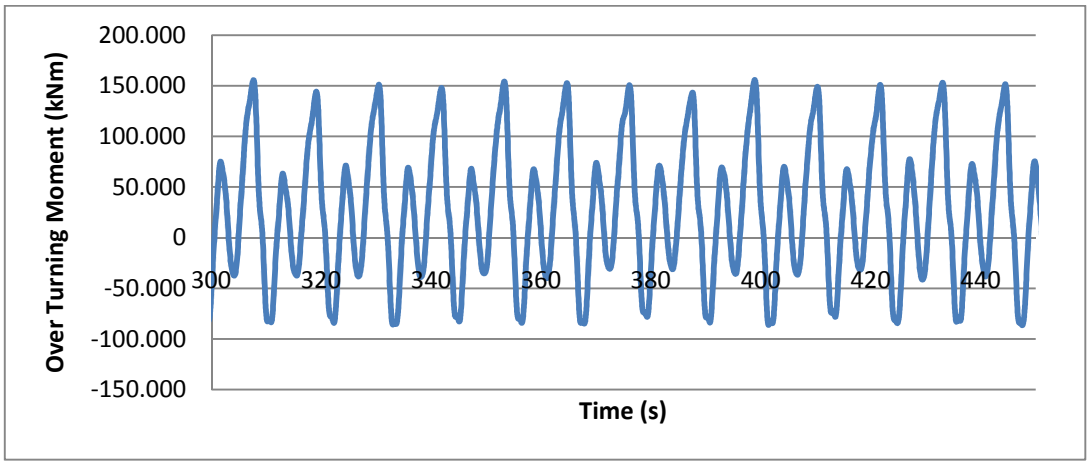

(c)

Figure 3.26. Time history data for seed number four, (a) Wind Speed, (b) Base Shear, (c) Over Turning Moment

Table 3.12. Maximum analysis results on structures for 100-year return period storm case

Seed	Wind Speed (m/s)	Base Shear (BS) (kN)	Overturning Moment (OTM) (MN·m)
1	64.9	5147	159.9
2	65.62	5171	159.4
3	62.9	5151	157.8
4	66.28	5126	160.0
5	69.11	5144	157.4
6	66.72	5158	160.3
7	67.75	5146	162.9
8	63.39	5130	156.9
9	65.61	5159	160.3
10	63.08	5132	162.0
Average		5146	159.7

3.2.3.4. Monopile Design Loads. The summary of the analyses result is presented in Table 3.13 below. Wind load on tower was also added to the design loads.

Table 3.13. Monopile design loads

Base Shear (kN)			
Storm Type	Coupled Wind-Wave	Tower Wind	Total
Operating Storm	2225	13.4	2238
50-year Storm	4048	195.4	4243
100-year Storm	5146	247.2	5393
Overturning Moment (MNm)			
Storm Type	Coupled Wind-Wave	Tower Wind	Total
Operating Storm	129.2	1.0	130.2
50-year Storm	136.4	14.7	151.1
100-year Storm	159.7	18.8	178.5

3.3. Strength Check

The strength check of the monopile was carried out according to API RP2A-WSD guidelines part 3.2. And, the method was mentioned previously section 2.5.2.

The allowable compression stress, F_a, the allowable bending stress, F_b, and, the allowable shear stress, F_v, for the monopile in this study are determined below (Equations 2.10 – 2.17).

Therefore,

$$F_{xe} = \frac{2CEt}{D} = 2520\ MPa$$

$$F_{xc} = F_y * \left[1.64 - 0.23 * (\frac{D}{t})^{\frac{1}{4}}\right] = 228.2\ MPa$$

$$F_{y,new} = Smaller\ (F_{xe}; F_{xc}) = 228.2$$

$$C_c = \left(\frac{2\pi^2 E}{F_{y,new}}\right)^{\frac{1}{2}} = \left(\frac{2\pi^2 21000}{228.2}\right)^{\frac{1}{2}} = 134.78$$

$$F_a = \frac{\left[1-\frac{\left(\frac{Kl}{r}\right)^2}{2C_C^2}\right] * F_{y,new}}{\frac{5}{3} + \frac{3\left(\frac{Kl}{r}\right)}{8C_C} - \frac{\left(\frac{Kl}{r}\right)^3}{8C_C^3}} = 104.8 \text{ MPa}$$

$$F_b = \left[0.72 - 0.58\frac{F_y D}{Et}\right] * F_y = \left[0.72 - 0.58\frac{250*6}{21000*0.06}\right] * 250 = 162.74\ MPa$$

$$F_v = 0.4 * F_y = 0.4 * 250 = 100\ MPa$$

Afterwards, the applied forces, f_t, f_b, and f_v were calculated. The forces at 4 meters below mudline are shown table below.

Table 3.14. Monopile design loads for strength check

Case	BS (kN)	OTM (MNm)	Axial Load (kN)
Operating Storm	2238	130.2	9366
50-year Storm	4243	151.1	9366
100-year Storm	5393	178.5	9366

3.3.1. Shear

The maximum shear stress, f_v, for the monopile was determined and checked by the equation 2.15 and 2.16.

$$f_{v,operation} = \frac{V}{0.5*A} = \frac{2.238}{0.5*1.11966} = 3.998\ MPa < 100\ MPa$$

$$f_{v,50year} = \frac{V}{0.5*A} = \frac{4.243}{0.5*1.11966} = 7.579\ MPa < 100\ MPa$$

$$f_{v,100year} = \frac{V}{0.5*A} = \frac{5.394}{0.5*1.11966} = 9.634\ MPa < 100\ MPa$$

All cases show that monopile is in safe side with respect to base shear.

3.3.2. Compression

$f_a < F_a$ Should be checked so that it is safe or not.

$f_a = \frac{Total\ Mass}{A} = \frac{9.366}{1.119665} = 8.365\ MPa < 104.8\ MPa$, so it is in safe side.

3.3.3. Combined Axial Compression and Bending

According to Equation 2.18;

$I = \pi(6^4 - 5.88^4)/64 = 4.94m^4$

$$f_{bx,operation} = \frac{M*y}{I} = \frac{130.2*6/2}{4.94} = 79.07\ MPa < F_b = 162.74\ MPa$$

$$f_{bx,50year} = \frac{M*y}{I} = \frac{151.1*6/2}{4.94} = 91.78\ MPa < F_b = 162.74\ \ MPa$$

$$f_{bx,100year} = \frac{M*y}{I} = \frac{178.5*6/2}{4.94} = 108.4\ MPa < F_b = 162.74\ \ MPa$$

$$f_{by,operation} = f_{by,50year} = f_{by,100year} = 0$$

Operational storm case: $\frac{f_a}{0.6F_y} + \frac{\sqrt{f_{bx}^2+f_{by}^2}}{F_b} = 0.5416 \leq 1.0$

50-year RP storm case: $\frac{f_a}{0.6F_y} + \frac{\sqrt{f_{bx}^2+f_{by}^2}}{F_b} = 0.6197 \leq 1.0$

100-year RP storm case: $\frac{f_a}{0.6F_y} + \frac{\sqrt{f_{bx}^2+f_{by}^2}}{F_b} = 0.7219 \leq 1.0$

All cases show that monopile is in safe side with respect to combined axial load and bending.

The percentage results are shown in the table below. The results show that the maximum utilization ratio is 72% of the pile capacity under combined axial and bending loads for 100-year storm case.

Table 3.15. Member utilization ratios for monopile

Storm Type	% percent capacity used	
	Combined Axial Load and Bending	Shear
Operating Storm	54.16	4.00
50-year Storm	61.97	7.58
100-year Storm	72.19	9.63

4. PARAMETRIC ANALYSIS

As a first design step, the monopile dimensions are obtained based on the resonance avoidance requirement. Afterwards, the strength requirement is checked. Resonance avoidance criterion requires that the first wave and the structural period should be well separated; however, in this study, it was found that the dynamic response of the structure is very sensitive to the wave period, because of the higher wave harmonic. This is discussed in the following sections.

4.1. Sensitivity of Dynamic Response to Higher Wave Harmonics

The wind turbines can be considered as single degree of freedom (SDOF) around their resonance regions. Around these regions, the linear elastic response of the structure to wave loading is amplified due to inertia effect. Commonly, the offshore structures are designed for their periods well apart from the predominant wave period; therefore, there is no significant dynamic amplification factor (DAF). The wave period is 8.37 sec for the operating speed case of the site; however, there might be a variation in the wave period that is discussed in the Section.2.3.2.3. It can be expected that the wave period can vary between 5 sec or 9 sec in operating speed case shown in the figure below.

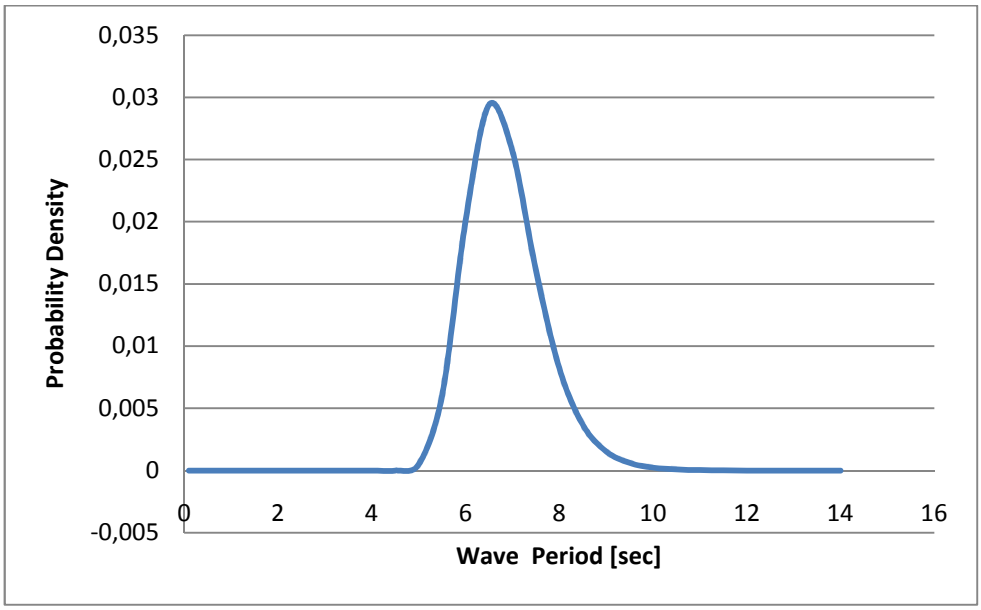

Figure 4.1. Probability density of wave period at a fixed values of the wave height 7.17m

Figure 4.2 shows the total (dynamic) responses of structure in terms of overturning moment of two different wave periods of 8 sec and 9 sec. The other properties of the waves are the same with the operating case wave properties.

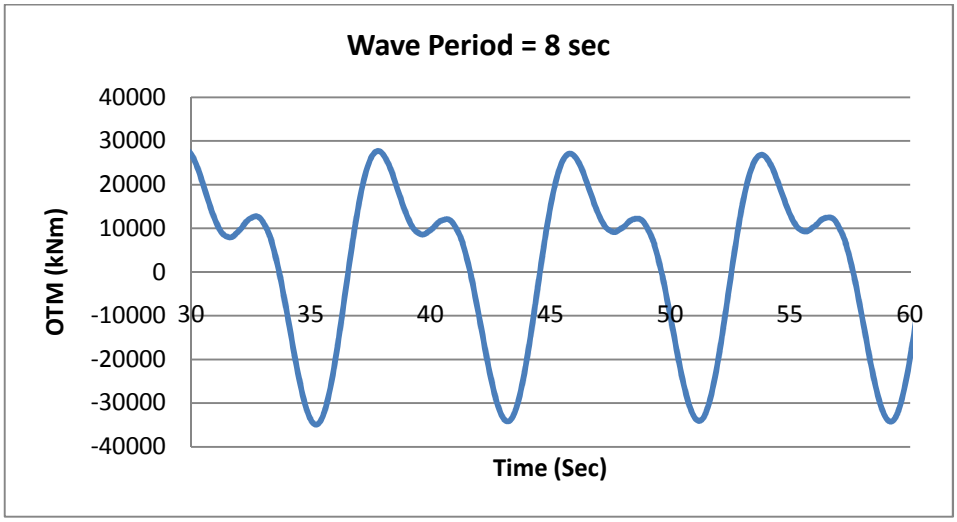

(a)

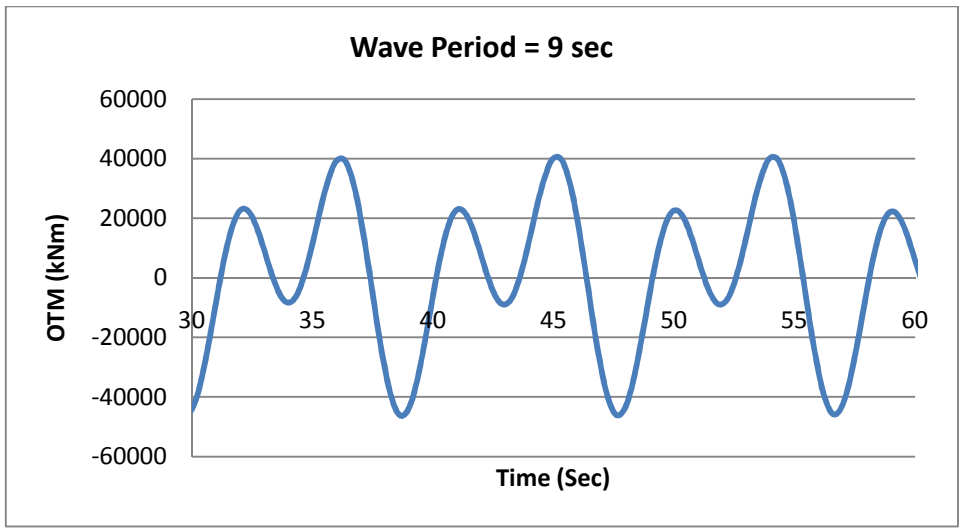

(b)

Figure 4.2. Total response of structure for overturning moment (a) 8 sec wave, (b) 9 sec wave

The total response of structure in Figure 4.2.a is smaller than the total response of the structure in Figure 4.2.b. All the variables are the same in both cases, but the wave periods. The overturning moment (OTM) values were obtained under wave loading only (i.e. there is no wind loading). There is a 45 % of increase in OTM (OTM for 8 sec wave period is 27970 kNm and OTM for 9 sec wave period is 40580 kNm). This much of

increase in dynamic response is much greater than the dynamic amplification traditionally encountered. The following analyses had been performed to understand the reasons of the situation.

4.1.1. Fast Fourier Transform Analyses

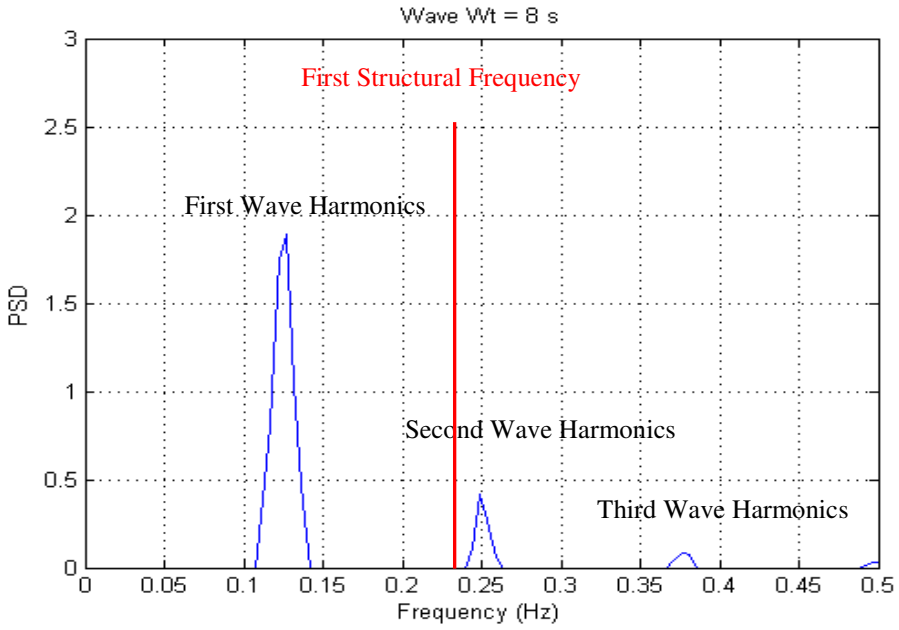

(a)

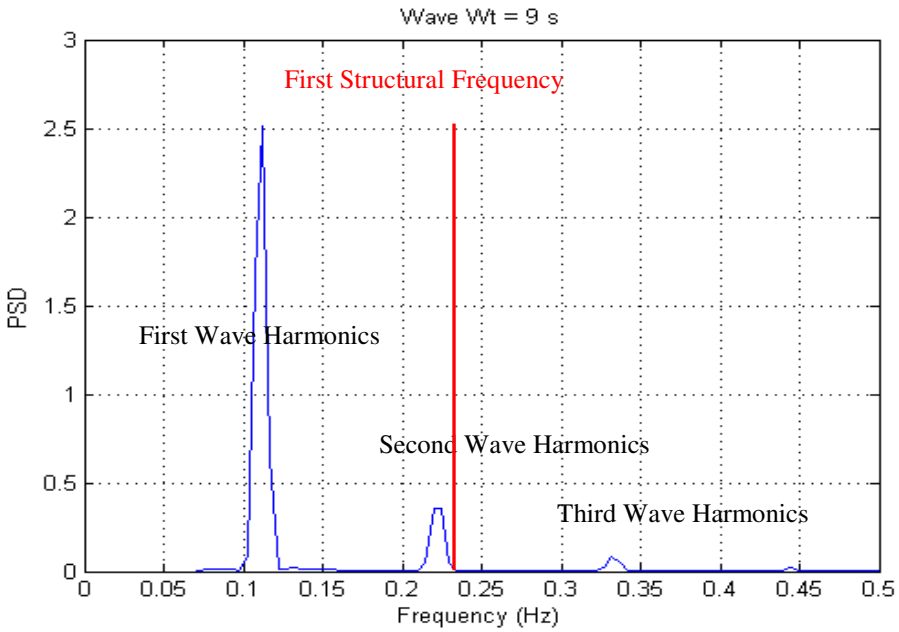

(b)

Figure 4.3. Spectral density of (a) wave period of 8 sec, (b) wave period of 9 sec

The Fast Fourier Transform (FFT) analyses were performed for the forcing and the response values. The forcing quantity was the wave with two different periods and the response quantity was overturning moment itself.

Firstly, the power spectral density of the input wave was obtained by FFT analyses shown in Figure 4.2. The figure shows the first four wave harmonics for two different wave periods.

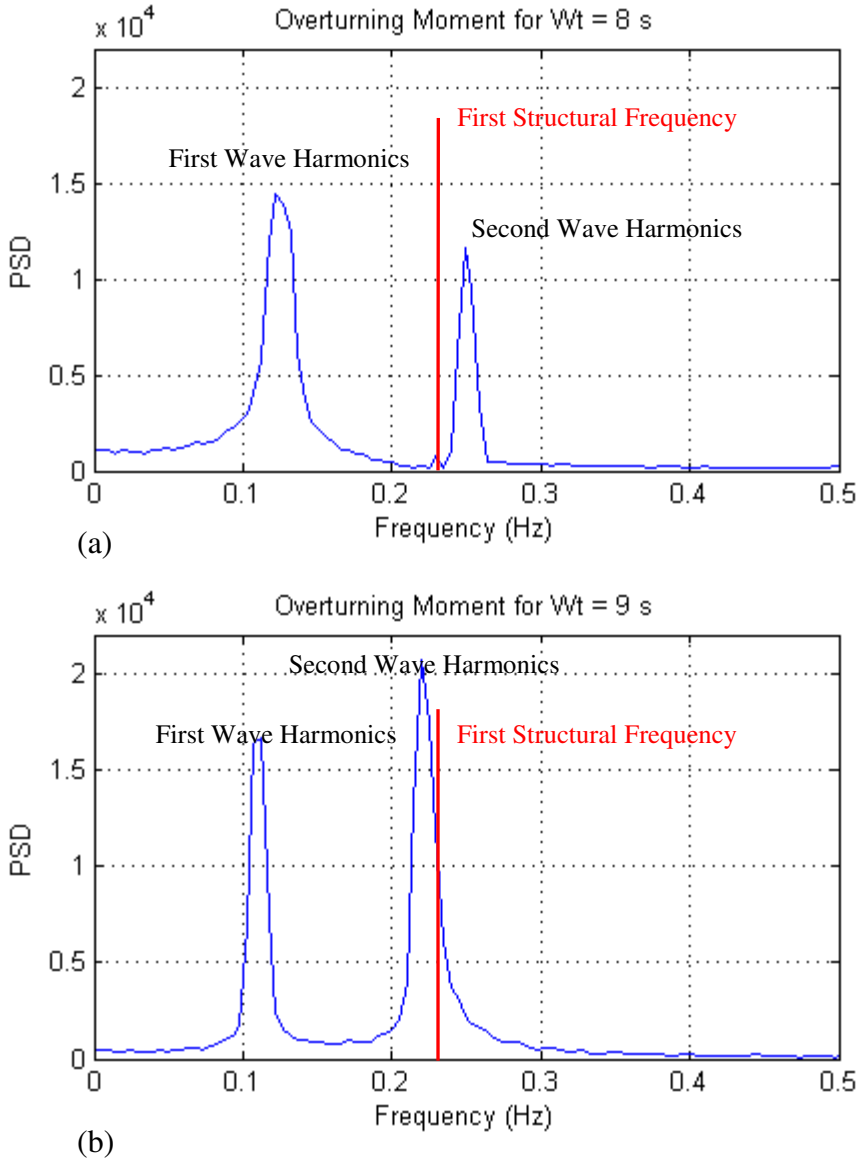

Figure 4.4. Spectral density of the structural response for overturning moment (a) wave period of 8 sec, (b) wave period of 9 sec

Natural period of the OWT analyzed in this thesis was 4.35 sec according to SAP 2000 analyses. Therefore the frequency of the structure is 0.23 Hz. This frequency is very close to second wave harmonics in both figures. The only difference is that, in Figure 4.3.a, the first structural frequency is smaller than the second wave harmonic, and, it is bigger than the second wave harmonics in Figure 4.3.b.

The frequency analysis of the response quantity in terms of overturning moment of the monopile was presented in Figure 4.4. Some observations can be made based on the Figure 4.4 as follows. The first structural frequency is closer to the second wave harmonics for two different wave periods. When the structural frequency is smaller than the second wave frequency (out of phase), response of the structure is less than the one when the structural frequency is greater than the second wave frequency (in-phase). The next section gives more details about the frequency response functions (FRF) and the response values (overturning moment and base shear of monopile at mudline).

4.1.2. Frequency Response Function and Response Values

Figure 4.5 shows the response function for the structure with two wave harmonics of different periods. The figure below was plotted according to Equation 2.1.

Figure 4.5 shows that second harmonic of wave with 8 sec period is on the right hand side of the peak of the response curve. However, there is “deamplification” in the dynamic response (i.e. linear elastic response and the inertia response are out of phase). Moreover, second harmonic of the wave with 9 sec period is on the left hand side of the peak. There is “amplification” in the response. And, inertia force is in-phase with the linear elastic response of the structure. The mathematical representations of these responses are presented in Appendix A.

The response values for overturning moments for different wave periods are presented in Figure 4.6 below. The solid green line shows where the second wave harmonic coincides with the first structural period and the dashed purple line shows where the third wave harmonic coincides with the first structural period.

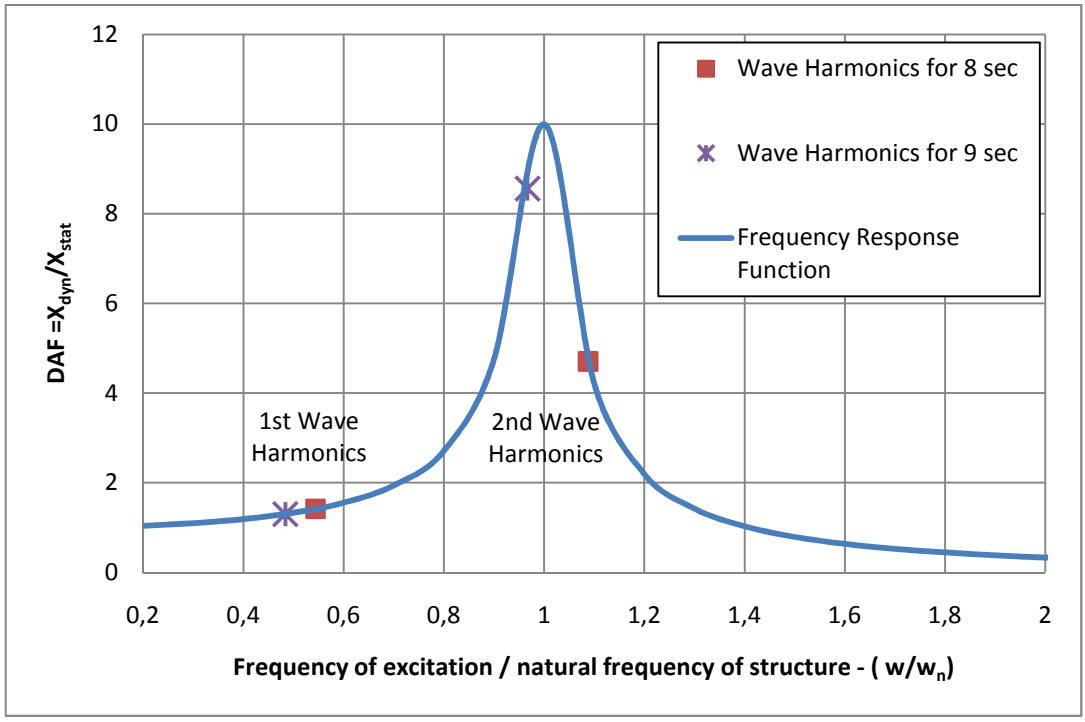

Figure 4.5. Frequency response function for structure (T = 4.35 sec)

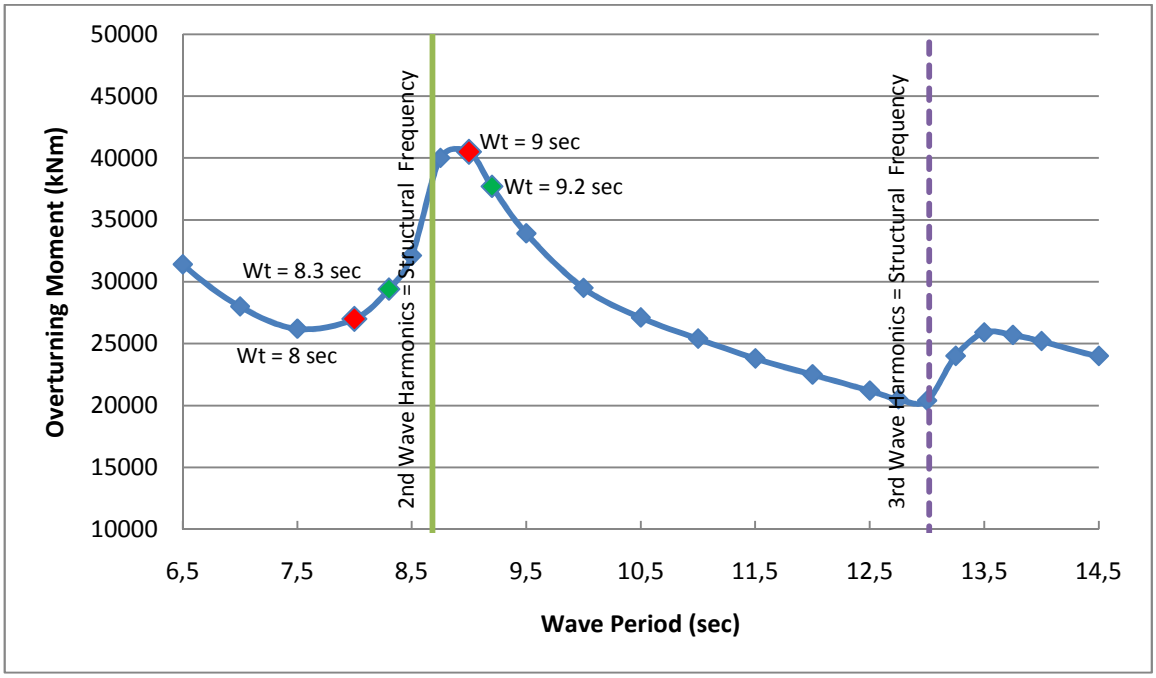

Figure 4.6. Total structural overturning moment response for different wave periods

According to the Figure 4.6, although the first structural period is well separated with the first wave harmonic which is compulsory, second and third wave harmonics may coincide with the structural period causing significant increase in the structural response.

Note that, for Massachusetts site, 2nd harmonics of the maximum wave period in operating case (i.e. 8.37 sec / 2 = 4.18 sec) is close to the 1st structural period (i.e. wave period of 4.35 sec). On the other hand, it may be expected that the 3rd harmonics of the maximum wave period in any extreme storm conditions (i.e. wave period of 13 sec) are close to the 1st structural period but this is not the case in the extreme storm conditions in Massachusetts site.

Figure 4.6 also shows that it can be expected that the response of the structure in terms of OTM (i.e. 27000 kNm & 40500 kNm) in the operating case could be increased by 45% due to 1 sec change in the wave period (i.e. having 8.0 sec, and 9.0 sec periods). Furthermore, the response of structure for OTM (i.e. 20400 kNm & 25900 kNm) in the extreme storm case may increase by 30% due to 0.5 sec change in maximum wave periods (i.e. having 13.0 sec, and 13.5 sec periods).

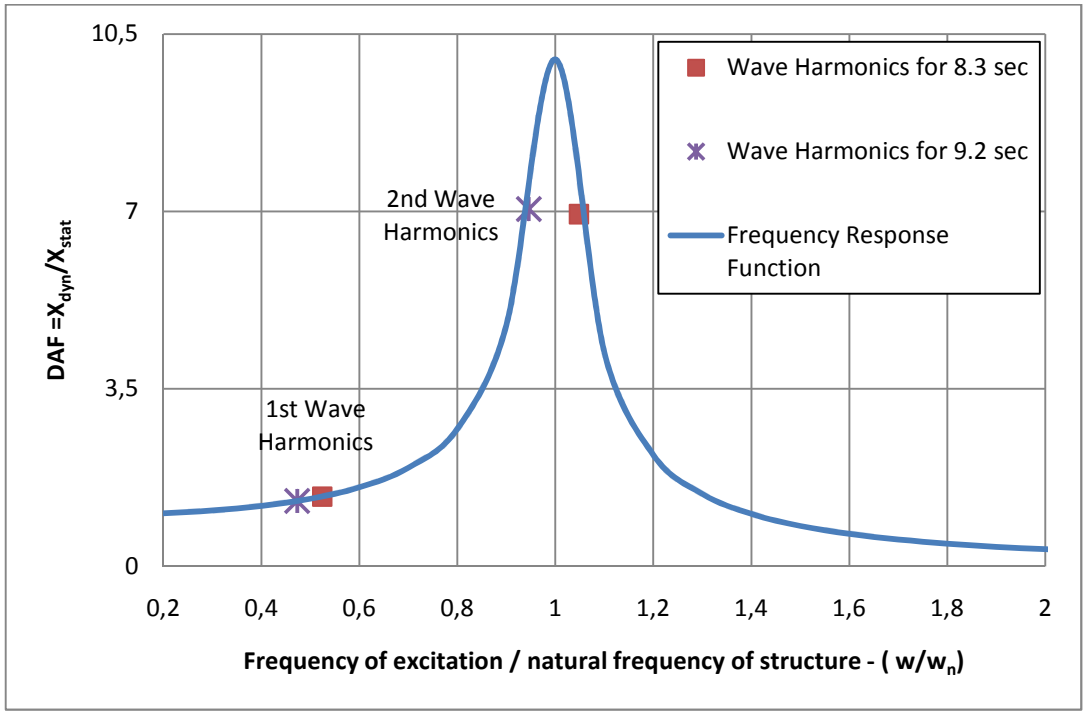

Figure 4.7. Frequency response function for structure (T = 4.35 sec) under two different wave period with same DAF

In addition to these, Figure 4.5 (i.e. the response function with 5% damping) shows that for the wave period of 8 sec, DAF is equal to 4.8. On the other hand, for the wave period of 9 sec, the DAF is 8.8. Therefore, it can be assumed that the correlation between

the structural responses seem to be proportional to the correlation between the DAF values. However, when the waves have 8.3 sec and 9.2 sec periods so that DAF is the about same for the second harmonic of the wave for any damping value (Figure 4.7). However, the responses are not the same. According to Figure 4.6, the OTM values for the two waves (i.e. having 8.3 sec, and 9.2 sec periods) are 29400 kNm and 37700 kNm, respectively. There is still approximately 30% difference in the response. That is because, the response is effected not only by the second wave harmonic but also by the first wave harmonic which should be added to the frequency response function to get correct DAF.

It is concluded that the structural response vary significantly due to the higher wave harmonics. And, DAF does not give correct amplification of the response because of the higher wave harmonic effects. It is also expected that the 1st structural frequency may vary with penetration depth and thickness of pile, or soil condition. These conditions are explained in details in following sections.

4.2. Environmental Condition

It should be noticed that there will be a variation in the design wave period at a site. Figure 4.8 shows the experimental wave data (dots) observed in the site, and the selected wave data (line) for the Massachusetts site. These experimental data has a shape fitted to the dimensionless joint probability density function in Figure 2.16 in Section 2.3.2.3.

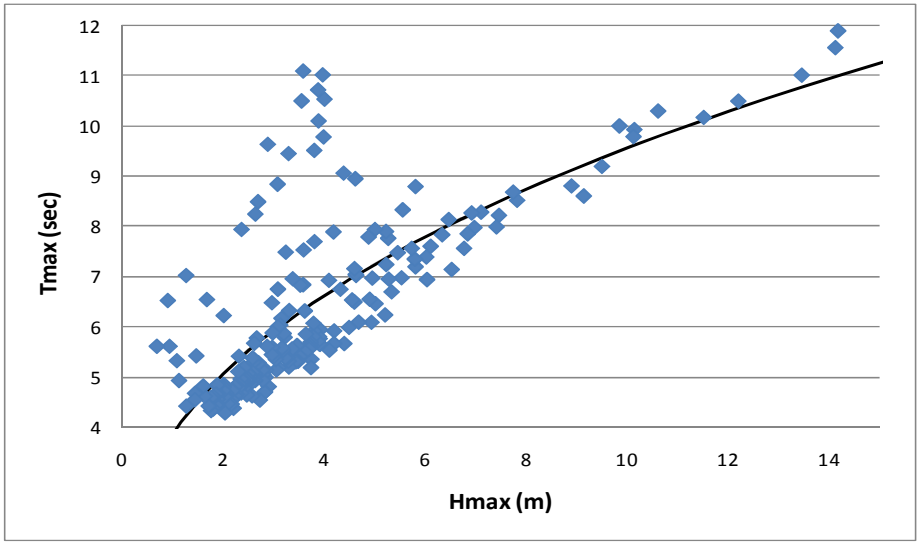

Figure 4.8. Variation of wave height with wave period [33]

It can be observed that period may vary for a given wave height. Traditionally, the design of OWTs is made for extreme and operating storm conditions. In this study, it was shown that the variation in maximum wave period should be considered to take the higher wave harmonic effect into account.

4.3. Structural Randomness

Besides the environmental condition, the penetration depth of monopile and the soil condition may change the structural period.

4.3.1. Penetration Depth

In general, when the penetration depth of a monopile structure increases, its structural period gets lower; however, there is a limit how small this period will be. After a certain depth of penetration, the period reaches its lowest value. Figure 4.8 shows how three structural periods reach their lowest values for three different monopile diameters with same thicknesses, while penetration depths change.

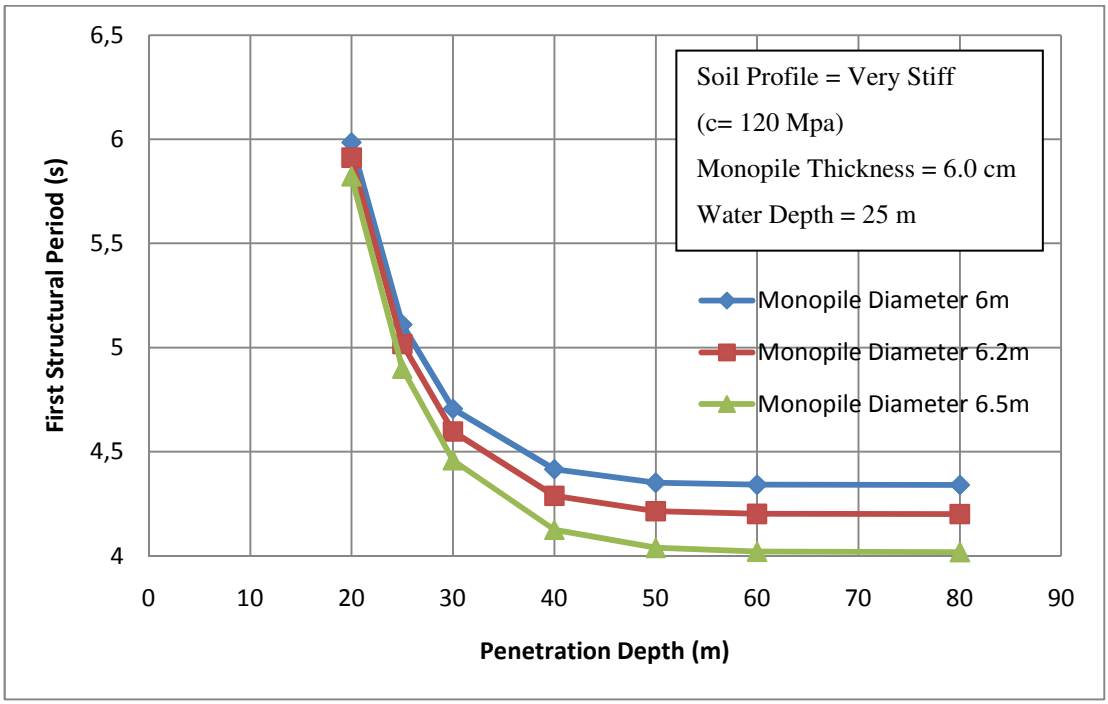

Figure 4.9. Change in the first structural period due to penetration depth for three different monopile diameters

According to the Figure 4.8, after 50 m of penetration depth, the structure period stays the same. Moreover, Figure 4.9 shows the percentage change in the first structural period with respect to the penetration depth. If a monopile has 40m of penetration depth, the period of structure changes 2% for its diameter of 6m or 6.5m. The less penetration depth may cause 40% increase in structural period. And, the change in the period is more sensitive for larger diameters.

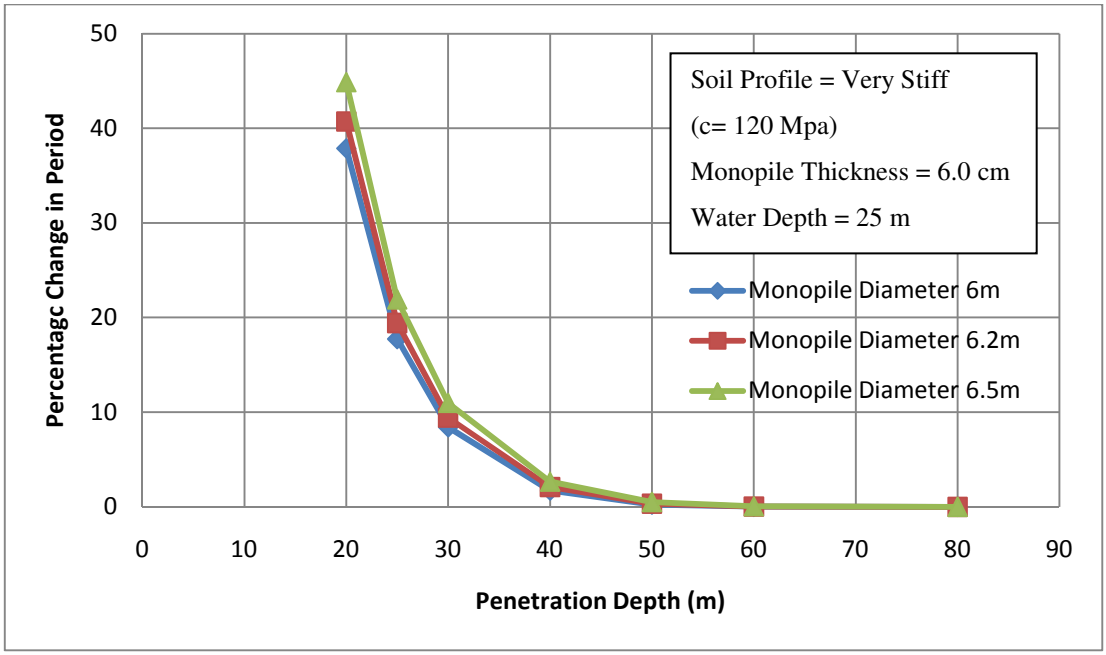

Figure 4.10. Percent change in first structural period according to penetration depth for three different monopile diameters

4.3.2. Soil Stiffness

The soil type in Massachusetts site is very stiff clay. The design analyses were made for this case. However, the change in soil itself causes the variation in structural period. Figure 4.10 shows the percent change in the period with the soil conditions presented in Table 4.1. The penetration depth is chosen to be deep enough (80 m) to eliminate its effect.

As it is seen in the figure below, the $\pm$ 60% change in soil causes 7% change in the structural frequency. It seems that it is not much of a variation in the period but it is high enough the change the "deamplified" structural response to "amplified" one (referring to section 4.1).

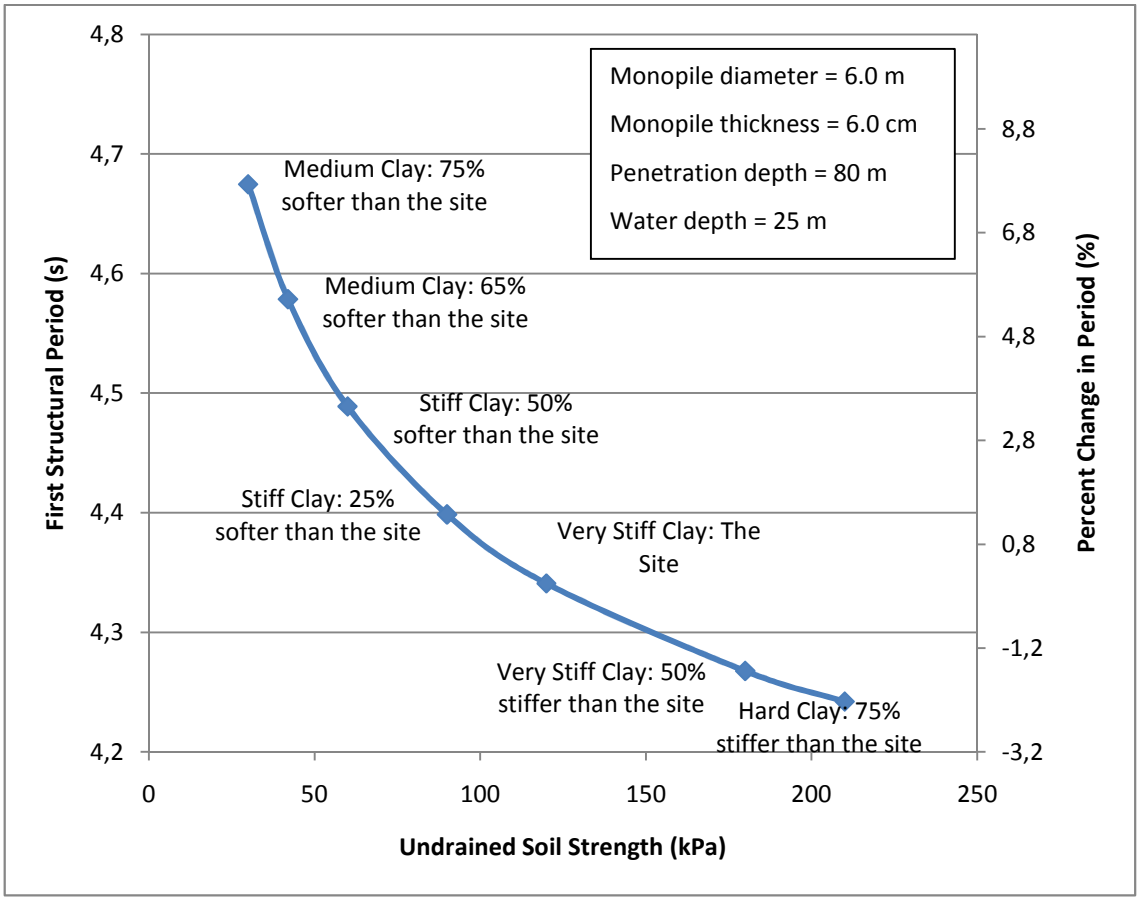

Figure 4.11. Change in first structural period according to soil profile

Table 4.1. Change in stiffness of soil profiles

Case	c (kPa)	Increase	Consistency	p-y Curve		t-z Curve		Q-z Curve
				k_1 (kN/m)	k_2 (kN/m)	k_1 (kN/m)	k_2 (kN/m)	k_1 (kN/m)
1	210	75%	Hard	46116	12682	21000	11550	87500
2	180	50%	Very Stiff	39528	10871	18000	9900	75000
3 Massach.	120	0%	Very Stiff	26352	7247	12000	6600	50000
4	90	-25%	Stiff	19764	5435	9000	4950	37500
5	60	-50%	Stiff	13176	3624	6000	3300	25000
6	42	-65%	Medium	9223	2536	4200	2310	17500
7	30	-75%	Medium	6588	1812	3000	1650	12500
8	18	-85%	Soft	3953	1087	1800	990	7500

In the study [40], monopiles are designed using p-y curve based on finite element (FE) modeling. The study shows that the standard p-y method (according to API RP2A)

overestimates the pile-soil stiffness of large diameter piles. And, modification for p-y curve is needed. However, that modification was not considered in this thesis, so the soil was actually assumed stiffer than it should be in the calculations above.

On the other hand, generally, penetration depth for OWTs is chosen to be less than 40 meters. For this case the soil conditions has great effect on the structural period. This situation was explained in the optimization study. Moreover, the percent change in soil conditions were not modeled i.e. only the in-situ data of very stiff clay was considered.

5. OPTIMIZATION ANALYSIS

The structure was designed for 5MW turbines at 25m water depth. Dimensions of the members were determined to avoid the resonance. The ultimate strength check was performed for the final member dimensions, as well.

Monopile structures have three design parameters which are monopile diameter, *D*, thickness, *t*, and the penetration depth, *L*. All of these parameters affect the frequency of monopile. The monopile has diameter of 6 meters, the thickness of 6 cm, and, penetration depth of 60 meters. However, this might not be the optimum solution in terms of the material. Therefore, several optimization studies were carried out.

5.1. Pile Penetration Effect

The structure gets softer as the penetration depth become less. The structural period might increase 40 %, if the penetration is not deep enough.

Figure 5.1 shows the structure period change due to penetration depth for three different soil condition having same diameter and thickness. Because the soil is very stiff in Massachusetts site, 40 - 50 m of penetration depth is deep enough to have necessary such that target period. However, if the soil gets softer, the structural period becomes more sensitive to the penetration depth.

An optimization study was performed to determine the required pile penetration depth which gives the lowest steel weight for a target period, shown in the Figure 5.2. The steel volume was 106.4 m^3 in the analyzed monopile (6 m of diameter with 60 m of penetration depth) in this thesis. However the optimization study shows that steel volume can be reduced to 85.7 m^3 with same target period. That gives 20 m^3 of reduction in steel. Therefore it is more economic to make the monopile diameter 6.2 m with constant *D/t* ratio, and penetration depth of 36m.

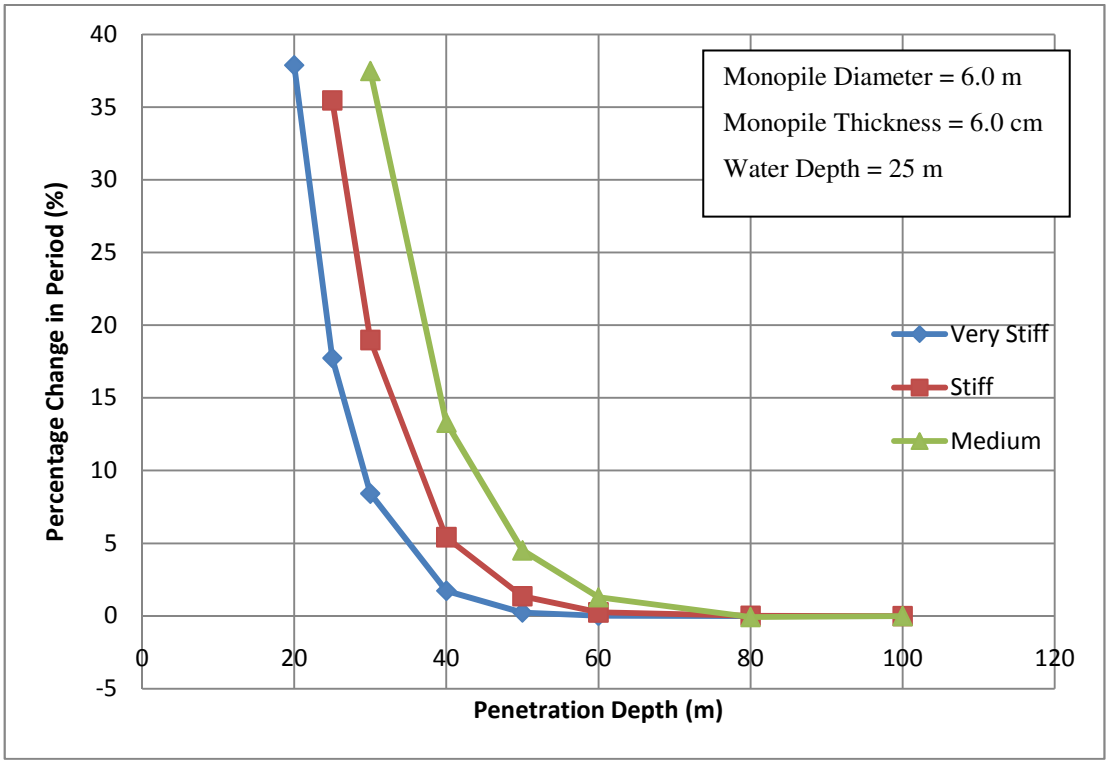

Figure 5.1. Percent change in first structural period according to penetration depth for three different soil conditions

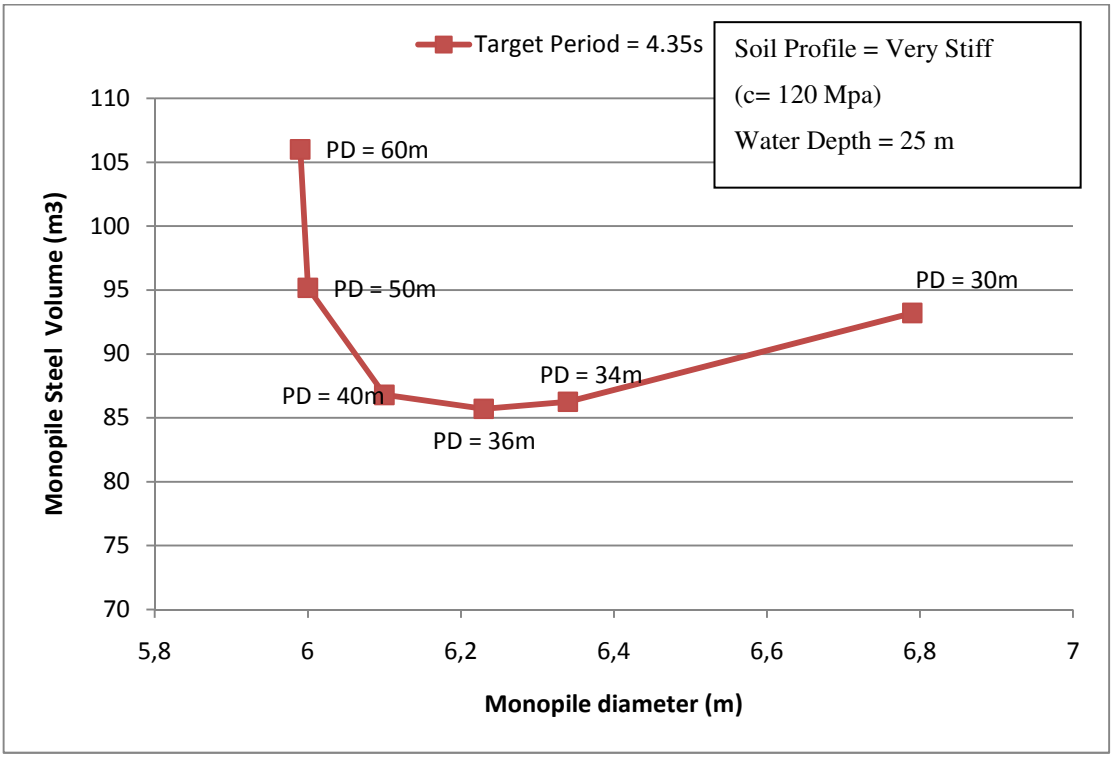

Figure 5.2. Optimization study for penetration depth

5.2. Thickness Effect

In the previous section the minimum weight was obtained by changing penetration depth while keeping D/t ratio constant. However, thickness of the pile can also be changed while keeping the penetration depth as 60 m.

Figure 5.3 shows that the optimum steel volume is where strength and resonant avoidance curves intersect. These two lines are obtained by keeping the diameter of monopile same while changing the thickness of the monopile to comply with the strength requirement (dashed line) and frequency requirement (i.e. resonance avoidance) (solid line). Therefore, the smallest volume i.e. most economical solution can be achieved. The strength requirement is fulfilled with minimum thickness, and frequency requirement is fulfilled with target period of 4.35 sec.

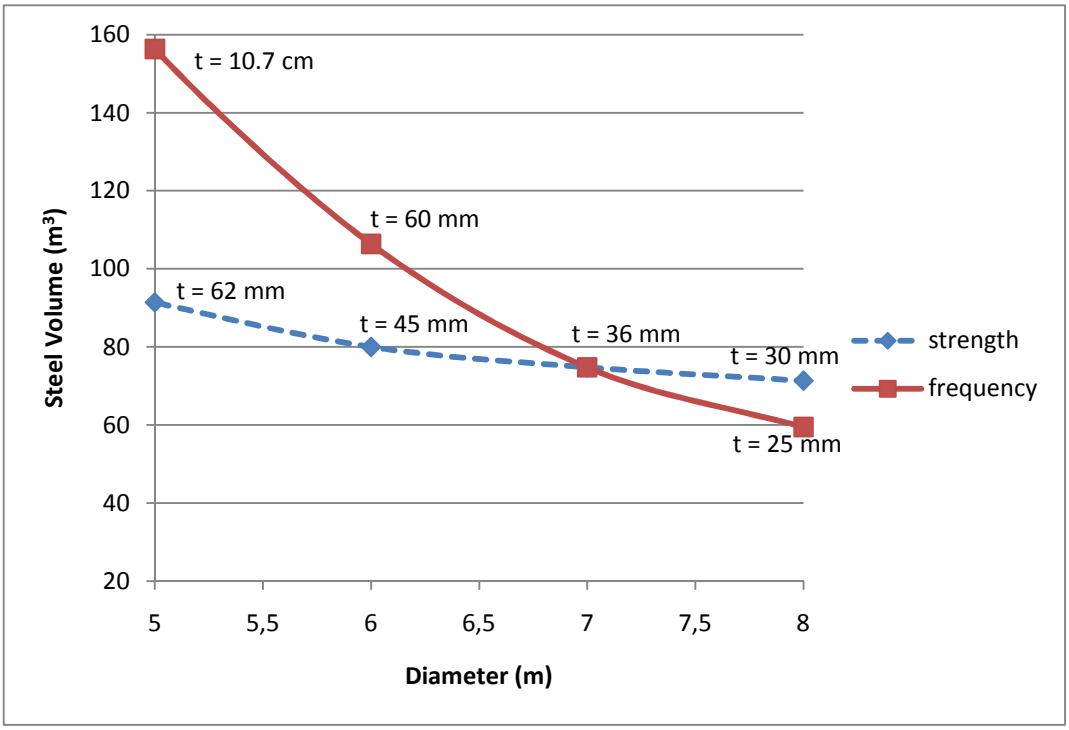

Figure 5.3. Optimization study for monopile thickness

The intersection indicates a monopile having a diameter of 7 meters. And, the thickness of 36 mm gives the most economical solution. However, *D/t* ratio equal to 195 which may not meet the drivability requirement for 60 meters of penetration depth. Drivability check was not taken into account in this thesis.

Note that, the point (t = 30mm) on strength line in the Figure 5.3 also meets the requirements. And, it is a little bit lighter than the intersection point. Because D/t ratio increases great amount in this case, it is not considered as a better solution.

5.3. Cost of a Turbine System

The optimization study has to be done for any wind farm before construction, because the cost of a turbine is extremely high. It has already mentioned in the literature review that €2/kg can be assumed for the monopile cost (installation not included). In addition to the estimation, the study "the economics of wind power" has published by European Wind Energy Association (EWEA) [42]. The study compares all the available and in construction wind farms (onshore and offshore).

Three monopile offshore wind farm are chosen for this thesis. The wind farms North Hoyle and Burbo Bank have been installed in United Kingdom shore, and the third fram, Horns Rev I has been installed in Denmark shore. All wind farms are smaller compared to the 5MW wind turbine examined in this thesis.

The general properties are presented the Table 5.1 below.

Table 5.1. Key information on three offshore wind farms

	North Hoyle (UK)	Burbo Bank (UK)	Horns Rev I (DK)
Operation Year	2003	2007	2002
Number of Turbine	30	24	80
Turbine Size (MW)	2	3.6	2
Total Capacity (MW)	60	90	160
Water Depth (m)	5 - 12	10	6 - 14
Distance from Shore (m)	7.5	5.2	14 - 17
Investment cost (€ million)	121	181	272
€ million / MW	2	2	1.7

Burbo Bank and North Hoyle have the same investment per megawatt. Horns Rev I, Burbo Bank and North Hoyle have the same investment per megawatt. Horns Rev I is the biggest wind farm. EWEA has extra cost study for the Horns Rev I, presented in the document [42]. The total cost of Horns Rev I was around €270 million. This price includes not only the turbine upper part (rotor and nacelle),but olso transmission cable cost, foundation cost, design and project management cost, and environmental analysis cost.

The share of the parts in total cost are summarised below,

- Sea transmission cable cost has 21% share of total cost,
- Upper part of the turbine cost has 49% share of total cost (turbine transportation and erection included),
- Foundation cost has 21% share of total cost,
- Design and project management cost has 6% share of total cost,
- Environmental analysis cost has 3% share of total cost.

Foundation cost is 1/5 of the total cost. It can be calculated easily that cost of a 2MW offshore turbine foundation is €700.000. However, it is highly site depended. Moreover, because the massive tower construction is required for offshore wind farms, the construction cost is also higher than many onshore wind farms. On the other hand, while an offshore turbine foundation costs 21% of the total cost of turbine, an onshore turbine foundation cost is normally around 5- 9 % [42].

5.4. Summary of Optimization Study

The summary of this chapter is shown in the table below. Reminding that, the steel density has been chosen 8500 kg/m^3 for monopile.

Table 5.2. Summary of the optimization study

Case	Diameter (m)	Thickness (m)	D/t	Penetration Depth (m)	Steel Volume (m^3)	Steel Weight (tons)
1	6.23	0.0623	100	36	85.7	728.45
2	7	0.036	195	60	74.8	635.8

The second case gives the economical solution, however the D/t ration may not stiff enough to penetrate the pile for 60 meters. Furthermore, the cost of the monopile in the second case can be increased by the transportation, installation, drivability, and hamming effects.

Therefore, the first case is chosen to be the most economical solution because of the drivability. Compared to the monopile considered in this thesis, the steel volume can be reduced 20 m^3 that is 19% reduction in weight and the cost of the foundation.

6. CONCLUSION

Throughout this study, several concepts for monopile type OWT design were presented. The following specific conclusions can be drawn.

For design studies;

- The constant wind speed should not be used for analyses because the response of the structure for stochastic wind speed was more than twice of the responses for constant wind speed. And also, due to the stochastic nature of the turbulent wind load, there can be 15% variation in overturning moment for each simulation. Means of 10 simulations was acceptable for the level of accuracy of the response.
- Regarding to the foundation models (i.e. distributed spring model, effective fixity length approach, and coupled spring model), all three models show less than 1 % difference in the first structural periods. The effective fixity length model is less complicated than the other two models.
- The support structure was designed to avoid resonance due to the OWT rotor. According to the Campbell diagram, the first structural period of the OWT was chosen between 1P and 3P range (i.e. soft-stiff range). The first wave excitation was also avoided in that region. Therefore, the target structural frequency was selected as 0.22 Hz (i.e. structural period is 4.5 sec).
- The design results showed the maximum utilization ratio of the pile is 72% to its capacity under combined axial and bending loads for 100-year storm case.

For parametric studies;

- According to joint probability density function of wave, the wave period may vary at the same maximum wave height. Therefore, it is observed that the response of the structure in terms of OTM in the operation case may increase by 45% due to 1 sec change in the wave period. And, response of structure for OTM in the extreme storm case may increase by 30% due to 0.5 sec change in maximum wave period.

- It is concluded that the structural response may vary significantly due to the wave harmonics. DAF does not give always plausible amplification of the response because of the higher wave harmonic effects.
- In the scope of this thesis penetration depth lower than 30m may cause 40% increase in structural period. The period is more sensitive to higher diameters.
- The $\pm$ 60% change in soil stiffness which is reasonable due to high uncertainties in soil modeling causes 7% change in the structural frequency at 60 meters of penetration depth. This level of change is high enough for the "deamplified" structural response to be "amplified".

For optimization studies;

- Regarding to the monopile considered in this thesis, the steel volume can be reduced 20 m^3 that is 19% reduction in weight and the cost of the foundation.

Further studies;

- The monopile can be designed by modified p-y curves and taking drivability condition into account so that the modeling of the soil-structure interaction is more accurate, and the optimization study is more extensive.
- The higher wave harmonics on the other type of support structures (e.g. jacket type, ground base support type structures) for OWTs can be examined for further studies.
- Fatigue analyses can be performed. And the optimization can be done for the OWT in resonance by taking precaution for the fatigue, so that the comparison can be made for the cost of the lighter structure having extra strengthening with the cost of commonly designed OWTs.

APPENDIX A: RESPONSE TO HARMONIC VIBRATION

The differential equation (equation of motion) governing the respoonse of SDOF systems subject to an external force is presented in the Equation A.1.

$$F(t) = m\ddot{u} + c\dot{u} + ku \tag{A.1}$$

Where;

$F(t)$ = external dynamic force, N,

$u = u(t)$ = displacement, m,

m = mass, kg,

k = stiffness, kg/s^2, $k = \omega_n^2 m$,

c = damping coefficient, kg/s, $c = 2m\omega_n\zeta$,

ζ = damping ratio,

The response of SDOF system to harmonic force is

$$F(t) = F_0 \sin \omega t = m\ddot{u} + c\dot{u} + ku \tag{A.2}$$

The complete solution of the Equation A.2 is

$$u(t) = u_c(t) + u_p(t) = \underbrace{e^{-\zeta\omega_n t}(A \sin \omega_D t + B \cos \omega_D t)}_{\text{Transient response}} + \underbrace{C \sin \omega t + D \cos \omega t}_{\text{steady-state response}} \tag{A.3}$$

Where, $\omega_D = \omega_n\sqrt{1-\zeta^2}$.

When force is applied on the system the total response of it becomes sum of the transient and steady-state responses together. However, transient response decays exponentially with time at a rate depending on ω/ω_n ratio and damping. After a while, essentially the forced response remains. This response is called steady-state response that is the focus on this chapter.

The particular solution $u_p(t)$ (i.e. the steady-state part) of this differential equation,

$$u_p(t) = C \sin \omega t + D \cos \omega t \tag{A. 4}$$

The Equation A.2 is modified by dividing equation into m.

$$\frac{F_0}{m} sin\, \omega t = \ddot{u} + 2\zeta \omega_n \dot{u} + \omega_n^2 u \tag{A. 5}$$

Substitute A.4 into its first and second derivative into A.5.

$$\frac{F_0}{m} \sin \omega t = [(\omega_n^2 - \omega^2)C - 2\zeta \omega_n \omega D] \sin \omega t + [\, 2\zeta \omega_n \omega C + \, (\omega_n^2 - \omega^2)D \,] \cos \omega t \tag{A. 6}$$

To find the C and D, divide the Equation A.6 by ω_n^2 and using the relation $k = \omega_n^2 m$

$$\left[1 - \left(\frac{\omega}{\omega_n}\right)^2\right] C - \left(2\zeta \frac{\omega}{\omega_n}\right) D = \frac{F_0}{k} \tag{A. 7}$$

$$\left(2\zeta \frac{\omega}{\omega_n}\right) C + \left[1 - \left(\frac{\omega}{\omega_n}\right)^2\right] D = 0 \tag{A. 8}$$

Therefore,

$$C = \frac{F_0}{k} \frac{1 - (\omega/\omega_n)^2}{[1 - (\omega/\omega_n)^2]^2 + [2\zeta(\omega/\omega_n)]^2} \tag{A. 9}$$

$$D = \frac{F_0}{k} \frac{-2\zeta(\omega/\omega_n)}{[1 - (\omega/\omega_n)^2]^2 + [2\zeta(\omega/\omega_n)]^2} \tag{A. 10}$$

Finally, the steady state deformation becomes by using C and D found above.

$$u(t) = C \sin \omega t + D \cos \omega t \tag{A. 11}$$

It is convenient to rewrite Equation A.11 in the form,

$$u(t) = u_0 \sin(\omega t - \phi) \tag{A.12}$$

or,

$$u(t) = u_0 \cos\phi \sin\omega t - u_0 \sin\phi \cos\omega t \tag{A.13}$$

Where,

ϕ = phase angle, deg,

u_0 = the dynamic response

$C = u_0 \cos\phi \;\; and \;\; D = -u_0 \sin\phi$

Thus, $u_0 = \sqrt{C^2 + D^2}$ and $\phi = \tan^{-1}(-D/C)$. Substituting C and D gives,

$$u_0 = \frac{F_0}{k}\left[\frac{1}{\sqrt{[1-(\omega/\omega_n)^2]^2 + [2\zeta(\omega/\omega_n)]^2}}\right] \tag{A.14}$$

$$\phi = \tan^{-1}\left(\frac{2\zeta(\omega/\omega_n)}{1-(\omega/\omega_n)^2}\right) \tag{A.15}$$

We know that static deformation (i.e. linear elastic) due to harmonic force is,

$$u_{st}(t)_0 = \frac{F_0}{k}\sin\omega t \tag{A.16}$$

The maximum value of static deformation is,

$$(u_{st})_0 = \frac{F_0}{k} \tag{A.17}$$

Therefore, Equation A.14 becomes,

$$DAF = \frac{u_0}{(u_{st})_0} = \left[\frac{1}{\sqrt{[1-(\omega/\omega_n)^2]^2 + [2\zeta(\omega/\omega_n)]^2}}\right] \quad (A.18)$$

DAF is called deformation amplification factor.

Equation A.12 is plotted in Figure A.1 for three values of ω/ω_n and a fixed value of $\zeta = 0.2$. In addition to that, DAF (Equation A.18) and phase angle (Equation A.15) with a fixed value of $\zeta = 0.2$ are plotted in Figure A.2.

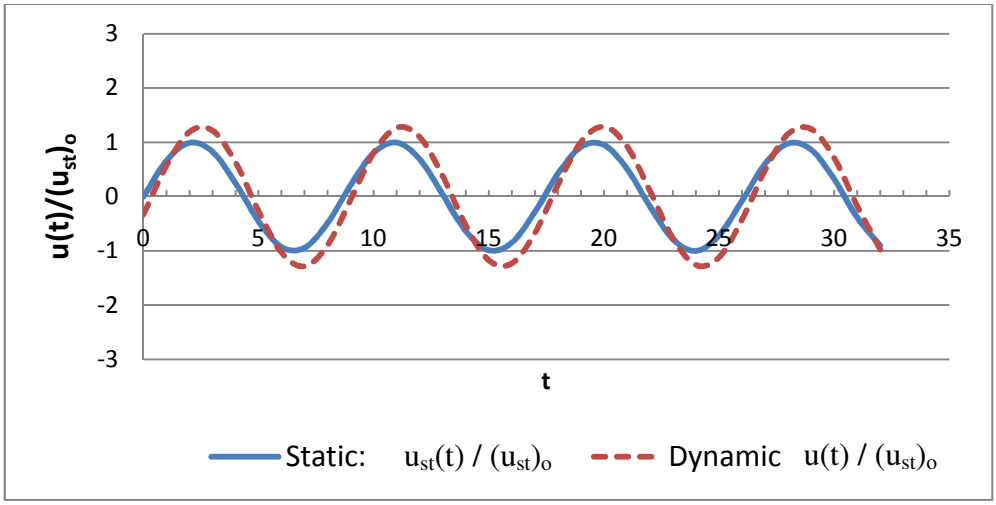

(a)

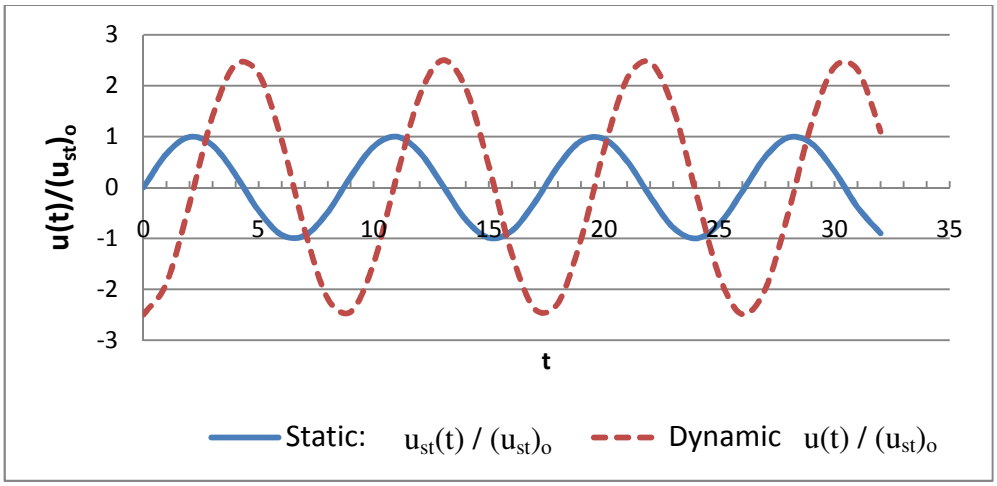

(b)

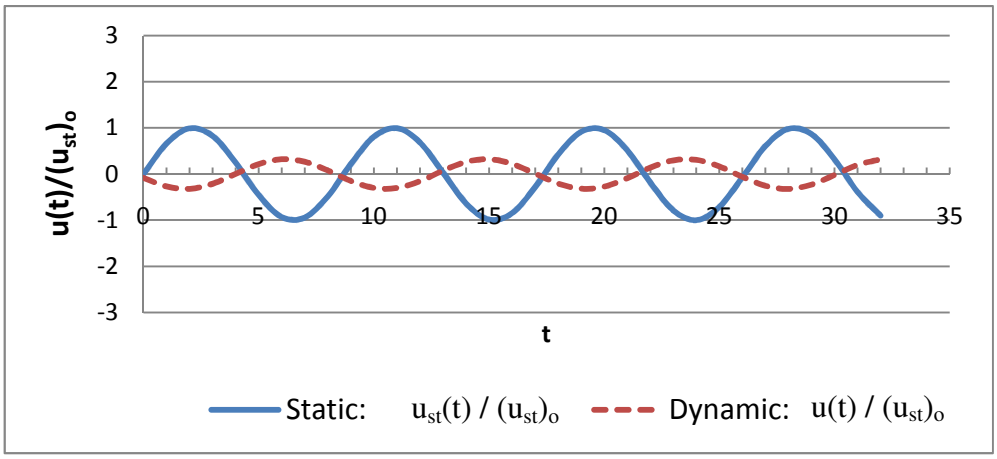

(c)

Figure A.1.Steady state response ($\zeta = 0.2$) to sinusoidal force for three frequency ratios (a) $\omega/\omega_n = 0.5$, (b) $\omega/\omega_n \approx 1$, (c) $\omega/\omega_n = 2$.

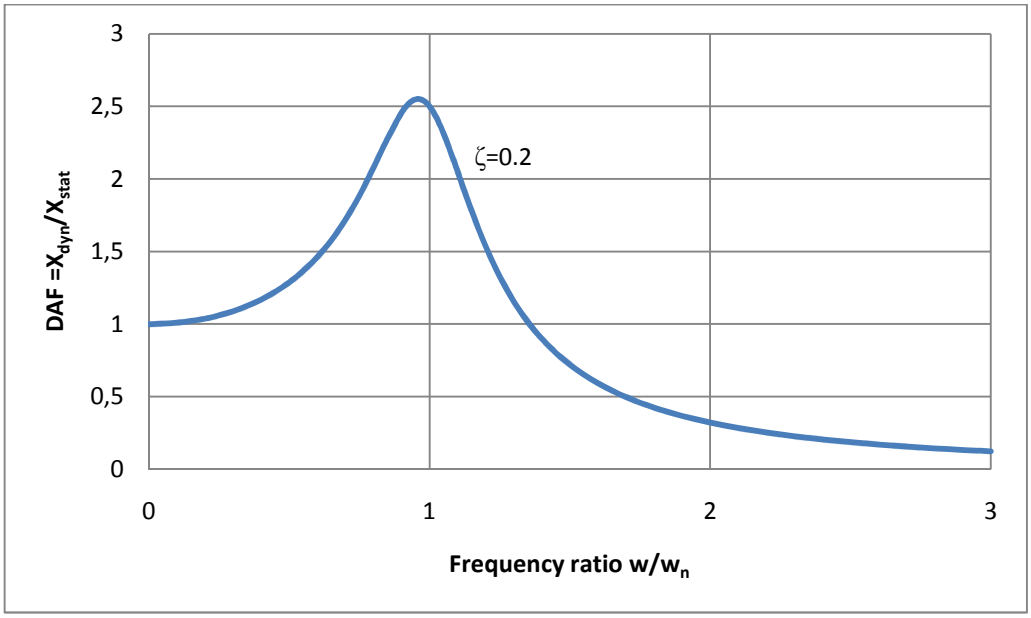

(a)

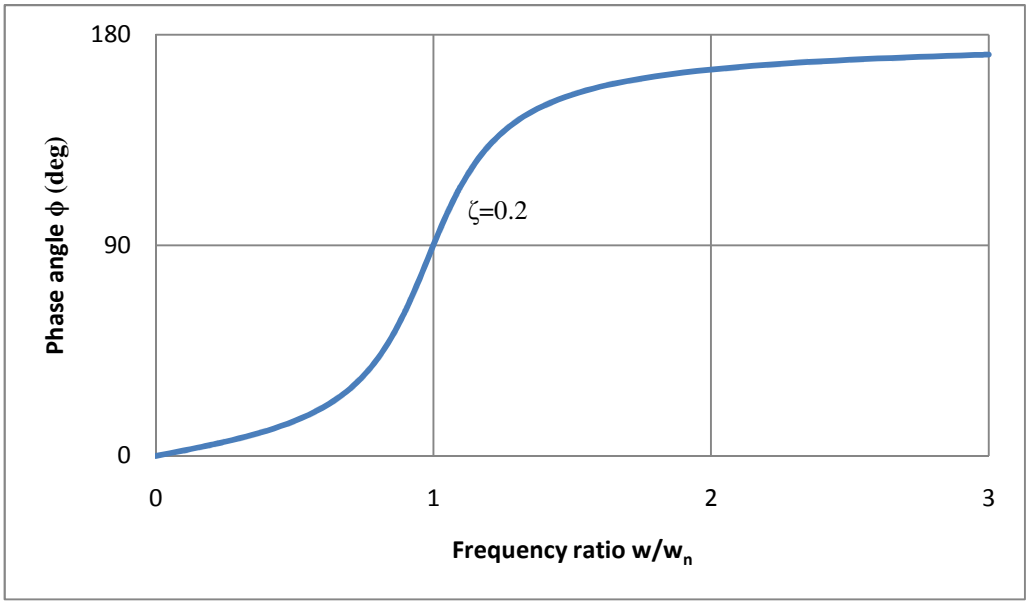

(b)

Figure A.2.Frequency response function (FRF). (a) Magnitude versus frequency (i.e. DAF), (b) Phase angle versus frequency

APPENDIX B: WAVE THEORIES

B.1. Linear Wave Theory

The most elementary wave theory was developed by Airy (1845) and called linear wave theory. Mathematically, the linear wave theory can be considered a first approximation of a complete theoretical description of wave behavior.

Figure 1 gives the general definitions for two-dimensional, linear water wave theory for which the following notation is needed:

$\eta(x,t)$ = the free water surface; t = time

u,w = velocity components in the x,z directions, respectively

$\phi(x,z,t)$ = the two-dimensional velocity potential (a function of the basic wave parameters H,d,T, or L, the spatial position x, z, and time t)

ρ = the fluid density; g = gravitational acceleration

a = wave amplitude = $H/2$; H = wave height

k = wave number = $2\pi/L$; L = wave length

ω = wave frequency = $2\pi/T$; T = wave period

d = mean water depth; C = wave celerity = L/T

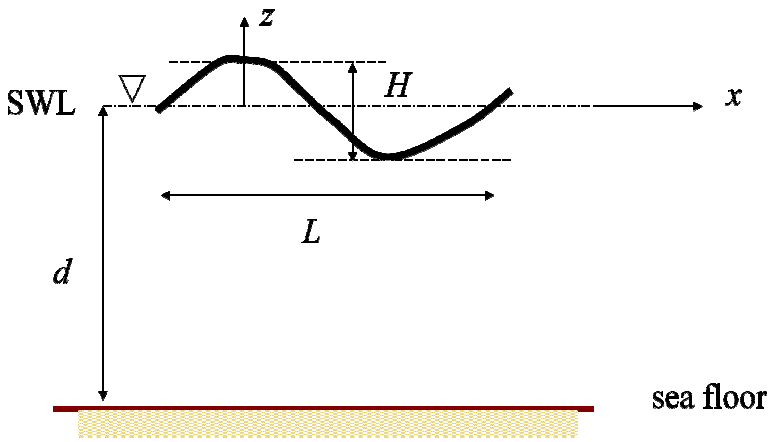

Figure B.1. Two-dimentional periodic wave

Linear wave theory is a solution of the Laplace equation:

$$\frac{\partial^2 \phi}{\partial x^2} + \frac{\partial^2 \phi}{\partial z^2} = 0 \tag{B.1}$$

The particular flow in any condition is determined by the boundary conditions. The Laplace Equation is subject to the specific boundary conditions (at the free surface of the sea and at the bottom)

Bottom boundary condition:

$$w = \frac{\partial \phi}{\partial z} = 0 \quad at \quad z = -d \tag{B.2}$$

Free surface dynamic boundary condition:

$$\frac{1}{2}(u^2 + w^2) + g\eta + \frac{\partial \phi}{\partial z} = 0 \quad at \quad z = \eta \tag{B.3}$$

The solution of the velocity potential function satisfying the Laplace Equation subject to the boundary conditions is,

$$\phi = \frac{gH}{2\omega} \frac{\cosh k(d+z)}{\cosh kd} \sin \theta \tag{B.4}$$

Where, $\theta = kx - \omega t$

On the other hand, the surface elevation is given by,

$$\eta(x,t) = a \cos \theta \tag{B.5}$$

The dispersion relationship gives the relationship between wave period *T* and wave length *L*.

$$\omega^2 = gk \tanh kd \tag{B.6}$$

$$\text{or,} \qquad L = \frac{gT^2}{2\pi}\tanh\frac{2\pi d}{L}$$

$$\text{or,} \qquad C = \sqrt{\frac{gL}{2\pi}\tanh\frac{2\pi d}{L}}$$

In deep water, $d/L > 1/2$ then,

$\tanh (2\pi d/L) \approx 1.0$, and $\cosh kd \approx \sinh kd \approx e^{kd}/2$.

In shallow water, $d/L < 1/20$ then,

$\tanh (2\pi d/L) \approx 2\pi d/L$, $\cosh kd \approx 1$, and $\sinh kd \approx kd$.

By using equation 4 and 6 the alternative velocity potential becomes,

$$\phi = \frac{\omega H}{2k}\frac{\cosh k(d+z)}{\sinh kd}\sin\theta \qquad \text{(B. 7)}$$

Horizontal particle velocity becomes,

$$u = \frac{\partial\phi}{\partial x} = \frac{\pi H}{T}\frac{\cosh k(d+z)}{\sinh kd}\cos(kx - \omega t) \qquad \text{(B. 8)}$$

And, vertical particle velocity becomes,

$$w = \frac{\partial\phi}{\partial z} = \underset{1}{\left(\frac{\pi H}{T}\right)}\underset{2}{\left(\frac{\sinh k(d+z)}{\sinh kd}\right)}\underset{3}{(\sin(kx - \omega t))} \qquad \text{(B. 9)}$$

These three components of velocity called;

- Surface deep water particle speed,

- Exponential decrease in particle velocity with increasing distance below the free surface, and,
- Cyclic velocity variation through a wave phase, respectively.

Moreover, the acceleration components become,

$$a_x = \frac{\partial u}{\partial t} = \frac{2\pi^2 H}{T^2}\frac{\cosh k(d+z)}{\sinh kd}\sin(kx - \omega t) \tag{B.10}$$

$$a_z = \frac{\partial w}{\partial t} = \frac{2\pi^2 H}{T^2}\frac{\sinh k(d+z)}{\sinh kd}\cos(kx - \omega t) \tag{B.11}$$

An finally, the horizantal water particle displacement ξ, and vertical water particle displacement ζ are presented below,

$$\xi(x_1, z_1, t) = -\boxed{\frac{H}{2}\frac{\cosh k(d+z_1)}{\sinh kd}}\sin(kx_1 - \omega t) \tag{B.12}$$

$$\zeta(x_1, z_1, t) = \boxed{\frac{H}{2}\frac{\sinh k(d+z_1)}{\sinh kd}}\cos(kx_1 - \omega t) \tag{B.13}$$

or,

$$\xi(x_1, z_1, t) = -\boxed{A}\sin(kx_1 - \omega t) \tag{B.14}$$

$$\zeta(x_1, z_1, t) = \boxed{B}\cos(kx_1 - \omega t) \tag{B.15}$$

B.2. Stokes Wave Theory

Stokes assumed that all variation in a direction can be represented by Fourier series and that the coefficients in these series can be written as perturbation expansions in terms of a parameter which increases with wave height. A first order Stokes wave is idential to a linear (Airy) wave. A presentation of Stokes theory, retaining terms to fifth order, is made by Fenton (1985) [46].

It is convenient to use the dimensionless wave height in the form $\varepsilon = kH/2$, where k is the wave number $k = 2\pi/\lambda$, where λ is wave length. The theory can be presented completely in terms of dimensionless wave height and dimensionless wave depth (i.e. kd). The coefficients used in the theory are presented in the table below [46].

If the three dimensions, water depth d, wave height H and wave length λ are known, then all the coefficients can be calculated. Stokes theory provides an equation for $\bar{u}$ (mean wave speed) in which mean current is zero. And the perturbation expansion in terms of ε is,

$$\bar{u}\left(\frac{k}{g}\right)^{1/2} = C_0 + \varepsilon^2 C_2 + \varepsilon^4 C_4 + \ldots \qquad (B.16)$$

On the other hand, the expression for the volume flow rate per unit span Q from the theory is,

$$Q\left(\frac{k^3}{g}\right)^{1/2} = C_0 kd + \varepsilon^2(C_2 kd + D_2) + \varepsilon^4(C_4 kd + D_4) + \ldots \qquad (B.17)$$

$$= \bar{u}d\left(\frac{k^3}{g}\right)^{1/2} + \sum_{i=1}^{\infty} \varepsilon^i D_i$$

The fluid velocities in (x,y) frame are given by $u = \partial\phi/\partial x$ and $w = \partial\phi/\partial z$, where the velocity potential ϕ is given by,

$$\phi(x,z,t) = -\bar{u}x + C_0\left(\frac{g}{k^3}\right)^{1/2} \sum_{i=1}^{5} \varepsilon^i \sum_{j=1}^{i} A_{ij} \cosh jkz \sin jk\,(x - ct) + \ldots \qquad (B.18)$$

And finally, the surface elevation is given by,

$$k\eta(x,t) = kd + \sum_{i=1}^{5} \varepsilon^i \sum_{j=1}^{i} B_{ij} \cosh jk(x - ct) + \ldots \qquad (B.19)$$

Table B.1. Coefficients used in Stokes theory in terms of hyperbolic functions of *kd*, including S = *sech(2kd)*.[46]

$$
\begin{aligned}
A_{11} &= 1/\sinh kd \\
A_{22} &= 3S^2/(2(1-S)^2) \\
A_{31} &= (-4-20S+10S^2-13S^3)/(8\sinh kd(1-S)^3) \\
A_{33} &= (-2S^2+11S^3)/(8\sinh kd(1-S)^3) \\
A_{42} &= (12S-14S^2-264S^3-45S^4-13S^5)/(24(1-S)^5) \\
A_{44} &= (10S^3-174S^4+291S^5+278S^6)/(48(3+2S)(1-S)^5) \\
A_{51} &= (-1184+32S+13232S^2+21712S^3+20940S^4+12554S^5-500S^6-3341S^7-670S^8) \\
&\quad /(64\sinh kd(3+2S)(4+S)(1-S)^6) \\
A_{53} &= (4S+105S^2+198S^3-1376S^4-1302S^5-117S^6+58S^7)/(32\sinh kd(3+2S)(1-S)^6) \\
A_{55} &= (-6S^3+272S^4-1552S^5+852S^6+2029S^7+430S^8)/(64\sinh kd(3+2S)(4+S)(1-S)^6) \\
B_{11} &= 1 \\
B_{22} &= \coth kd(1+2S)/(2(1-S)) \\
B_{31} &= -3(1+3S+3S^2+2S^3)/(8(1-S)^3) \\
B_{33} &= -B_{31} \\
B_{42} &= \coth kd(6-26S-182S^2-204S^3-25S^4+26S^5)/(6(3+2S)(1-S)^4) \\
B_{44} &= \coth kd(24+92S+122S^2+66S^3+67S^4+34S^5)/(24(3+2S)(1-S)^4) \\
B_{51} &= -(B_{53}+B_{55}) \\
B_{53} &= 9(132+17S-2216S^2-5897S^3-6292S^4-2687S^5+194S^6+467S^7+82S^8) \\
&\quad /(128(3+2S)(4+S)(1-S)^6) \\
B_{55} &= 5(300+1579S+3176S^2+2949S^3+1188S^4+675S^5+1326S^6+827S^7+130S^8) \\
&\quad /(384(3+2S)(4+S)(1-S)^6) \\
C_0 &= (\tanh kd)^{1/2} \\
C_2 &= (\tanh kd)^{1/2}(2+7S^2)/(4(1-S)^2) \\
C_4 &= (\tanh kd)^{1/2}(4+32S-116S^2-400S^3-71S^4+146S^5)/(32(1-S)^5) \\
D_2 &= -(\coth kd)^{1/2}/2 \\
D_4 &= (\coth kd)^{1/2}(2+4S+S^2+2S^3)/(8(1-S)^3) \\
E_2 &= \tanh kd(2+2S+5S^2)/(4(1-S)^2) \\
E_4 &= \tanh kd(8+12S-152S^2-308S^3-42S^4+77S^5)/(32(1-S)^5)
\end{aligned}
$$

APPENDIX C: PROBABILITY DENSITY FUCTION CALCULATIONS

Longuet-Higgins formulates the dimensionless joint probability density function as,

$$f(r,n) = \frac{2}{\sqrt{\pi}\nu}\left(1+\frac{\nu^2}{4}\right)\left(\frac{r}{n}\right)^2 exp\left\{-r^2\left[1+\left(1-\frac{1}{n}\right)^2\frac{1}{\nu^2}\right]\right\} \qquad (C.1)$$

Where,

r = dimensionless wave amplitude, $\frac{a}{\sqrt{2M_0}}$,

n = dimensionless wave period, $\frac{T}{T_{mean}}$,

a = H/2, m,

T_{mean} = $2\pi\frac{M_0}{M_1}$, sec,

ν = $\sqrt{\frac{M_0 M_2}{M_1^2}-1}$

For the spectrum the spectral moments are given approximately as [48],

$$M_0 = \frac{1}{16}H_s^2 \qquad (C.2)$$

$$M_1 = \frac{1}{16}H_s^2\omega_{max}\frac{6.8+\Upsilon}{5+\Upsilon}$$

$$M_2 = \frac{1}{16}H_s^2{\omega_{max}}^2\frac{11+\Upsilon}{5+\Upsilon}$$

Where, ω_{max} = Maximum angular wave frequency, 2π / T_{max}.

If no particular values are given for the peakedness parameter Υ, the following value may be used [48],

$$\Upsilon = e^{5.75-1.15T_{max}/\sqrt{H_s}} \quad for \quad 3.6 \le \frac{T_{max}}{\sqrt{H_s}} \le 5 \qquad (C.3)$$

All the calculation are presented in Table C.1 and Table C.2 by using the formulas above.

Table C.1. Calculation parameters for joint probability density functions.

Parameters		Operating Speed Case	50 Years RP Case	100 Years RP Case
H_{max}	[m]	7.17	14.10	15.70
T_{max}	[sec]	8.37	10.90	11.40
H_s	[m]	3.99	8.67	9.81
T_z	[sec]	6.97	9.16	9.57
ω_{max}	[Hz]	0.75	0.58	0.55
$T_{max}/\sqrt{H_s}$		4.19	3.70	3.64
Υ		2.54	4.45	4.78
M_0		1.00	4.70	6.01
M_1		0.93	3.22	3.93
M_2		1.01	2.55	2.95
v		0.41	0.39	0.39
T_{mean}	[sec]	6.76	9.16	9.63
a	[m]	3.59	7.05	7.85
r		2.54	2.30	2.26

Table C.2. Calculation for joint probability density functions at fixed wave heights.

	Operating Speed Case		50 Years RP Case		100 Years RP Case	
T [sec]	$n = T/T_{mean}$	$f(r,n)$	$n = T/T_{mean}$	$f(r,n)$	$n = T/T_{mean}$	$f(r,n)$
0.1	0.015	0.000	0.011	0.000	0.010	0.000
0.5	0.074	0.000	0.055	0.000	0.052	0.000
1	0.148	0.000	0.109	0.000	0.104	0.000
1.5	0.222	0.000	0.164	0.000	0.156	0.000
2	0.296	0.000	0.218	0.000	0.208	0.000
2.5	0.370	0.000	0.273	0.000	0.260	0.000
3	0.444	0.000	0.328	0.000	0.312	0.000
3.5	0.518	0.000	0.382	0.000	0.364	0.000
4	0.592	0.000	0.437	0.000	0.415	0.000
4.5	0.666	0.000	0.491	0.000	0.467	0.000
5	0.740	0.000	0.546	0.000	0.519	0.000
5.5	0.814	0.006	0.601	0.000	0.571	0.000
6	0.888	0.020	0.655	0.000	0.623	0.000
6.5	0.962	0.029	0.710	0.001	0.675	0.000
7	1.036	0.026	0.765	0.005	0.727	0.001
7.5	1.110	0.016	0.819	0.022	0.779	0.010
8	1.184	0.008	0.874	0.051	0.831	0.033
8.5	1.258	0.004	0.928	0.075	0.883	0.065
9	1.332	0.002	0.983	0.082	0.935	0.089
9.5	1.406	0.001	1.038	0.071	0.987	0.094
10	1.480	0.000	1.092	0.052	1.039	0.081
10.5	1.554	0.000	1.147	0.034	1.091	0.061
11	1.628	0.000	1.201	0.021	1.143	0.042
11.5	1.702	0.000	1.256	0.012	1.194	0.026
12	1.776	0.000	1.311	0.007	1.246	0.016
12.5	1.850	0.000	1.365	0.004	1.298	0.009
13	1.924	0.000	1.420	0.002	1.350	0.005
13.5	1.998	0.000	1.474	0.001	1.402	0.003
14	2.072	0.000	1.529	0.001	1.454	0.002

APPENDIX D: GUMBEL METHOD

The Gumbel method involves 5 main steps for processing of wind speed data to model extreme wind data [34]:

Step1: Data (V_{max}) is ranked in order from smallest to largest: 1, 2, 3, …, m, to N

V_{max} = maximum annual wind speeds, m/s

(To be sorted from lowest maximum to highest maximum)

m = rank of the wind speeds from lowest to highest

N = total number of annual maximum observation

Step 2: Probability of non-exceedance, P according to:

$$P = m/(N+1) \tag{D.1}$$

Step 3: Negative of the natural logarithm of P, taken twice

$$r = -ln(-ln(P)) \tag{D.2}$$

Step 4: Wind speed is plotted against y, and a line of best fit is drawn.

In general, by means of linear regression,

c = mode = intercept of the line, $1/a$ = slope of the line.

Step 5: For large values of return period a simple equation can be used to determine extreme wind speed.

$$V_R = c + \frac{1}{a}\ln(RP) \tag{D.3}$$

Alacatı is one of the onshore sites in Turkey, so, it was chosen for analysis. Wind data were recorded for a period of time (Jul 2000 – Dec 2000). Although it is short period of time, the data divided into 10 days of periods. North was chosen as dominant wind direction, and, one maximum wind speeds in each 10 days were considered. Then, Gumble method is applied in 10 days bins of 6 months wind data. The calculations presented in Table D.1 below and plotted in Figure D.1.

The maximum wind speed at 30m height are taken from the data and converted to the wind speed at 90 m height according to Equation 2.8. Then the return period calculations are presented in Table D.2.

Table D.1. Probabilistic calculation for maximum annual wind speed

Vs at (30m) (m/s)	*Vs* at (90m) (m/s)	*m*	*N*	*p*	*-ln(p)*	*r = -ln(-ln(p))*
13.2	15.4	1	17	0.056	2.890372	-1.061385
14.2	16.6	2	17	0.111	2.197225	-0.787195
16.4	19.2	3	17	0.167	1.791759	-0.583198
16.6	19.4	4	17	0.222	1.504077	-0.408180
16.7	19.5	5	17	0.278	1.280934	-0.247589
17	19.9	6	17	0.333	1.098612	-0.094048
17.2	20.1	7	17	0.389	0.944462	0.057140
18.8	22.0	8	17	0.444	0.810930	0.209573
19.2	22.5	9	17	0.500	0.693147	0.366513
19.3	22.6	10	17	0.556	0.587787	0.531391
19.9	23.3	11	17	0.611	0.492476	0.708309
20.8	24.3	12	17	0.667	0.405465	0.902720
23.2	27.1	13	17	0.722	0.325422	1.122631
24.7	28.9	14	17	0.778	0.251314	1.381050
25	29.2	15	17	0.833	0.182322	1.701983
26.1	30.5	16	17	0.889	0.117783	2.138911
30.5	35.7	17	17	0.944	0.057158	2.861929

Table D.2. Return period for maximum annual wind speed

Return Period (RP)	*1/a*	*c*	ln(*RP*)	*VR* (m/s)
1	4.9818	20.737	1E-06	20.737005
10	4.9818	20.737	2.302585	32.2080184
50	4.9818	20.737	3.912023	40.2259162
100	4.9818	20.737	4.60517	43.6790368
500	4.9818	20.737	6.214608	51.6969346
1000	4.9818	20.737	6.907755	55.1500552
5000	4.9818	20.737	8.517193	63.167953
10000	4.9818	20.737	9.21034	66.6210737
100000	4.9818	20.737	11.51293	78.0920921
1000000	4.9818	20.737	13.81551	89.5631105

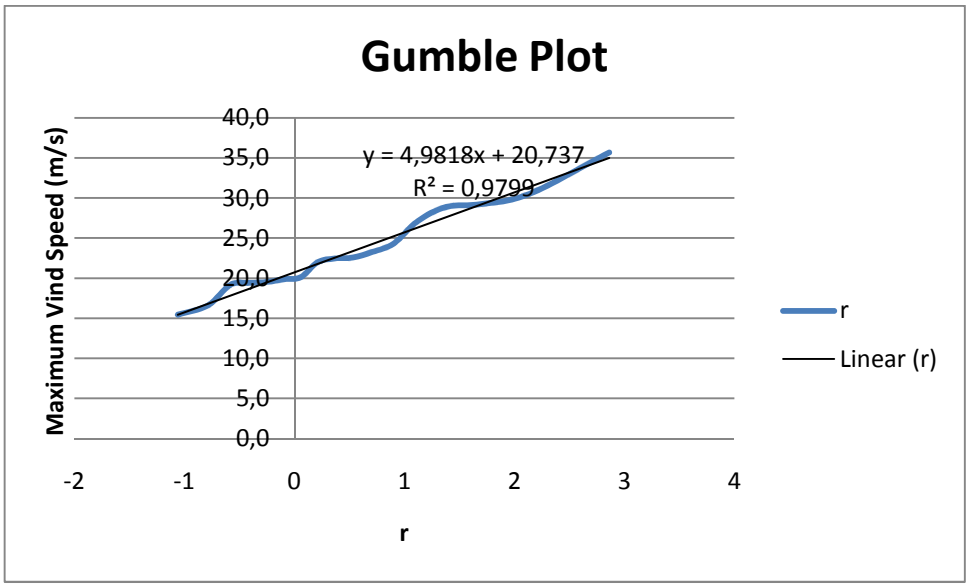

Figure D.1. Gumble Plot

The wind data for Massachusetts site is compared with the Figure D.2. There is a slight difference between return periods of 50 and 100 years in Alacatı (40.22 m/s and 43.67 m/s respectively) and Massachusetts site (42.98 m/s and 48.35 m/s respectively). One reason for that, Alacatı site wind data was measured from onshore area and

Massachusetts site data from offshore area. Furthermore, there is not much data for Alacatı site.

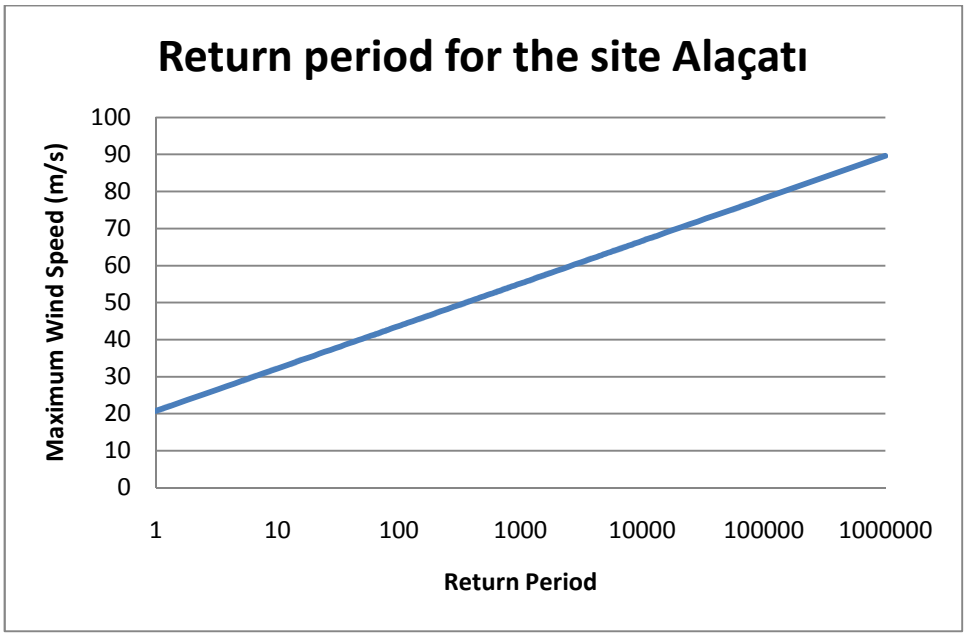

Figure D.2. Return period for the site Alaçatı.

APPENDIX E: WIND ON TOWER

Table E.1. Wind load on the tower for operating case

Average *Ws*, 90m (m/s)	ρ (kg/m3)	C_s
11.40	1.225	0.5

Operating Case

Width (m)	Height (m)	Area (m^2)	Wind Speed (m/s)	ΔF (kN)	Moment Arm (m)	ΔM (MNm)
	90	0.00	11.40	0.000	119	0.000
3.87	87.6	9.68	11.36	0.382	116.6	0.045
4.01	82.6	20.06	11.26	0.779	111.6	0.087
4.15	77.6	20.77	11.16	0.792	106.6	0.084
4.30	72.6	21.48	11.06	0.804	101.6	0.082
4.44	67.6	22.19	10.94	0.814	96.6	0.079
4.58	62.6	22.90	10.82	0.822	91.6	0.075
4.72	57.6	23.61	10.70	0.827	86.6	0.072
4.86	52.6	24.32	10.56	0.830	81.6	0.068
5.01	47.6	25.03	10.41	0.830	76.6	0.064
5.15	42.6	25.74	10.24	0.827	71.6	0.059
5.29	37.6	26.45	10.06	0.820	66.6	0.055
5.43	32.6	27.16	9.86	0.809	61.6	0.050
5.57	27.6	27.87	9.63	0.791	56.6	0.045
5.72	22.6	28.58	9.36	0.766	51.6	0.040
5.86	17.6	29.29	9.03	0.731	46.6	0.034
6.00	12.6	30.00	8.61	0.681	41.6	0.028
6.00	10.1	60.60	7.54	1.056	34.05	0.036
Total				**13.363**		**1.001**

Table E.2. Wind load on the tower for 50-year return period case

Average *Ws*, 90m (m/s)	ρ (kg/m3)	C_s
42.98	1.225	0.5

50-Year Return Period Case

Width (m)	Height (m)	Area (m^2)	Wind Speed (m/s)	ΔF (kN)	Moment Arm (m)	ΔM (MNm)
	90	0.00	42.98	0.000	119	0.000
3.87	87.6	19.35	42.81	10.863	106.6	1.158
4.01	82.6	20.06	42.46	11.074	111.6	1.236
4.15	77.6	20.77	42.08	11.263	106.6	1.201
4.30	72.6	21.48	41.68	11.428	101.6	1.161
4.44	67.6	22.19	41.26	11.568	96.6	1.117
4.58	62.6	22.90	40.81	11.679	91.6	1.070
4.72	57.6	23.61	40.33	11.758	86.6	1.018
4.86	52.6	24.32	39.81	11.801	81.6	0.963
5.01	47.6	25.03	39.24	11.804	76.6	0.904
5.15	42.6	25.74	38.62	11.760	71.6	0.842
5.29	37.6	26.45	37.94	11.661	66.6	0.777
5.43	32.6	27.16	37.18	11.496	61.6	0.708
5.57	27.6	27.87	36.30	11.248	56.6	0.637
5.72	22.6	28.58	35.28	10.894	51.6	0.562
5.86	17.6	29.29	34.04	10.395	46.6	0.484
6.00	12.6	30.00	32.46	9.678	41.6	0.403
6.00	10.1	60.60	28.44	15.012	34.05	0.511
Total				**195.381**		**14.752**

Table E.3. Wind load on the tower for 100-year return period case

Average *Ws*, 90m (m/s)	ρ (kg/m3)	C_s
48.35	1.225	0.5

100-Year Return Period Case

Width (m)	Height (m)	Area (m^2)	Wind Speed (m/s)	ΔF (kN)	Moment Arm (m)	ΔM (MNm)
	90	0.00	48.35	0.000	119	0.000
3.87	87.6	19.35	48.16	13.747	116.6	1.603
4.01	82.6	20.06	47.76	14.014	111.6	1.564
4.15	77.6	20.77	47.34	14.253	106.6	1.519
4.30	72.6	21.48	46.89	14.463	101.6	1.469
4.44	67.6	22.19	46.41	14.639	96.6	1.414
4.58	62.6	22.90	45.91	14.779	91.6	1.354
4.72	57.6	23.61	45.36	14.879	86.6	1.289
4.86	52.6	24.32	44.78	14.934	81.6	1.219
5.01	47.6	25.03	44.14	14.938	76.6	1.144
5.15	42.6	25.74	43.45	14.882	71.6	1.066
5.29	37.6	26.45	42.68	14.757	66.6	0.983
5.43	32.6	27.16	41.82	14.548	61.6	0.896
5.57	27.6	27.87	40.84	14.234	56.6	0.806
5.72	22.6	28.58	39.69	13.787	51.6	0.711
5.86	17.6	29.29	38.30	13.155	46.6	0.613
6.00	12.6	30.00	36.51	12.247	41.6	0.509
6.00	10.1	60.60	31.99	18.997	34.05	0.647
Total				**247.254**		**18.806**

REFERENCES

1. Jonkman, J., "NREL's Baseline Wind Turbine Aeroelastic Model for Use in Various Offshore Analysis Concept Studies", NRELOffshrBsline5MW.doc, *NREL/NWTX*, www.ieawind.org, 2006.

2. Zaaijer, M.B., "Comparison of Monopile, Tripod, Suction Bucket and Gravity Base Design for A 6MW Turbine", *Proceedings of the OWEMES,* Delft University of Technology, the Netherlands, 2003.

3. Fischer, T. and M. Kühn, "Site Sensitive Support Structure and Machine Design for Offshore Wind Farms", *Endowed Chair of Wind Energy (SWE),* the Institute of Aircraft Design, Universitat Stuttgart, Germany, 2009.

4. AlHamaydeh, M. and S. Hussain, "Optimized Frequency-Based Foundation Design for Wind turbine Towers utilizing Soil-Structure Interaction", *Journal of Franklin Institute*, doi:10.1016/j.jfranklin.2010.04.013, 2010.

5. Kühn, M., "Soft or Stiff – A Fundamental Question for Designers of Offshore Wind Energy Converters", *European Wind Energy Conference EWEC 97*, Dublin, Ireland, October 1997.

6. van der Tempel, J. and D.P. Molenaar, "Wind Turbine Structural Dynamics – A Review of the Principles for Modern Power Generation, Onshore and Offshore", *Wind Engineering*, Volume 26, No.4, pp. 211-220, 2002.

7. Saigal, R.K. and D. Dolan, MMI Engineering, Inc.; Der Kiureghian, A., University of California, Berkeley; Camp, T., Garrad Hassan & Partners Ltd.; and Smith, C.E., Minerals Management Service; "Comparison of Design Guidelines for Offshore Wind Energy Systems", *2007 Offshore Technology Conference*, OTC 18984-PP, 2007.

8. Camp, T.R., M.J. Morris, R. van Rooij, J. van der Tempel, M. Zaaijer, A. Handerson, K. Argyriadis, S. Schwartz, H. Just, W. Grainger and D. Pearce, "Design Methods for

Offshore Wind Turbines at Exposed Sites", *Final Report EU Joule III Project*, JOR3-CT95-0284, November 2003.

9. Veers, P.S. and S. Butterfield, "Extreme Load Estimation for Wind Turbines: Issues and Opportunities for Improved Practice", *Sandia National Laboratory and National Renewable Energy Laboratory*, USA, 2001.

10. Lesny, K., S.G. Paikowsky and A. Gurbuz, "Scale Effects in Lateral Load Response of Large Diameter Monopiles", *GeoDenver*, Denver, USA, February 2007.

11. Krolis, V.D., J. van der Tempel and W. de Vries, Evaluation of Foundation Design for Monopile Support Structures for Offshore Wind Turbines, *2007 European Offshore Wind Conference*, Delft University of Technology, The Netherlands, 2007.

12. Wiemann, J., K. Lesny and W. Richwien, "Evaluation of Pile Diameter Effects on Soil-Pile Stiffness", *7th German Wind Energy Conference DEWEK*, 2004.

13. Passon, P., "Memorandum – Derivation and Description of the Soil-Pile Interaction Models", *IEA-Annex XXIII Subtask 2,* University of Stuttgart, Germany, July 2006.

14. M.B.Zaaijer, "Foundation Modelling to Assess Dynamic Behaviour of Offshore Wind Turbines", *Applied Ocean Research*, pp.45-57, Delft, 2006.

15. Argyriadis, K., L. Gill and S. Schwarts, "Loads for Offshore wind Turbines: The 2nd Edition of The GL Wind Guideline", *Germanischer Lloyd Wind Energie GmbH*, Germany, 2004.

16. Seidel, M., M. von Mutius and D. Steudel, "Design and Load Calculations for Offshore Foundations of A 5MW Turbine", *7th German Wind Energy Conference DEWEK*, 2004.

17. van der Tempel, J., *Design of Support Structures for Offshore Wind Turbine*, PHD Thesis, Delft Technical University, April 2006.

18. Livingstone, P., *NOF Energy Market Visit to Denmark*, http://www.nofenergy.co.uk/editorfiles/NOF Energy Market Visit to Denmark 2010.pdf, 2010.

19. WWEA, *World Wind Energy Report 2009*, http://www.wwindea.org/home/index.php.

20. Ender, C., "Wind Energy Use in Germany – Status 31.12.2009", *Dewi Magazin*, No.36, pp. 28-41, February 2010.

21. Kurtaran, C., "Calm before the Storm in Turkey", *Dewi Magazin*, No.36, pp.24-27, February 2010.

22. Kurul, K., "An Incentive in the Form of Production Credit can be Worked on (Interview with Kor Özay)", *Clean Energy Magazine*, pp. 32-34, June 2010.

23. Musial, W. and B. Ram, "Large-Scale Offshore Wind Power in the United States - Assessment of Opportunities and Barriers", *NREL*, September 2010.

24. Jonkman, J., "Definition of the Floating Systems for Phase IV of OC3, *NREL*, 2010.

25. Jonkman, J.M. and Jr.M.L. Buhl, "FAST User's Guide," NREL/EL-500-38230. Golden, *National Renewable Energy Laboratory*, Colorado, August 2005.

26. Jonkman, B.J., "TurbSim User's Guide (Version 1.50)", NREL/TP-500-46198, *National Renewable Energy Laboratory*, September 2009.

27. Goda, Y., "Random Seas and Design of Maritime Structures", *Advanced Series on Ocean Engineering*, Vol. 5, 2000.

28. Anbarasan, M., *Offshore Structural Design,* www.docstoc.com/docs/5874616/Offshore-Structural-Design, 2009.

29. Piggott, H., *Centre for Alternative Technology Windpower Course Notes*, www.scoraigwind.com/wpNotes/bladeDesign.pdf.

30. DET NORSKE VERITAS., "Design of Offshore Wind Turbine Structures", *DNV Offshore Standard*, DNV-OS-J101, 2007.

31. American Petroleum Institute (API), "Recommended Practice for Planning, Designing and Constructing Fixed Offshore Platforms-Working Stress Design", *American Petroleum Institute*, API RP-2A-WSD, 21st Edition 2000.

32. The Danish Energy Agency's Approval Scheme for Wind Turbines, *Recommendation for Technical Approval of Offshore Wind Turbines*, December 2001.

33. Jha, A., D. Dolan, T. Gur, S. Soyoz and C. Alpdogan, "Comperison of API & IEC Standards for Offshore Wind Turbine Applications in the U.S. Atlantic Ocean: Phase II", *MMI Engineering*, July 2009.

34. Holmes, J., *Wind Loading on Buildings*, SPON press, 2001.

35. Reese L.C., W.M. Isenhower and S.T. Wang, *Analysis and Design of Shallow and Deep Foundations*, John Wiley & Sons Inc, 2006.

36. Zaaijer, M.B., *Offshore Wind Farm Design - Loads, Dynamics and Structural Design*, ocw.tudelft.nl/fileadmin/ocw/opener/Offshorewindfarmhfd6.pdf, 2008.

37. Barltrop, N.D.P. and A.J. Adams, *Dynamics of Fixed Marine Structures*, Oxford: Butterworth Heinemann Ltd, 1991.

38. van Bussel, G.J.W., C. Schontag, T.T. Cockerill, R. Harrison, J. van der Tempel, L.A. Harland, J.H. Vugts and M. Kühn, "Methods Assisting the Design of Offshore Wind Energy Conversion Systems", *Institute for Wind Energy*, Opti-OWECS final report, Vol. 2., Delft, 1998.

39. Leblanc, C., *Design of Offshore Wind Turbine Support Structures*, DCE Thesis No. 18, Ph.D. Thesis, Aalborg University, Denmark, 2009.

40. Lesny, K. and J. Wiemann, ”Design Aspects of Monopile in German Offshore Wind Farms”, *ISFOG 2005*, Perth – Western Australia, September 2005.

41. Zaaijer, M.B., *Properties of Offshore Support Structures for Large Scale Wind Turbines*, Delft University of Technology, the Netherlands, 2001.

42. Morthorst, P.E., H. Auer, A. Garrad and I. Blanco, “Wind Energy-The Facts: Part III: The Economics of Wind Power”, *International Institute for Environment and Development*, London, UK, 2008.

43. Borgen, E., “Floating Wind Power in Deep Water – Competitive with Shallow-water Wind Farms”, *Modern Energy Review*, Volume 2 Issue 1, Touch Brietings, pp. 49-53, March 2010.

44. DET NORSKE VERITAS., “Environmental Conditions and Environmental Loads”, *DNV Recommended Practice*, DNV-RP-C205, 2007.

45. Le Mehaute, B., *An Introduction to Hydrodynamics and Water Waves*, Springer-Verlag New York Inc, 1976.

46. Fenton, J.D., “Nonlinear Wave Theories”, *Ocean Engineering Science*, Volume 9, New York, 1990.

47. Ochi, K.M., *Ocean Waves – The Stochastic Approach*, Cambridge Ocean Technology, Series 6, 1998.

48. DET NORSKE VERITAS., “State of the Art Review on Wave Description in Current Design Practice and Marine Operation”, *DNV Maxwave*, Report No. 2001-1491, Revision No. 1, 2002.

REFERENCES NOT CITED

Akova, I., 2008, *Yenilenebilir Energy Kaynakları*, Nobel publication, February.

Chopra, A.K., 1995, *Dynamics of Structures – Theory and Application to Earthquake Engineering*, Prentice Hall Inc., New Jersey.

Kooijman, H. J. T., C. Lindenburg, D. Winkelaar and E. L. van der Hooft, 2003, "Dowec 6 MW pre-design: Aero-elastic modeling of the DOWEC 6 MW pre-design in PHATAS", *Energy Research Center of the Netherlands*, September.

Peterson, P., K.B. Nielsen and T. Feld, 2005, "Design Basis for Offshore Wind Structures", *Det Norske Veritas-Global Wind Energy*, Copenhagen, Denmark.

Sumer, B.M. and J. Fredsoe, 1997, "Hydrodynamics Around Cylindrical Structures", *Advanced Series on Ocean Engineering*, Volume 12.